

**CHARACTERIZATION OF THE PRESSURE WAVE FROM A SHOCK TUBE  
USING NUMERICAL SIMULATIONS**

by

Mukul Bokil

A thesis submitted to the faculty of  
The University of Utah  
in partial fulfillment of the requirements for the degree of

Master of Science

Department of Mechanical Engineering

The University of Utah

December 2010

Copyright © Mukul Bokil 2010

All Rights Reserved

**The University of Utah Graduate School**

**STATEMENT OF THESIS APPROVAL**

The thesis of **Mukul Bokil**

has been approved by the following supervisory committee members:

<b>Kenneth Monson</b>	, Chair	<b>07/28/2010</b>
<b>Todd Harman</b>	, Member	<b>07/28/2010</b>
<b>K. Larry DeVries</b>	, Member	<b>07/28/2010</b>

and by **Timothy Ameal**, Chair of  
the Department of **Mechanical Engineering**

and by Charles A. Wight, Dean of The Graduate School.

## **ABSTRACT**

Research presented in this thesis stems from rising concern about blast-induced traumatic brain injury (TBI). It has been hypothesized that brain tissue is damaged by the blast wave generated during an explosion, but the mechanism of tissue injury is unknown. The pressure wave produced by a typical explosion includes a peak pressure, or overpressure, and positive and negative pressure phases; each component of this blast wave may make a unique contribution to injury. A simple device called a shock tube is capable of generating the characteristics associated with the blast wave. This thesis presents a computational model of a shock tube being used in our laboratory to investigate the above-mentioned characteristics of the blast wave. The shock tube is approximately 135 cm long and has a 2.54 cm inner diameter.

This research has two primary objectives. The first is to characterize blast wave properties as a function of shock tube independent parameters. In our shock tube, the independent parameters are driver section length and initial pressure. Because the purpose of this research is to study injury due to pressure wave loading alone, the target is placed outside the tube to avoid interaction with venting gases. Quantifying the appropriate region for testing is the second main objective of this research.

Shock behavior within the shock tube was characterized with 1D simulations, while expansion of the wave after it exits the tube was modeled using primarily 2D but

also 3D simulations. The numerical code used for this research (called Uintah) was previously developed at the University of Utah.

Results show that peak overpressure and positive phase duration increase with driver pressure, and negative phase duration decreases with driver pressure. Response time of the expansion waves is controlled by the driver section length. Expansion waves travel in the reverse direction to the shock wave and reflect back from the shock tube wall. These reflected expansion waves eventually overtake the shock wave, and decrease its peak pressure, increasing the positive phase duration. Results from 2D simulations show that the region lying above  $45^\circ$  angle from the shock tube axis is the most appropriate region for testing of primary blast effects. Preliminary 3D simulations generally agree but suggest that this boundary may be overly conservative so that some of the region below this line is likely also appropriate for testing. As anticipated, the 2D approach has quantitative limitations in modeling 3D behavior. However, comparison with the 3D solution indicates that the 2D approach effectively simulates trends in shock tube behavior. In addition to these findings, an investigation of boundary conditions and potential sources of error in the numerical code are also discussed.

## TABLE OF CONTENTS

ABSTRACT.....	iv
ACKNOWLEDGEMENTS.....	ix
1 INTRODUCTION.....	1
1.1 Motivation.....	1
1.2 Compressible fluids.....	2
1.2.1 Sound waves and speed of sound.....	3
1.2.2 Mach number.....	3
1.3 Shock waves and expansion waves.....	5
1.3.1 Introduction.....	5
1.3.2 Compression wave.....	5
1.3.3 Expansion waves.....	7
1.3.4 Blast wave.....	8
1.4 Shock tube.....	10
1.4.1 Introduction.....	10
1.4.2 Operation of shock tube.....	11
1.4.3 Strength of shock wave.....	13
1.4.4 Blast wave in the shock tube.....	14
1.5 Research objectives.....	15
1.5.1 Parameter study.....	15
1.5.2 Region for testing.....	17
1.6 Numerical simulations.....	18
1.6.1 Introduction.....	18
1.6.2 Theory of numerical simulation.....	19
1.6.3 Uintah.....	20

1.6.4	Governing equations .....	21
1.7	Introduction of upcoming chapters .....	23
2	ONE-DIMENSIONAL SOLUTION.....	24
2.1	Introduction .....	24
2.2	Objective of the 1D simulations.....	24
2.3	Defining geometry and input parameters .....	25
2.4	Governing equations .....	27
2.5	Resolution study.....	28
2.6	Validation of the numerical code .....	30
2.6.1	Description of exact solution .....	30
2.6.2	Comparison of simulated results with the exact solution .....	30
2.7	Data processing .....	33
2.8	Parameter study .....	33
2.8.1	Variation of $P_{dr}$ .....	34
2.8.2	Variation of $L_{dr}$ .....	38
2.8.3	Numerical errors .....	40
2.9	Discussion of the 1D study.....	50
3	TWO-DIMENSIONAL SIMULATIONS.....	52
3.1	Introduction .....	52
3.2	Objective of the 2D simulations.....	52
3.3	Defining geometry and input parameters .....	53
3.3.1	Theoretical geometry of 2D shock tube.....	53
3.3.2	Geometry defined in 2D simulations .....	53
3.4	Governing equations .....	54
3.5	Resolution study.....	55
3.6	Validation of the 2D code .....	58
3.6.1	Description of the explosion problem.....	58
3.6.2	Exact solution.....	60
3.6.3	Validation against the exact solution .....	60

3.7	Data processing .....	60
3.8	Results .....	62
3.8.1	Quantifying an area where target is not affected .....	62
	by the exhaust gas vent .....	62
3.8.2	Parameter study.....	72
3.9	Conclusions .....	79
4	INTRODUCTION TO 3D SOLUTION.....	80
4.1	Introduction .....	80
4.2	Comparisons between 2D and 3D simulations .....	80
4.2.1	Comparison between 2D and 3D geometry .....	80
4.2.2	Comparison between 2D and 3D results.....	82
4.3	Additional results from 3D simulations .....	86
4.4	Discussion .....	88
5	SUMMARY, CONCLUSIONS, AND FUTURE WORK .....	89
5.1	Summary .....	89
5.2	Conclusions .....	90
5.3	Future work .....	92
	APPENDIX.....	93
	REFERENCES .....	124

## **ACKNOWLEDGEMENTS**

I would like to gratefully and sincerely thank Dr. Kenneth Monson for his guidance, understanding, and patience during my graduate studies in the University of Utah. I would like to thank the Department of Defense for providing partial funding to this project through the grant W81XWH-08-1-0295. I sincerely thank Dr. Todd Harman for his great help throughout my research. Finally, I would also like to thank my other lab mates for their help and cooperation throughout the span of this project and especially on the day of my defense.

# 1 INTRODUCTION

## 1.1 Motivation

Awareness of traumatic brain injuries has increased over the past few years because of the recent rise in terrorist activities and the need to increase safety in military areas. A traumatic brain injury is defined as a blow to the head or a penetrating head injury that disrupts the functions of a brain. Over 1.4 million Americans suffer traumatic brain injury each year [1]. Main causes of traumatic brain injury are motor vehicle accidents (around 20%), falls, physical violence, and blasts or explosions, the latter of which are a major concern in the military. The effects of blasts, or explosions, are classified into primary, secondary, and tertiary effects [2]. Every explosion, or blast, generates a pressure wave that originates from the center of the blast and spreads out spherically from the origin of the explosion. Due to the high energy it carries, this pressure wave causes damage to living animal tissues; these are termed primary, or direct, effects. Secondary and tertiary effects (also described as indirect effects) of the blast are associated with the damage caused by projectiles thrown into a person and by a person being thrown.

Some recent blast experiments suggest that primary effects may play a significant role in neurological damage in animals but the mechanism of injury under primary loading is not clear. There is a possibility that blast loads impair the circulatory or

respiratory system, which subsequently leads to brain injury [1]. Hence, studying injuries caused by primary effects is of vital importance.

To study the primary effects on biological tissue, an experimental blast wave that simulates a real blast wave is required. Shock tubes can be used for this purpose, and such a tube is now under use in our laboratory. The objective of this thesis is to describe numerical simulations used to characterize the performance of this shock tube.

This chapter covers fundamentals of compressible fluids, shock waves and expansion waves in Sections 1.2, and 1.3, respectively, operation of a simple shock tube in Section 1.4, research objectives in Section 1.5, and the description of the applied numerical approach and governing equations in Section 1.6.

## **1.2 Compressible fluids**

All fluids are technically compressible but they are categorized into compressible and incompressible fluids, depending on their degree of compressibility. A fluid whose density varies in an appreciable amount when subjected to high pressure is called a compressible fluid. The main difference between compressible and incompressible fluids is the rate at which forces are transmitted through the fluid. For example, if a pump fitted at one end of a pipeline filled with water is turned on, water will begin to flow almost immediately out of the other end. In compressible fluids, imposition of force at one end of the pipe does not cause immediate flow of fluid at the other end of the pipe. Instead, fluid in the area of application of force gets compressed and its density increases. The compressed fluid expands against the adjacent fluid, which is at a lower density. This results in the compression of adjacent fluid and sets in motion a compression pulse that

travels throughout the pipe. In some cases, this compression pulse will combine with others to form a shock wave.

### 1.2.1 Sound waves and speed of sound

All fluids are elastic in nature, so a pressure disturbance transmits in the form of successive compression and rarefaction waves. This pressure disturbance is called a finite disturbance when a perturbation in the thermodynamic state of quiescent gas causes variations in pressure and density the same order as that of local values of pressure and density. However, when the disturbance is very small ( $\Delta P/P \ll 1$ ), small perturbations (i.e. sound waves) propagate at a speed of sound  $c$ , as in Equation 1.1,

$$c^2 = \left( \frac{\partial p}{\partial \rho} \right) \quad (1.1)$$

where  $p$  and  $\rho$  are the pressure and density of the fluid, respectively.

However, when the strength of a disturbance becomes large enough, i.e. of almost the same order as  $p$ , the speed of the wave increases beyond the speed of a sound wave; this generated wave of higher amplitude is called a shock wave. Table 1.1 lists the difference between sound waves and shock waves.

### 1.2.2 Mach number

The Mach number is the ratio of the speed of a fluid particle in a medium to the speed of sound in that medium (pages 1-40 in [3]), as given in Equation 1.2.

**Table 1.1:** Fundamental differences between sound waves and shock waves

<b>Sound waves</b>	<b>Shock waves</b>
No particle flow across the sound wave	Particle flow across the shock wave
Thermodynamic state of gas remains unaltered due to passage of sound wave	Thermodynamic state of gas is altered due to the successive compression and rarefaction of gas
The process of formation of sound wave is isentropic	The process of formation of shock wave is irreversible

$$M = \frac{V}{c} = \frac{V}{\sqrt{\frac{\partial p}{\partial \rho}}} \quad (1.2)$$

where  $V$  is the speed of a fluid particle in a medium and  $c$  is the speed of sound in the same medium. The flow of fluid is divided into the following types according to the Mach number of fluid (Table 1.2).

**Table 1.2:** Mach number ranges

$M < 1$	Subsonic
$M = 1$	Sonic
$0.8 < M < 1.2$	Transonic
$M > 1$	Supersonic

### 1.3 Shock waves and expansion waves

This section covers the description of the shock wave and its complementary part expansion waves.

#### 1.3.1 Introduction

When high pressure gas suddenly comes into contact with low pressure gas, there is an expansion of the high pressure gas into the low pressure region, forming a weak compression wave that propagates into the low pressure gas. For a sufficiently high pressure difference between the gases (usually greater than 2.5), a number of compression waves coalesce to form a shock wave. Temperature increases almost instantaneously, and there is an increase in entropy across the shock, making the flow irreversible. They cause a discontinuous change in fluid properties such as speed (which changes from supersonic to subsonic), pressure, temperature, and density. When a compression shock wave progresses in one direction, there is also an expansion wave progressing in the reverse direction. The formation of both waves can be explained as follows.

#### 1.3.2 Compression wave

The description of the compression wave is adopted from pages 138 - 198 in [3]. Figure 1.1 shows the formation of a compression wave in a duct. High pressure gas can be described as a low mass piston when exposed suddenly to a low pressure gas. The velocity of the piston then increases by a small increment  $dV$  at each instant in time until it reaches a constant magnitude of  $V$ . After the first increment of piston to the right, a weak compression wave is created, which propagates through the low pressure gas.

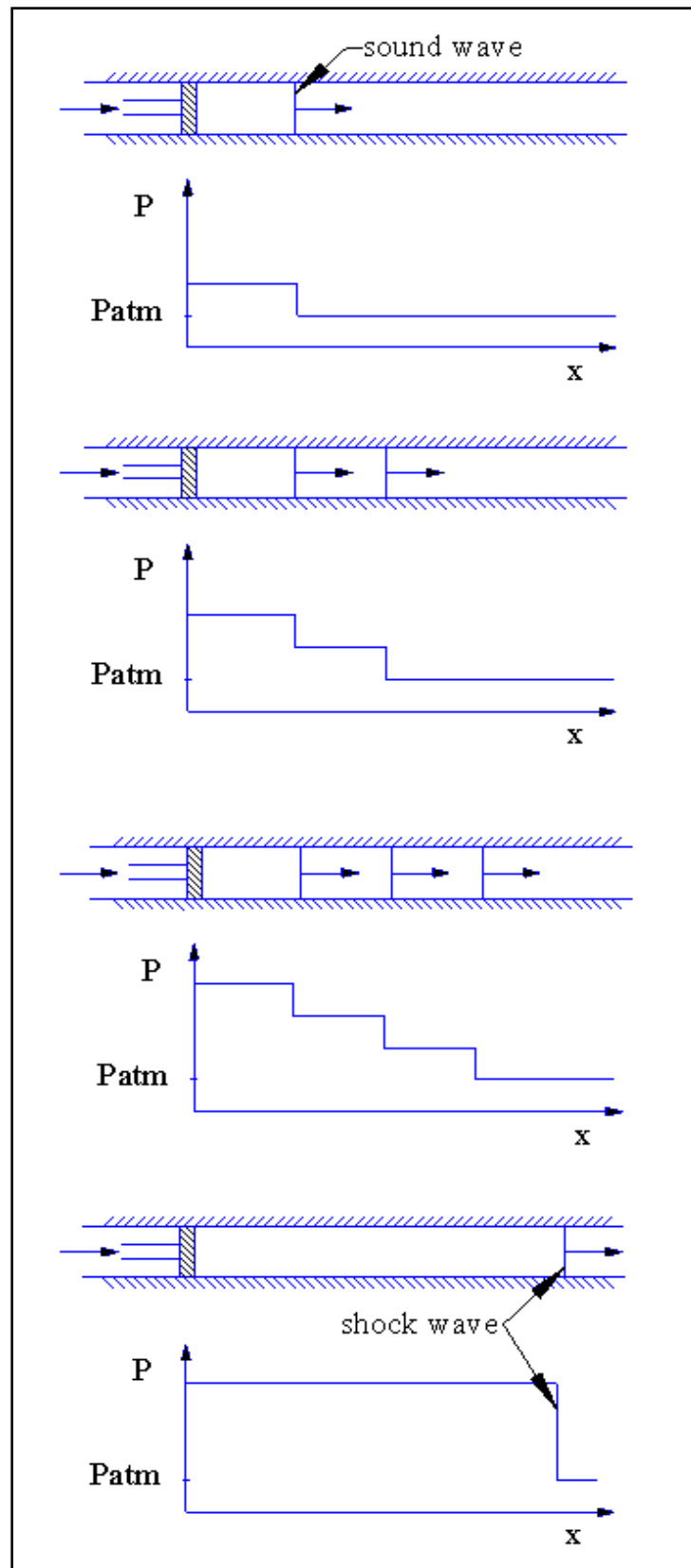


**Figure 1.1:** Shock wave formation (diagram re-created from Saad [3], Fig. 4.3)

Due to the passage of the wave, the pressure and temperature of the gas behind the wave increase, and the gas is set in motion to the right with velocity  $dV$ . When the piston is incremented by  $dV$  a second time, another wave is generated, which travels into the gas at a higher sonic speed than the first wave, because the gas through which it is traveling is already at a higher temperature and pressure due to the passage of the first wave. The speed of sound depends on the properties of the gas through which it is traveling, and so the second wave has the higher absolute velocity than the first wave, eventually overtaking it. Likewise, the third wave overtakes the first two. These waves reinforce each other to form a single compression shock wave of finite thickness.

### **1.3.3 Expansion waves**

The description of the expansion waves is adopted from pages 138 - 198 in [3]. The development of an expansion wave can be explained in a similar way. Applying the same piston analogy, if the piston is moved towards the left with a small increment of  $dV$ , a weak expansion wave travels to the right through a gas. Gas behind the wave is set in motion to the left at velocity  $dV$  due to the piston movement. Due to the passage of the expansion wave, the pressure and temperature of the gas behind it decrease. When the piston is incremented a second time, another expansion wave passes and has a lower speed than the first one, since the gas through which it is traveling is at a lower pressure and temperature. Unlike compression waves, expansion waves and the gas travel in opposite directions. As each successive expansion wave has a velocity lower than the preceding one, successive expansion waves do not reinforce each other to form a single expansion wave (Figure 1.2).

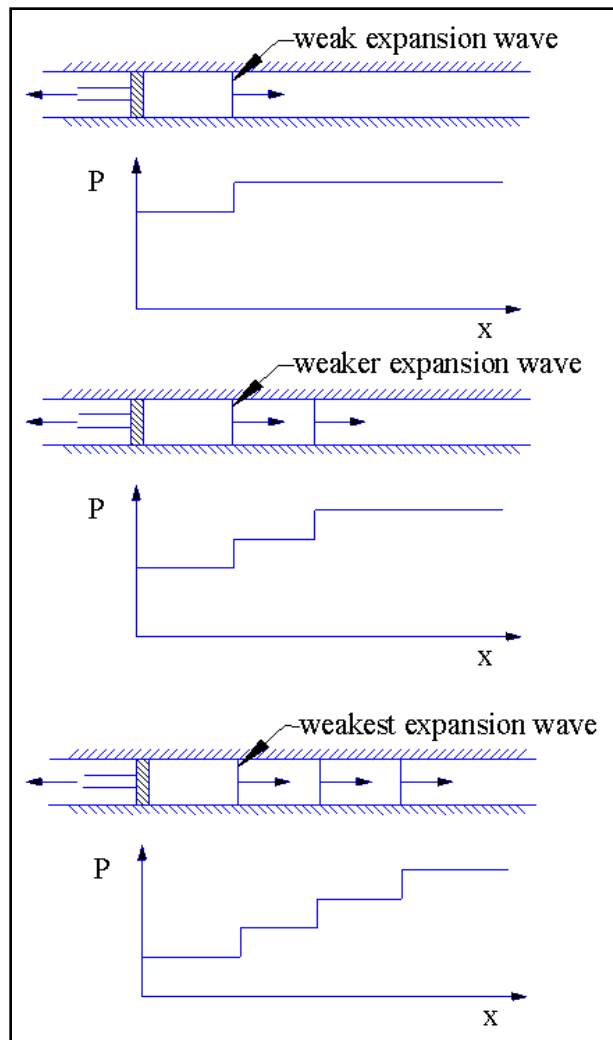


**Figure 1.2:** Expansion wave formation (diagram re-created from Saad [3], Fig. 4.4)

### 1.3.4 Blast wave

In an explosion, a wave system of both shock and expansion waves is generated. As the shock wave propagates into the surrounding space, expansion waves that propagate in the reverse direction reflect back from the origin of the explosion. These reflected waves, after a while, overtake the shock wave and slow it down. This degraded shock wave will be termed as a “blast wave” in this research, even though its characteristics are not very different from the incident shock. Around the origin of the

blast, reflected expansion waves create a zone of negative pressure, which is felt at the shock front very soon by means of the fluid molecules, and the flow is slowed down. This action degrades the shock wave to the blast wave. The complex wave pattern generated from an explosion can be approximated by the Friedlander wave [4], shown in Figure 1.3. The main characteristics of a blast wave are the peak pressure and positive and negative phase durations. Positive phase duration is the time over which the pressure is greater than the ambient pressure, while negative phase duration is the time over which the pressure is less than the ambient pressure.

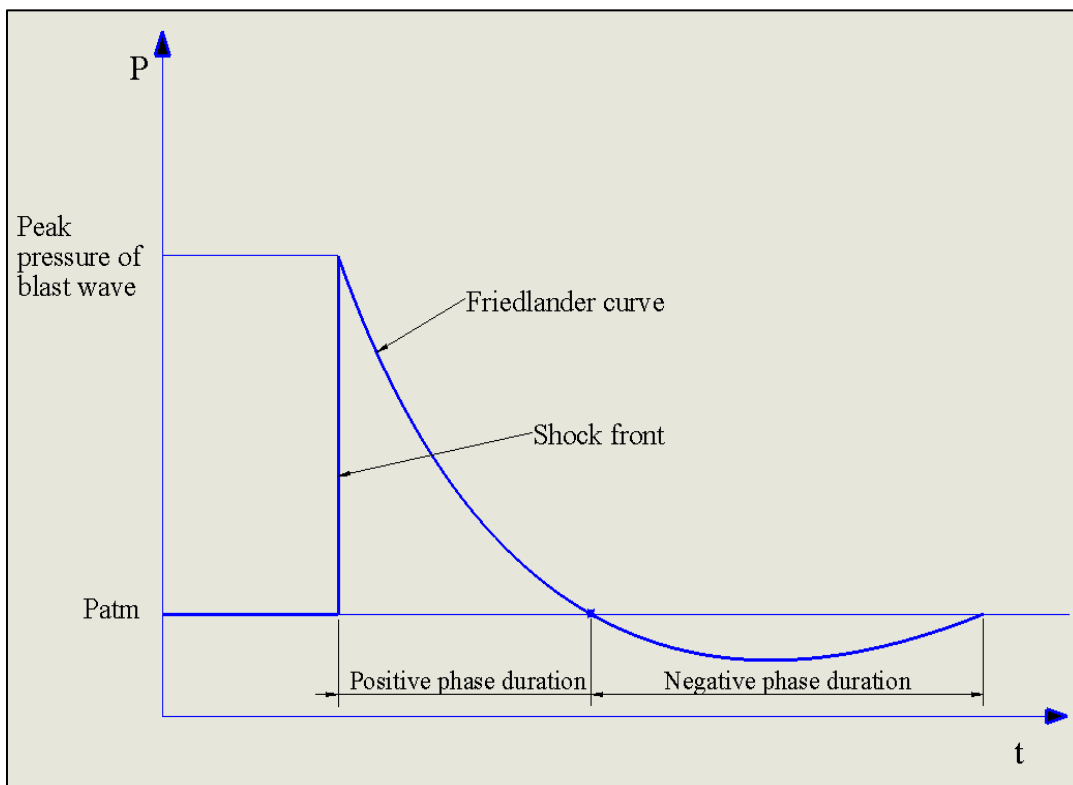


**Figure 1.3:** Friedlander, or ideal blast, wave

## 1.4 Shock tube

Shock tubes are commonly used to generate shock and blast waves in the laboratory. This section describes the operation of typical shock tubes and the approach used to generate blast waves using them.

### 1.4.1 Introduction

Compressed gas-driven shock tubes are a means to generate shock waves in the laboratory. The cross section can be circular or rectangular, depending on the application. It is closed at one end, while the other end can be kept open or closed depending upon the application. It is divided into high and low pressure regions by placing a diaphragm in between. The high pressure region is called the driver section and the low pressure region is called the driven section. The gas properties in these two regions can be the same or different. The length of the driven section ( $L_{dn}$ ) is usually greater than the length of the driver section ( $L_{dr}$ ). The ratio of the two is called the Length Ratio (LR; Equation 1.3) and is one of the most important parameters of the shock tube. The shock tube installed in our laboratory is closed at one end and open at the other, so the initial pressure in the driven section is atmospheric. Figure 1.4 shows the basic geometry of the shock tube.

$$LR = \frac{L_{dn}}{L_{dr}} \quad (1.3)$$

In order to generate a shock wave with a tube of this type, the driver section is pressurized. Under this pressure, the diaphragm deforms until it is ruptured by a blade placed at some minor distance from the diaphragm.

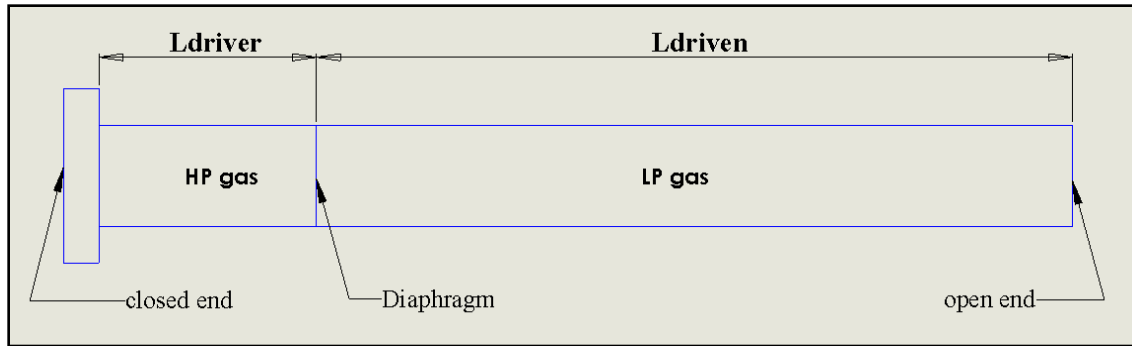


**Figure 1.4:** Theoretical shock tube geometry

Once the diaphragm ruptures, the high pressure gas suddenly comes into contact with the low pressure gas and generates a wave system of shock wave and expansion waves, as described in Section 1.3.

#### 1.4.2 Operation of shock tube

The description of the operation of the shock tube is adopted from pages 138 - 198 in [3]. The schematic diagram shown in Figure 1.5 is a shock tube separated in two sections of different pressures by means of a diaphragm. Region 4 is the driver section filled with high pressure gas. Region 1 is the driven section open to the atmosphere. Pressures in these regions are  $p_4$  and  $p_1$ , respectively, at time  $t = 0$ . At  $t = 0$ , the diaphragm is ruptured, and the high pressure gas comes in contact with the low pressure gas, initiating the formation of the shock and expansion waves. Successive compression waves rapidly coalesce to form a single constant shaped shock wave that travels at high speed, leaving the gas behind it in motion to the right at velocity  $V_2$ . According to the properties of the shock wave,  $p_2 > p_1$ ,  $T_2 > T_1$ , and  $\rho_2 > \rho_1$ . On the other side of the diaphragm (driver section), a series of expansion waves start traveling one behind the other in the

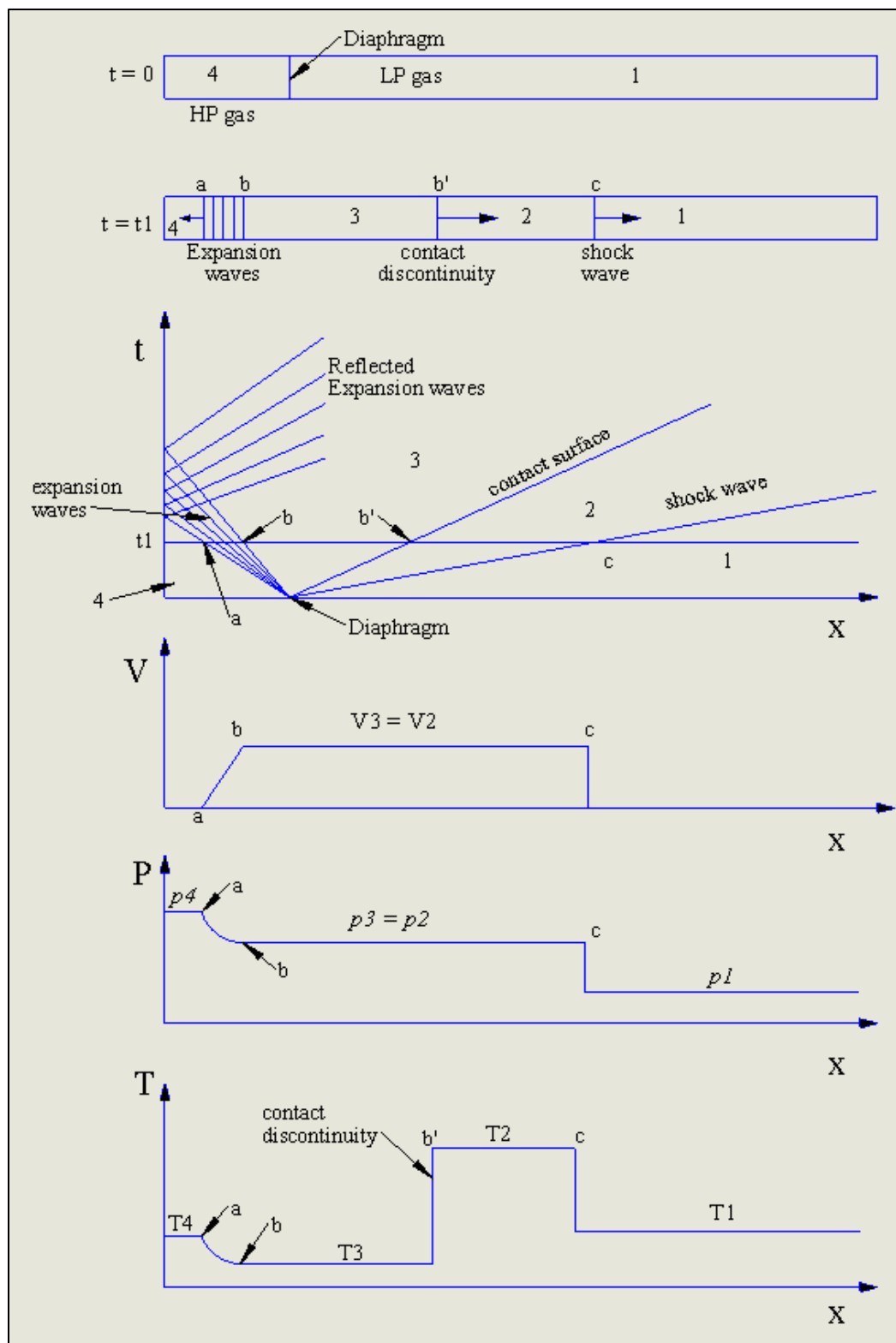


**Figure 1.5:** Operation of the shock tube (Diagram re-created from Compressible Fluid

Flow [3], Fig. 4.35)

direction opposite to that of the incident shock and reflect back from the wall. The leading expansion wave is shown to be traveling at a location “a” while the tail expansion wave is traveling at location “b.” The gas behind the tail expansion wave is set in motion to the right at velocity  $V_3 = V_2$ . Even though the shock and expansion waves move in opposite directions, the way they interact establishes the common pressure  $p_2 = p_3$  and the common velocity  $V_2 = V_3$ . The density and the temperature of the gases, though, differ in these regions, forming a surface of discontinuity, which moves to the right at velocity  $V_2$ . The physical properties described above are shown in Figure 1.5 at time  $t_1$ . As can be seen, the velocity and the pressure are constant in regions 2 and 3, but the temperature varies in these two regions. Temperature  $T_2$  is higher than temperature  $T_3$  because of the passage of the shock wave in region 2.

### 1.4.3 Strength of shock wave

The strength of shock is given by Equation 1.4 (pages 138 – 198 in [3]),

$$\frac{p_2}{p_1} = 1 + \frac{2\gamma_1}{\gamma_1 + 1} (M_s^2 - 1) \quad (1.4)$$

where  $\gamma_1$  is the specific heat ratio in Region 1 and  $M_s$  is the Mach number of an incident shock.

As Equation 1.4 shows, the strength of shock is independent of the lengths of the driver and the driven sections. It also represents the strength of a “pure” shock at one instant of time inside the shock tube. Equation 1.4 does not take into consideration the effect of the expansion wave.

#### 1.4.4 Blast wave in the shock tube

Section 1.4.3 illustrates how shock and expansion waves are formed inside a shock tube. Given a long enough tube, the reflected expansion waves shown in Figure 1.5 eventually overtake the shock front and degrade it down to a blast wave. This degradation principally means the reduction in the peak pressure and the velocity of the shock front. Figure 1.6 shows the difference between shock and blast waves as defined in this research. The blast wave is shown at the later time because it takes time for the expansion waves to reflect back and overtake the shock front.

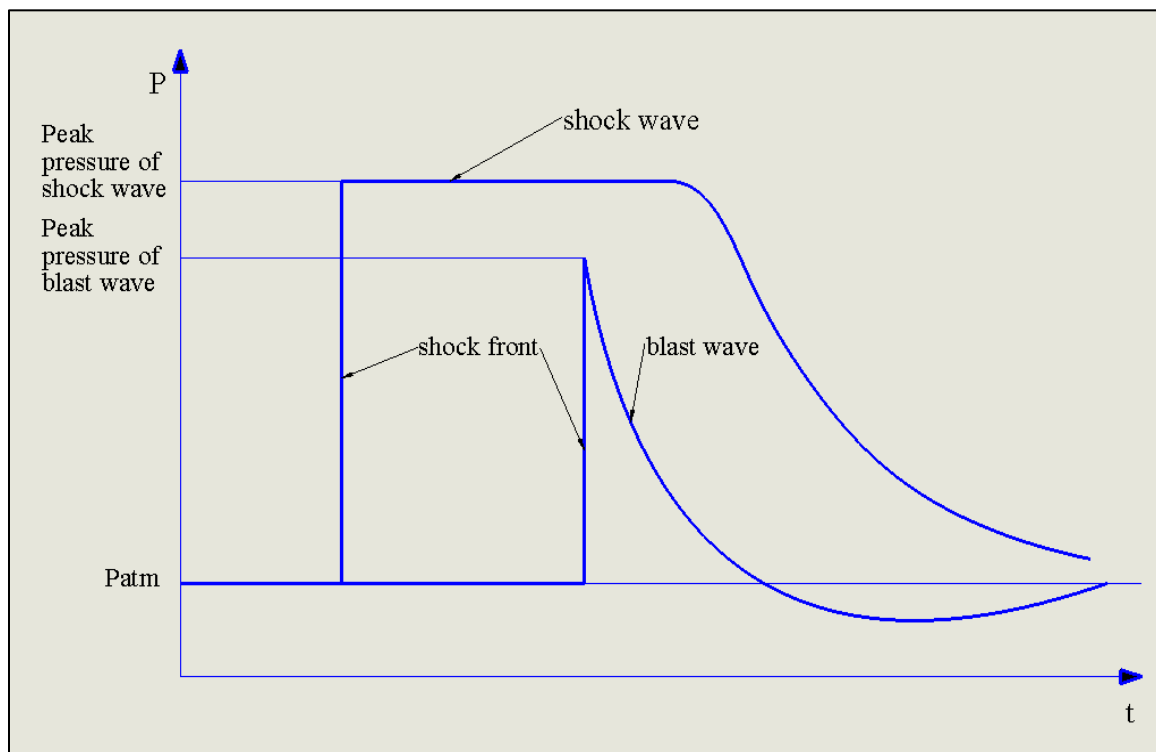


**Figure 1.6:** Comparison of shock wave and blast wave

## 1.5 Research objectives

There are two primary objectives of this research project: (1) definition of relationships between independent shock tube control variables and the resulting blast wave characteristics and (2) identification of a region appropriate for testing with the shock tube utilized in our laboratory.

### 1.5.1 Parameter study

Figure 1.7 shows the experimental shock tube in our laboratory, the design of which was completed at Florida Tech University. Use of this tube has been reported elsewhere [5]. The detailed dimensions of the tube are given in Chapter 3. The experimental shock tube shown in Figure 1.7 has variable driver section length ( $L_{dr}$ ) and a fixed driven section length. That implies the length ratio depends only on the driver section. The driven section of the tube is open to the atmosphere and the pressure in the driver section ( $P_{dr}$ ) can be regulated by a pressure regulator knob on the high pressure gas cylinder. The tube is designed to generate a shock that ultimately exits the driven section and expands to interact with a target. So, our tube has two independent variables, viz.  $P_{dr}$ ,  $L_{dr}$ , and three dependent variables of the blast wave, viz. peak pressure, positive phase duration, and negative phase duration. Therefore, the first objective of this research was to characterize the dependent variables of the blast wave as a function of the independent variables of the shock tube.

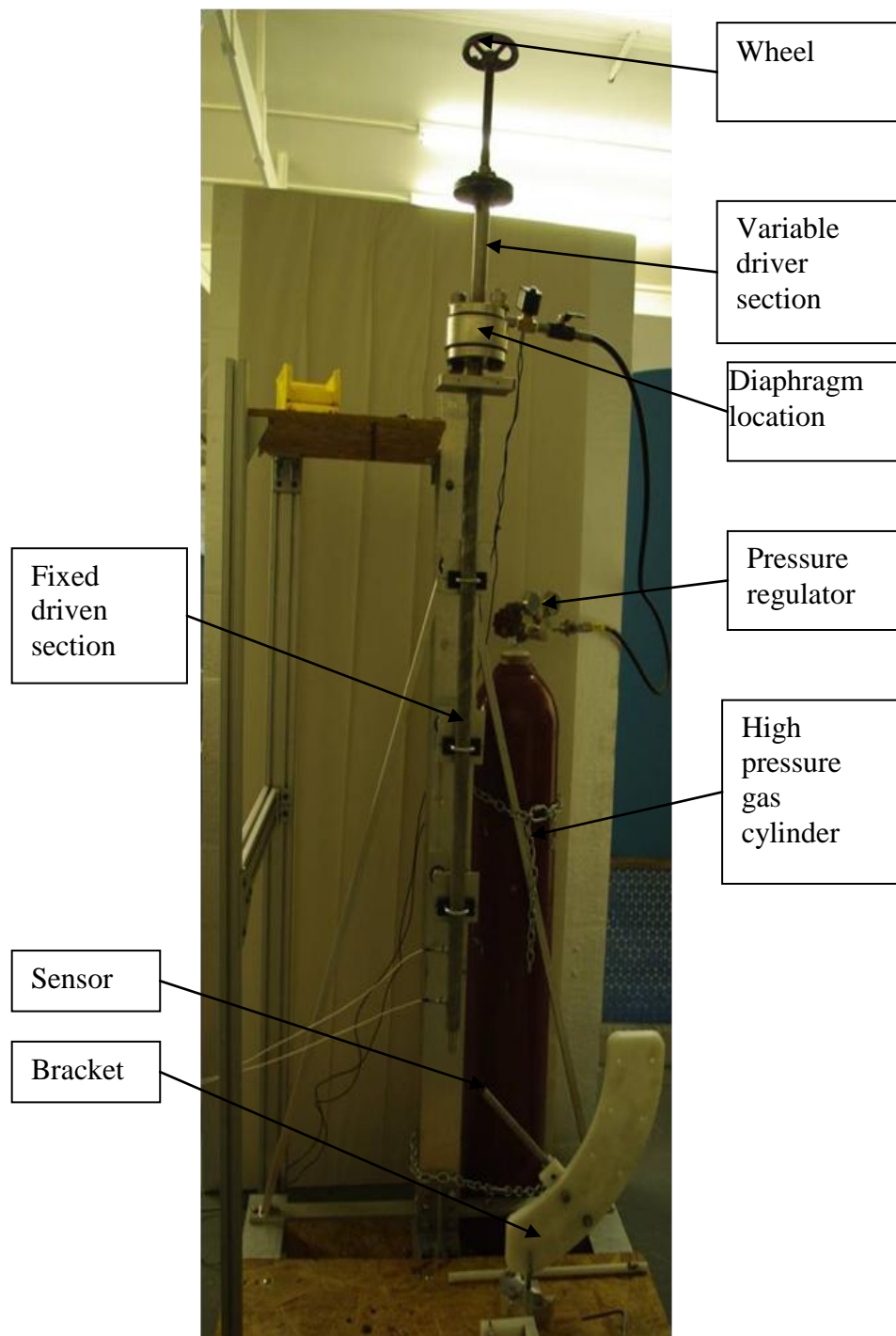


**Figure 1.7:** Experimental shock tube (courtesy Prof. Daniel Kirk, Florida Tech University)

### 1.5.2 Region for testing

In Figure 1.7, the sensor attached to the bracket is shown. The sensor is mounted not along the axis of the shock tube but, actually, off axis. The reason for that is first, the shock expands outside the tube axisymmetrically and then follows the jet of high pressure gases, which, also, expand outside the tube, conically. The primary injury is associated only with the blast wave and not the exhaust gas vent. Figure 1.8 shows the difference between the impact on the rat brain produced by the blast wave alone and the blast wave combined with the gas vent. Peak OP refers to the peak of the blast wave. From Figure 1.8, it seems that the impact due to the exhaust gas vent is significant and hence, isolating the target (rat) from the gas vent is important. Thus, the second objective of this research was to quantify the region for testing the samples (Figure 1.9).

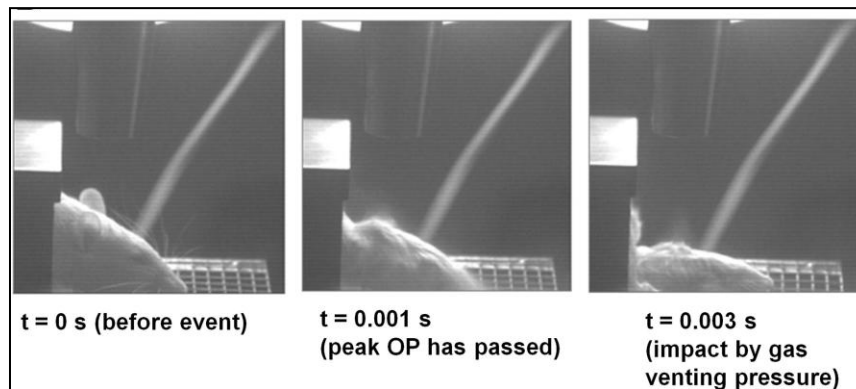


**Figure 1.8:** Rat head movement and deformation at different times; Peak OP refers to the peak of the blast wave. (Fig. 2(D) in [5])

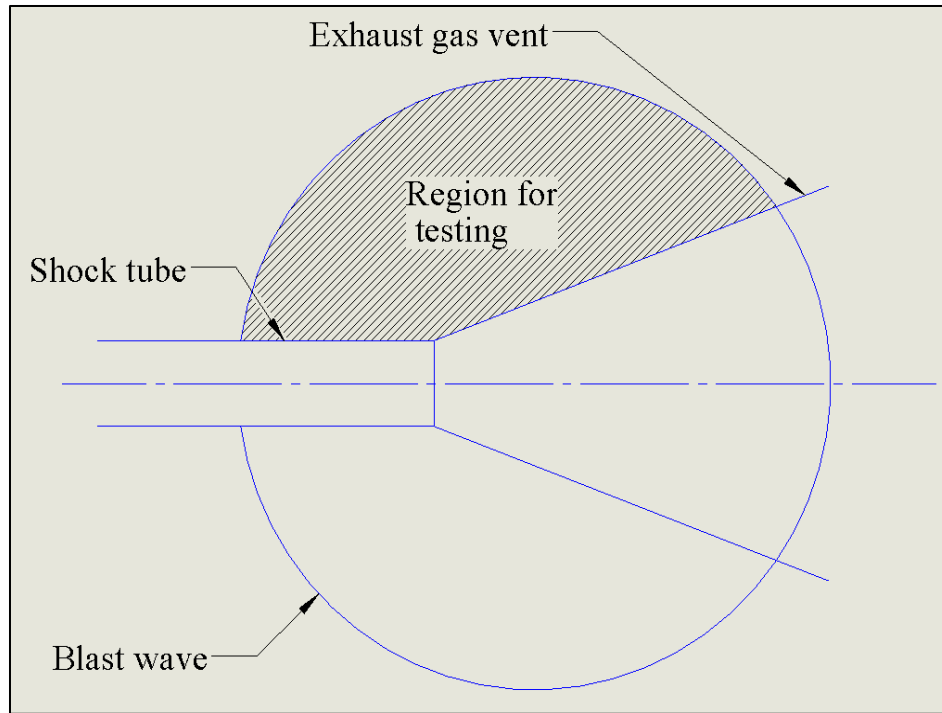


**Figure 1.9:** Region for testing

## 1.6 Numerical simulations

The objectives mentioned in the previous section can be pursued either with an experimental approach or a numerical approach. This thesis concentrates on the numerical approach. This section focuses on the theory of numerical simulations, followed by a description of the software used for this research. The section concludes with presentation of the governing equations used for the shock tube problem.

### 1.6.1 Introduction

Numerical simulations are a powerful companion to experimental testing. In contrast to experimental shock tubes, which require equipment like a high pressure tank, diaphragm rupturing mechanism, and sensors to record data, numerical simulations are

generally minimally expensive and allow considerable flexibility in exploring a large solution space of a given problem. Once the needed computer code is written, initial setup required to run numerical simulations simply requires an input file where the physical and geometrical parameters of the tube are specified, as opposed to the experimental setup, which includes diaphragm replacement, filling up gas in the driver section, etc. In experiments, data can be obtained only at limited locations where sensors are mounted. In numerical simulations, data can be recorded anywhere inside and outside the tube just by adding the probe points into the input file. For these reasons, a numerical model is an attractive approach for parameter studies.

While numerical simulations have many advantages, the speed of a simulation depends on the speed of the computer, the resolution used in the code, and the dimensionality of the problem. Three-dimensional simulations are computationally expensive and, unfortunately, many experimental systems, including the present shock tube, are naturally three-dimensional. Proper boundary conditions are also crucial and can be difficult to apply.

### **1.6.2 Theory of numerical simulation**

The physical laws of nature can be written in the form of mathematical equations, which are often in the form of differential and integral calculus [6]. Sometimes, the equations are so complex that they cannot be solved analytically. Hence, there are two popular approaches to solve the real world problems. The first is the experimental approach, which seeks to ascertain the physical laws through observation and experimentation, while the second is the numerical approach, which solves the equations governing a problem on the discrete number of points to obtain an approximate solution.

If the points are spaced more densely, the accuracy of the solution increases to a level that can be reasonably compared with physical reality. This point spacing has particular importance in numerical simulations under the concept of resolution.

In the case of studying dynamics of fluids, numerical simulations come under the description of Computational Fluid Dynamics (CFD). There are numerous different commercial CFD packages available, namely Fluent, OVERFLOW, CFL3D, and many more. The package used for this research is called Uintah.

### **1.6.3 Uintah**

“The Uintah Computational Framework consists of a set of software components and libraries that facilitate the solution of Partial Differential Equations (PDEs) on Structured Adaptive Mesh Refinement (AMR) grids using hundreds to thousands of processors” [7]. More information on AMR structure is given in Chapter 3. The University of Utah Center for Accidental Fires and Explosions (C-SAFE) group programmed Uintah [8]. Uintah can solve full physics simulations of dynamic fluid-structure interactions (FSI) involving large deformations and material transformations. A new application of the Uintah software is the shock tube problem described in this thesis. As the shock tube wall needs to be defined to restrict the flow inside it, the problem becomes the FSI problem with the assumption of no-wall-deformation. In Uintah, the method used for FSI is MPM-ICE. The Material Point Method (MPM) accounts for any structural behavior while the Implicit, Continuous-fluid, Eulerian (ICE) [9] method does the fluid analysis. MPM, originally developed by Sulsky [10, 11], is a particle method for structural mechanics simulations [8]. For this shock tube problem, the version of ICE utilized is a cell-centered, finite-volume, multimaterial, Eulerian method further

developed by Kashiwa and others at Los Alamos National Laboratory [12]. The governing multimaterial model equations are stated and described in the next subsection. The development of these equations can be found in [13].

#### 1.6.4 Governing equations

The governing equations used here are the multimaterial equations, in which each material is given a continuum description and defined over the complete computational domain [7, 8]. Multimaterial equations are used to determine the probability of finding a particular material at any location in space, together with its state (i.e. mass, momentum, energy). For a collection of  $N$  materials, the subscript  $r$  signifies one type of materials (for example, fluids), such that  $r = 1, 2, 3, \dots, N$ . The  $r$ -material average density in volume  $v$  is given as  $\rho_r = M_r/v$ .  $M_r$  is the mass of material  $r$  in the volume  $v$ .  $v$  can be thought of as a computational cell. The rate of change of the state in a volume moving with the velocity of  $r$ -material is given by the following equations.

$$\frac{1}{v} \frac{D_r M_r}{Dt} = \Gamma_r \quad (1.5)$$

$$\frac{1}{v} \frac{D_r (M_r u_r)}{Dt} = \theta_r \nabla \cdot \sigma + \nabla \cdot \theta_r (\sigma_r - \sigma) + \rho_r g + \sum_{s=1}^N f_{rs} + \sum_{s=1}^N u_{rs} \Gamma_{rs} \quad (1.6)$$

$$\frac{1}{v} \frac{D_r (M_r e_r)}{Dt} = -\rho_r p \frac{D_r \vartheta_r}{Dt} + \theta_r \tau_r : \nabla u_r - \nabla \cdot \theta_r q_r + \sum_{s=1}^N h_{rs} + \sum_{s=1}^N (e + p\vartheta)_{rs} \Gamma_{rs} \quad (1.7)$$

$\Gamma_r$  is the rate at which r-material mass is converted or depleted from the volume due to the conversions from other materials, typically by a chemical reaction.  $\Gamma_{rs}$  is the rate of conversion of mass between the r-material to another s-material. In the shock tube problem described earlier, there is no conversion of mass due to any chemical reaction or between the two materials. Hence, the terms containing  $\Gamma$  are eliminated.  $u_r$ ,  $\theta_r$ ,  $\sigma_r$ ,  $e_r$ , and  $\rho_r$  refer to the r-material velocity, volume fraction, stress, internal energy, and density, respectively.  $\sigma$  is the mean mixture stress,  $\tau_r$  is the deviatoric part of the material stress  $\sigma_r$ , and  $q_r$  is the heat flux. In this research, body forces, viscous forces, and heat flux are neglected, so the terms containing  $g$ ,  $\tau$ , and  $q$  are eliminated from the above equations.  $h_{sr}$  and  $f_{rs}$  represent the exchange of heat and momentum between r and s materials, respectively.  $\vartheta_r$  is the specific volume of the r-material. After eliminating the terms mentioned above, the governing equations for the shock tube problem are as follows.

$$\frac{1}{v} \frac{D_r M_r}{Dt} = 0 \quad (1.8)$$

$$\frac{1}{v} \frac{D_r (M_r u_r)}{Dt} = \theta_r \nabla \cdot \sigma + \nabla \cdot \theta_r (\sigma_r - \sigma) + \sum_{s=1}^N f_{rs} \quad (1.9)$$

$$\frac{1}{v} \frac{D_r (M_r e_r)}{Dt} = -\rho_r p \frac{D_r \vartheta_r}{Dt} + \sum_{s=1}^N h_{rs} \quad (1.10)$$

Equations 1.8, 1.9, and 1.10 are the conservation equations for mass, momentum, and energy for a multimaterial problem, respectively. In the problems pertaining to this research, material  $r$  is gas (air or nitrogen) and material  $s$  is the shock tube wall.

These three equations, along with the equations of state [14], are solved to determine density, pressure, and velocity in three directions, along with internal energy and temperature. Each of these variables is solved within each cell as a function of time. The generated data is then analyzed using different visualization tools and combinations of different scripts, which mainly include C-Shell scripting, GNUplot scripting, and Octave scripting.

## **1.7 Introduction of upcoming chapters**

The research described in this thesis was carried out mostly in one and two dimensions. Chapter 2 discusses the 1D solution to the shock tube problem. The objective of Chapter 2 is mainly to analyze the flow of compressed high pressure gases inside the tube. Chapter 3 discusses the 2D approximation to the shock tube problem. The objective of Chapter 3 is to analyze the pressure wave and the compressed high pressure gases after they exit the tube. Chapter 4 briefly discusses the 3D simulation and its comparison to 2D. Chapter 5 summarizes the overall findings and conclusions, and presents recommendations for future work.

## **2 ONE-DIMENSIONAL SOLUTION**

### **2.1 Introduction**

In the current experimental design, the target is exposed to a blast wave outside the shock tube. When the shock exits the tube, it expands axisymmetrically about the axis of the tube. However, inside the tube, all phenomena are one-dimensional, so a 1D model is sufficient. A 1D approach is used for this portion of the problem because it is relatively easy to run and requires less storage space and computer memory. This chapter principally covers the objective (Section 2.2), geometry, and input parameters of the 1D simulation (Section 2.3); followed by the governing equations (Section 2.4), resolution study (Section 2.5), and the validation of the numerical code (Section 2.6). Finally, results are discussed along with numerical errors in the simulation (Section 2.8).

### **2.2 Objective of the 1D simulations**

Although the ultimate goal of this research is to study the wave formation outside the tube, the blast wave characteristics inside the tube are studied using 1D simulations. 1D simulations are computationally less expensive and easier to run than a full problem. Therefore, the objective of 1D simulation is to understand the influence of the independent variables on the blast wave characteristics inside the tube.

### 2.3 Defining geometry and input parameters

A 1D shock tube can be represented as a line divided into two segments of initially different pressures. The lengths of the high pressure region and the low pressure region are denoted by  $L_{dr}$  and  $L_{dn}$ , respectively. The total length is denoted by  $L$  (see Figure 2.1). The gas in both regions is air. Table 2.1 gives a listing of parameters utilized in the simulation, including some that relate to the air. The initial pressure in the driver and the driven section is calculated by Equation 2.1:

$$p = \rho C_v T (\gamma - 1) \quad (2.1)$$

Some explanation is necessary for the last two parameters of Table 2.1, order of method and CFL number. Any partial derivative term can be expanded using Taylor's series. The order of method, or order of accuracy, is determined by the number of terms of the Taylor's series that are employed in the code.

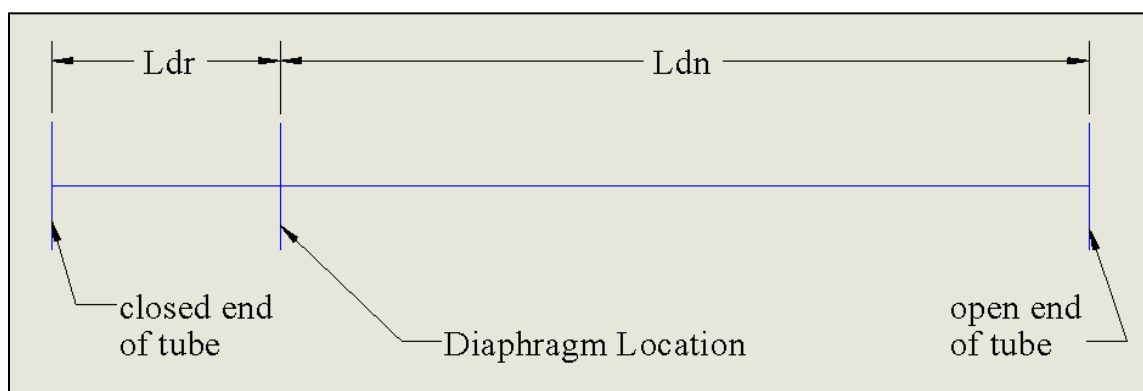


**Figure 2.1:** Geometry of 1D shock tube simulation

**Table 2.1:** The list of initial parameters to be declared in an input file

<b>Geometrical parameters</b>	<b>Units</b>
$L_{dr}$	m
$L_{dn}$	m
LR (length ratio)	-
<b>Physical parameters</b>	
Air Density ( $\rho$ )	kg/m <sup>3</sup>
Air Temperature (T)	K
Air Specific heat ( $C_v$ )	J/kg-K
Air Specific heat ratio ( $\gamma$ )	-
<b>Other parameters</b>	
Resolution (spacing between each cell)	mm
Physical time of the simulation (t)	sec
Order of method	-
CFL number	-

Accuracy increases with the number of terms used. Governing Equations 1.8 – 1.10 are in the form of partial derivatives with respect to time and space. In MPM, ICE, and MPM-ICE, partial derivatives with respect to time always have the first order of method, while partial derivatives with respect to space can have first or pseudo second order of method. Pseudo second order means that order of method will be second for the continuous part of the numerical solution, but at discontinuities like a shock, the partial derivatives of the advection terms with respect to space change to the first order of method. The reason for

this is that the second order of method induces a larger error at the discontinuities than the first order. In this thesis, the “pseudo second order of method” is referred just as the “second order of method” for simplicity.

In mathematics, while solving certain PDEs, the Courant–Friedrichs–Lewy (CFL) condition is necessary for the stability of the numerical solution [15]. As has been mentioned, in CFD, the domain is discretized into small cells. Let the length of each cell be  $\Delta x$  and the size of each timestep be  $\Delta t$ . Now, if the sound wave propagates through the fluid at velocity  $V$  in the cell, then for numerical stability, the time for the sound wave to travel the distance  $\Delta x$  should be greater than  $\Delta t$ , as given by Equation 2.2.

$$\Delta t \leq \frac{\Delta x}{(V + c)} \quad (2.2)$$

$$C = (V + c) \frac{\Delta t}{\Delta x} \leq 1 \quad (2.3)$$

Equation 2.3 is the CFL condition, where  $C$  is called the Courant number. The Courant number is represented by CFL in the input file.

## 2.4 Governing equations

There is no shock tube wall in the 1D shock tube model. Hence, the terms modeling momentum and thermal exchange between the solid and gas in Equations 1.8 - 1.10 are eliminated. So, the value of  $\theta$ , becomes 1. Equations 2.4 – 2.6 are the simplified set of equations solved for the 1D shock tube problem.

$$\frac{1}{v} \frac{D_r M_r}{Dt} = 0 \quad (2.4)$$

$$\frac{1}{v} \frac{D_r (M_r u_r)}{Dt} = \nabla \cdot \sigma \quad (2.5)$$

$$\frac{1}{v} \frac{D_r (M_r e_r)}{Dt} = -\rho_r p \frac{D_r \vartheta_r}{Dt} \quad (2.6)$$

## 2.5 Resolution study

The concept of resolution was introduced in Chapter 1. Higher resolution results in greater accuracy if the numerical scheme is convergent. Before validating the numerical code against the exact solution, it is necessary to test the convergence of the solution through a resolution study. Table 2.2 represents the set of initial values used for the resolution study. Of the parameters displayed in Table 2.2, the density and temperature in both high and low pressure regions remain the same for most of the simulations. Also, the specific heat ratio remains the same. In similar subsequent tables, only parameters that differ from those in Table 2.2 are displayed.

Resolution is defined as the length of the domain divided by the number of cells. But as the length of the domain is variable in this research, the resolution is expressed as the size of the cells. The resolution study was carried out evaluating the pressure versus time behavior at a distance of 0.35 m from the rear of the driver section. Figure 2.2 shows solutions at different resolutions. Results show that pressure profiles with cell spacing of 1.25 mm and 0.625 mm are nearly equivalent. Thus, the cell spacing of 1.25 mm was chosen for further study.

**Table 2.2:** Initial parameter declaration for resolution study

<b>Parameters</b>	<b>Values</b>	<b>Units</b>
$L_{dr}$	0.1	m
$L_{dn}$	0.9	m
LR	9	-
Resolution (spacing between each cell)	variable	mm
Density in HP region ( $\rho$ )	11.76	kg/m <sup>3</sup>
Density in LP region ( $\rho$ )	1.176	kg/m <sup>3</sup>
Temperature in HP region (T)	300	K
Temperature in LP region (T)	300	K
Specific heat ( $C_v$ )	716.4	J/kg-K
Specific heat ratio ( $\gamma$ )	1.4	-
Physical time of the simulation (t)	0.002	sec
Order of method	First	-
CFL	0.45	-

## **2.6 Validation of the numerical code**

### **2.6.1 Description of exact solution**

The exact solution used here is the Riemann problem for the 1D case, wherein the time dependent Euler's equations are solved for the ideal gas. The Riemann problem consists of a conservation law together with piecewise constant data having a single discontinuity, like a shock. The Riemann problem solved here is the one-dimensional shock tube problem. More details on the exact analytical solution can be found in the Toro's book [16].

### **2.6.2 Comparison of simulated results with the exact solution**

Boundary conditions applied to the Riemann problem are not discussed here because the simulation is terminated before the waves reach the boundary, thereby removing the effects of boundary conditions on the solution. A similar approach is used in the numerical simulation, where the physical time of the simulation is short enough to prevent the waves from reaching the boundaries. The shock and expansion waves propagate in opposite directions, so a length ratio of 1.0 was chosen, which divides the total length of the tube into high and low pressure regions equally. Table 2.3 shows the initial parameters declared in the simulation. Figure 2.3 compares the exact solution against the numerical solution. Figure 2.3 shows that using a second order method, the simulated results reasonably match with the exact solution for the length ratio of one.

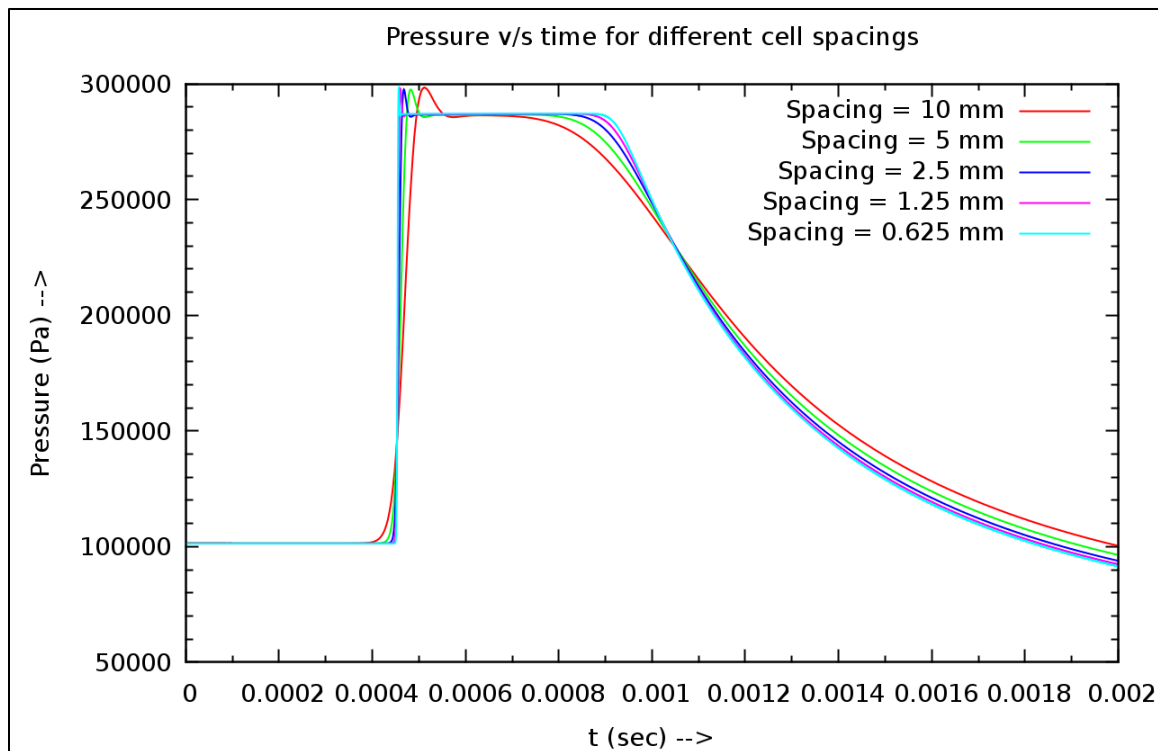


**Figure 2.2:** Pressure versus time for different cell spacing

**Table 2.3:** Parameter declaration for the validation study

Parameters	Values	Units
$L_{dr}$	0.5	m
$L_{dn}$	0.5	m
LR	1	-
Resolution (spacing between each cell)	1.25	mm
Specific heat ( $C_v$ )	716.4	J/kg-K
Physical time of the simulation (t)	0.002	sec
Order of method	second	-
CFL	0.45	-

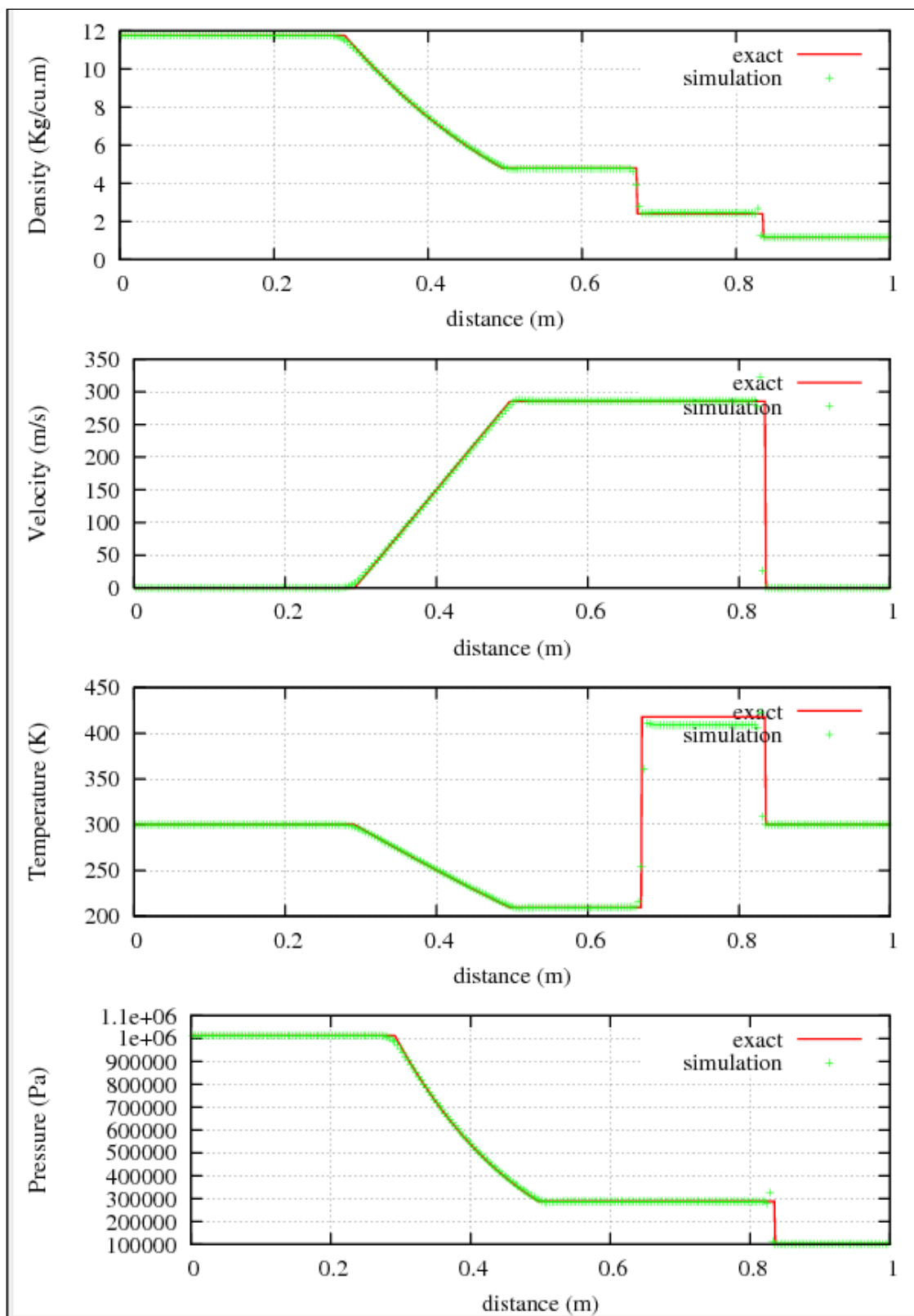


**Figure 2.3:** Comparison of the simulated results and the exact solution ( $t = 0.0006$  sec)

## 2.7 Data processing

Every shock tube problem pertaining to this research starts with the sudden exposure of the high pressure region to the low pressure region. The simulation, then, is allowed to run for a certain amount of time. The solver calculates the values of pressure, temperature, density, and velocity at every probe point specified in an input file at every timestep. An example input file of the shock tube problem is shown in Appendix A.3. Instead of recording the data at every single timestep, data are rather recorded at every few timesteps, the frequency of which can be adjusted in the input file. The data-file consists of the values of pressure, velocity, density, temperature, and spatial location at all specified times. The pressure profile against the time can be plotted directly from these files using GNUplot scripts. The values for peak pressure, positive phase duration, and negative phase duration are calculated from the same data files using Octave and C-shell scripting. The Octave script is called in the C-shell script. The C-shell script browses through each data file while the Octave script performs the operations on that file to calculate peak pressure and positive and negative phase duration. Examples of the C-shell and Octave scripts can be found in Appendix A.3.

## 2.8 Parameter study

The ultimate purpose of the 1D shock tube simulation is to characterize the pressure wave inside the tube as a function of tube geometry and initial air properties. Among the four input physical parameters, only driver pressure is variable; all others are fixed. The variable geometrical input parameters are  $L_{dr}$  and  $L_{dn}$ . The experimental shock tube that is being used for this research is made with only  $L_{dr}$  as a variable geometric

parameter. As a result, the 1D shock tube was characterized using two input variables,  $P_{dr}$  and  $L_{dr}$ . Validation of the numerical code was carried out before the waves reached the boundaries. Once a boundary is reached, the defined boundary conditions begin influencing the results. Three possible boundary conditions were explored, but in the end, none of them could accurately replicate the environment of the open end tube. A detailed description of the study on boundary conditions is presented in Appendix A.1. The length of the tube chosen for the parameter study is 5 m. The length ratio refers to the ratio of the distance between any chosen point in the driven section of the tube and the diaphragm to the  $L_{dr}$ . The reason for choosing a long tube is to eliminate the influence of the boundary conditions at the open end. Using this approach, a shorter tube could be chosen, still stopping the simulation before the wave reaches the boundary, but then the negative phase duration that occurs at later times cannot be studied.

### **2.8.1 Variation of $P_{dr}$**

In the experimental shock tube, the driver pressure most commonly used is approximately 700 psi. Hence, a driver pressure range of 600 to 900 psi (4830 to 6205 kPa), with an increment of 50 psi (344.7 kPa), was chosen for the simulations. In the presented plots, the driver pressure values are expressed in kPa. Table 2.4 gives the input conditions. As was mentioned in Section 2.3, pressure is not entered into the input file but is calculated by the code using Equation 2.1. So, in Table 2.4, density in the HP region is the variable parameter. The data is collected at 0.5 m from the driver section end of the tube. Figure 2.4 plots peak pressure against driver pressure and shows that the peak pressure increases with driver pressure in an approximately linear fashion.

**Table 2.4:** Input parameters for the study of driver pressure variation

Parameters	Values	Units
$L_{dr}$	0.1	m
$L_{dn}$	5	m
LR	13.15	-
Resolution (spacing between each cell)	1.25	mm
Density in HP region ( $\rho$ )	variable	kg/m <sup>3</sup>
Specific heat ( $C_v$ )	743	J/kg-K
Specific heat ratio ( $\gamma$ )	1.4	-
Physical time of the simulation (t)	0.003	sec
Order of method	First	-
CFL	0.45	-

Figure 2.5 shows the plot of positive phase duration against the driver pressure. The relationship between the two is nonintuitive. It starts with a linear increase of positive phase duration but then the slope of the line abruptly changes. To investigate this further, the pressure-time relationship was considered (Figure 2.6). From Figure 2.6 it is still not clear what is causing this difference as the pressure profiles look almost the same. It is clear, however, that differences in positive phase durations between the pressure profiles are very small. The positive impulse generated by these profiles is more or less the same. However, it is still not clear why positive phase duration varies bilinearly with driver pressure; this should be further investigated in the future.

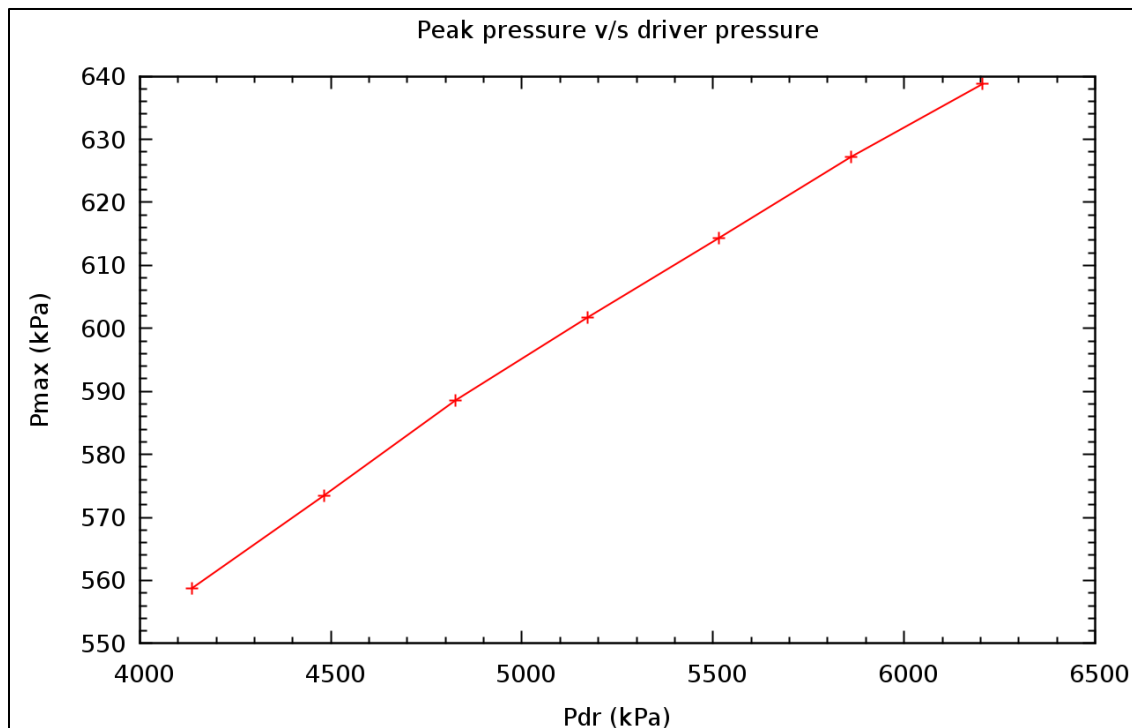


**Figure 2.4:** Peak pressure versus driver pressure

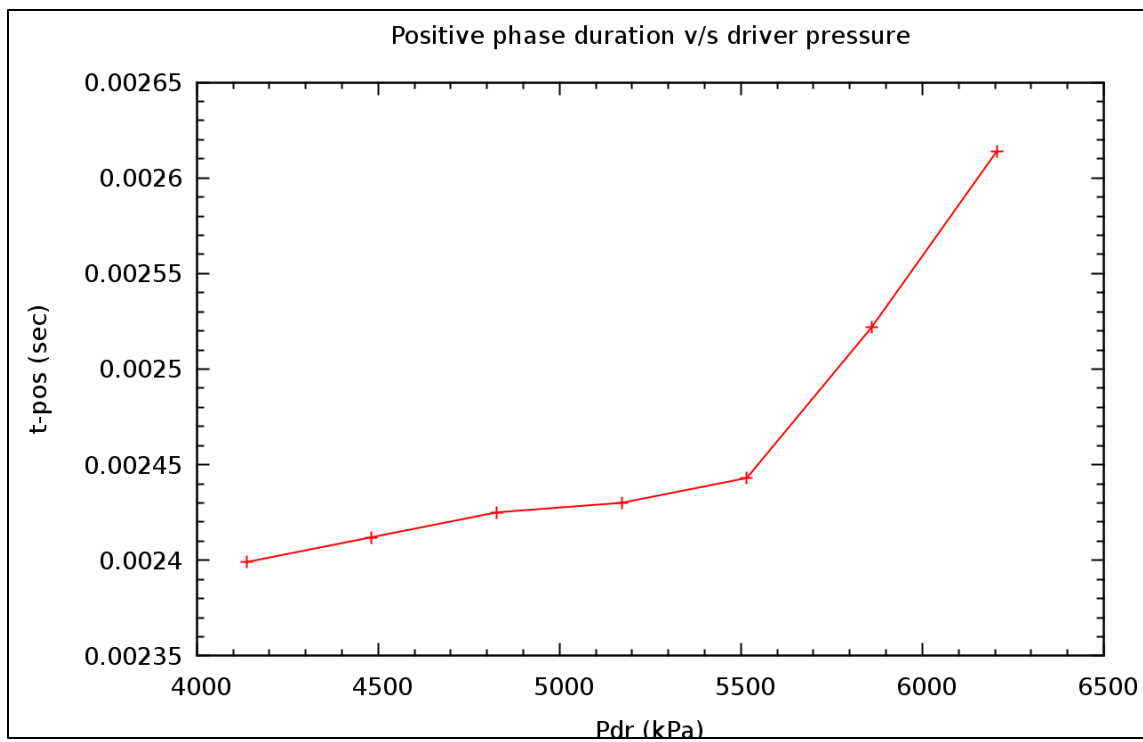


**Figure 2.5:** Positive phase duration versus driver pressure

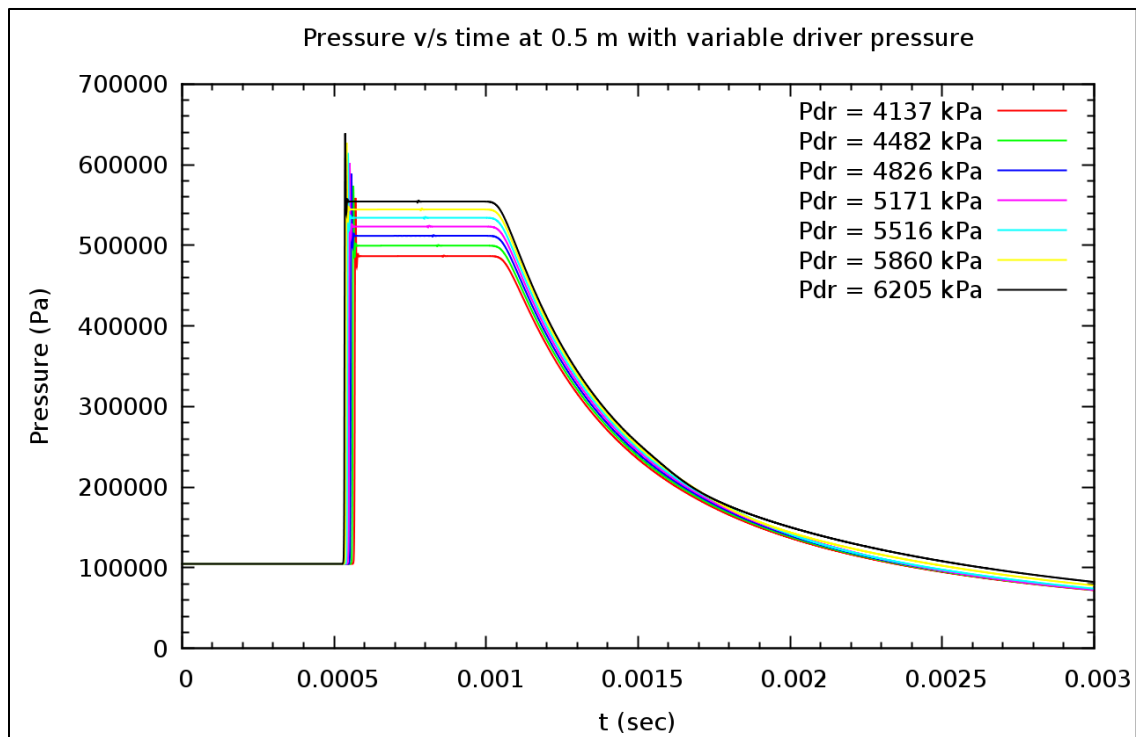


**Figure 2.6:** Pressure versus time at different driver pressures

Another point of interest in Figure 2.6 is that shock waves resulting from higher driver pressures travel with higher velocities. The shock wave in the case of 900 psi (6205 kPa) driver pressure arrives at the 0.5 m location earliest.

Figure 2.7 shows the plot of negative phase duration against the driver pressure. Similar to the positive phase duration, the trend here is also bi-linear. The only difference is that negative phase duration decreases with driver pressure. The reason for this behavior is similarly unclear.

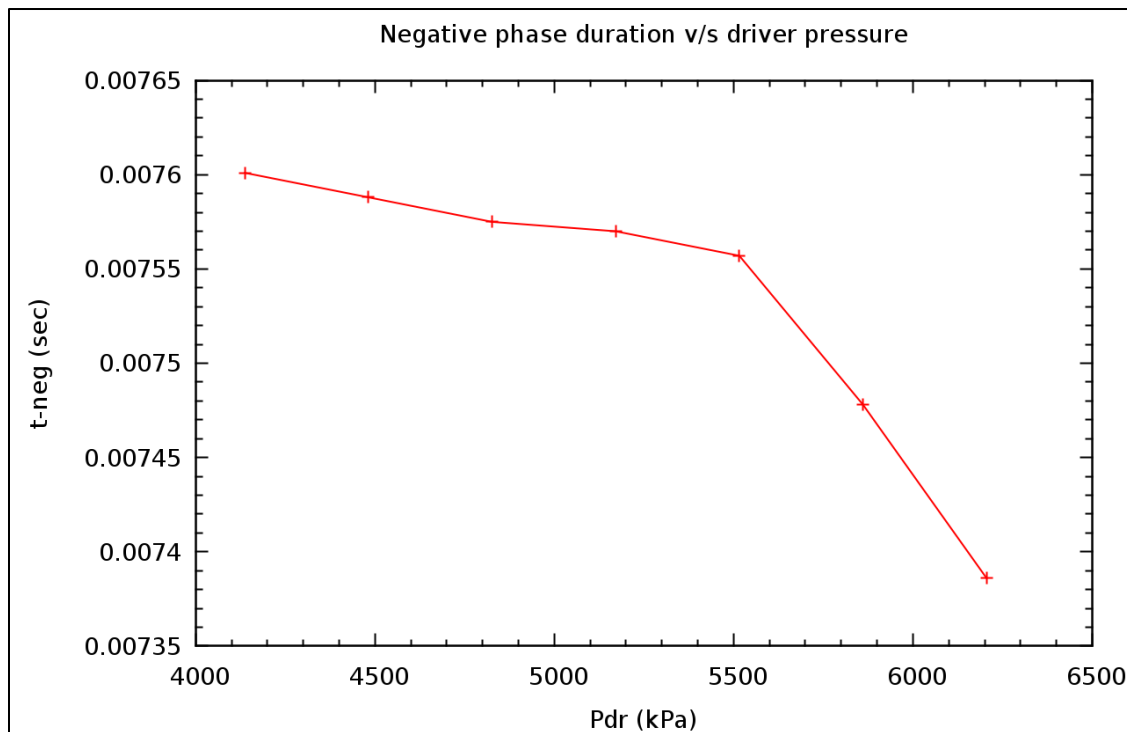


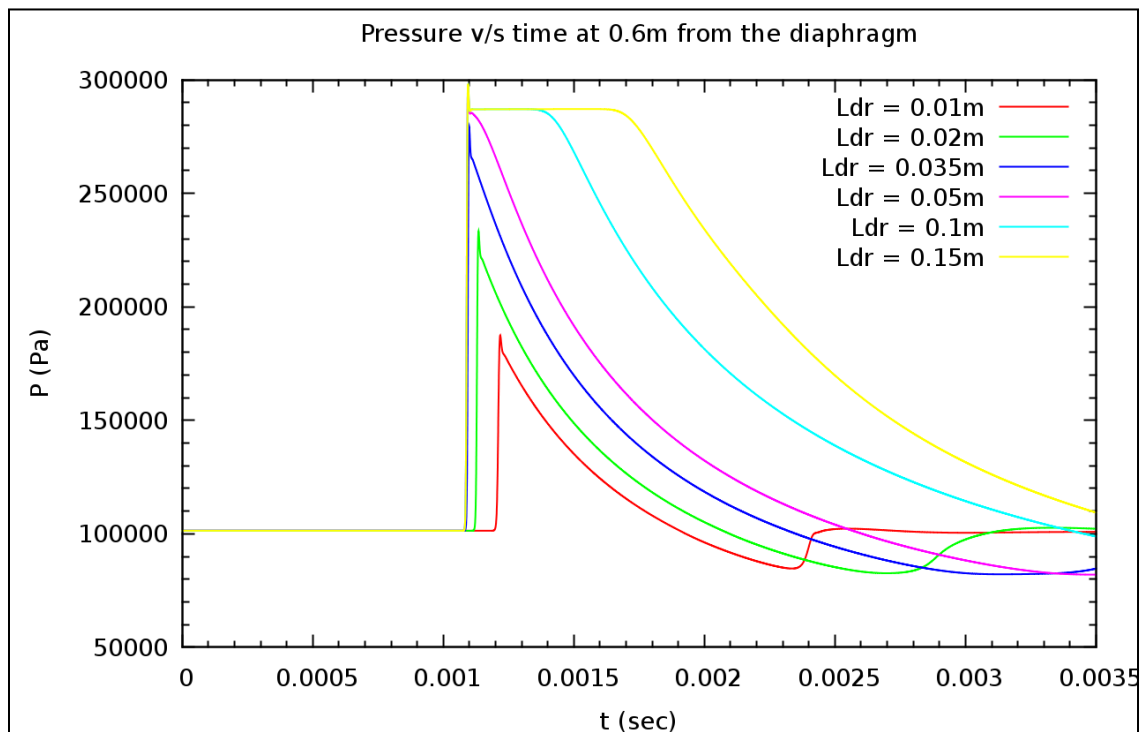
**Figure 2.7:** Negative phase duration versus driver pressure

### 2.8.2 Variation of $L_{dr}$

By changing only the driver section length, while keeping the total length of the tube constant, the difference in the pressure profiles of the shock wave due to the change in  $L_{dr}$  can be visualized. Table 2.5 indicates the input conditions. The study was carried out for the Driver length of 0.01, 0.02, 0.035, 0.05, 0.1, and 0.15 m. The first investigated characteristic of the shock wave is the peak pressure,  $P_{max}$ . Figure 2.8 shows the pressure profiles at different Driver length, and the probe point chosen is 0.6 m from the diaphragm. It can be observed from Figure 2.8 that peak pressure goes on increasing until it attains the approximate value of 298 kPa and then remains constant with additional increases in driver length.

**Table 2.5:** Input parameter declaration for studying the driver length variation

Parameters	Values	Units
$L_{dr}$	variable	m
Total length L	5	m
LR	variable	-
Resolution (spacing between each cell)	1.25	mm
Specific heat ( $C_v$ )	743	J/kg-K
Physical time of the simulation (t)	0.01	sec
Order of method	First	-
CFL	0.25	-

**Figure 2.8:** Pressure profiles for different driver lengths

The figure also shows that the shock waves with lower peaks rise at a later time than the ones that have attained the pressure of 298 kPa. In Equation 1.4, it was observed that the peak pressure is independent of the geometry of the tube, so these results were unexpected and prompted further investigation of possible sources of error in the code.

### **2.8.3 Numerical errors**

Study of potential numerical errors in the code was motivated by the parameter study. This section covers the classification of the numerical errors followed by the method used for analyzing them.

#### **2.8.3.1 The classification of errors**

Figure 2.9 illustrates the classification of the numerical errors. The governing equations used in this code are MPM-ICE equations [8], which have been previously used to solve the shock tube problem, so we can safely neglect the possibility of error caused by the governing equations. Boundary conditions are applied on the inlet and outlet of the shock tube. Applied inlet boundary conditions are appropriate for this study as explained in Appendix A.1. Outlet boundary conditions do not influence the solution until the shock wave reaches the end of the tube; this error study considers only the times before the shock wave reaches the outlet boundary.

Out of the numerical errors shown in Figure 2.9, the three main sources of error occurring in Uintah computational framework are the error due to the spatial resolution, temporal resolution, and order of method. The temporal resolution in the code is governed by the CFL number. The lower the CFL number, the higher the temporal

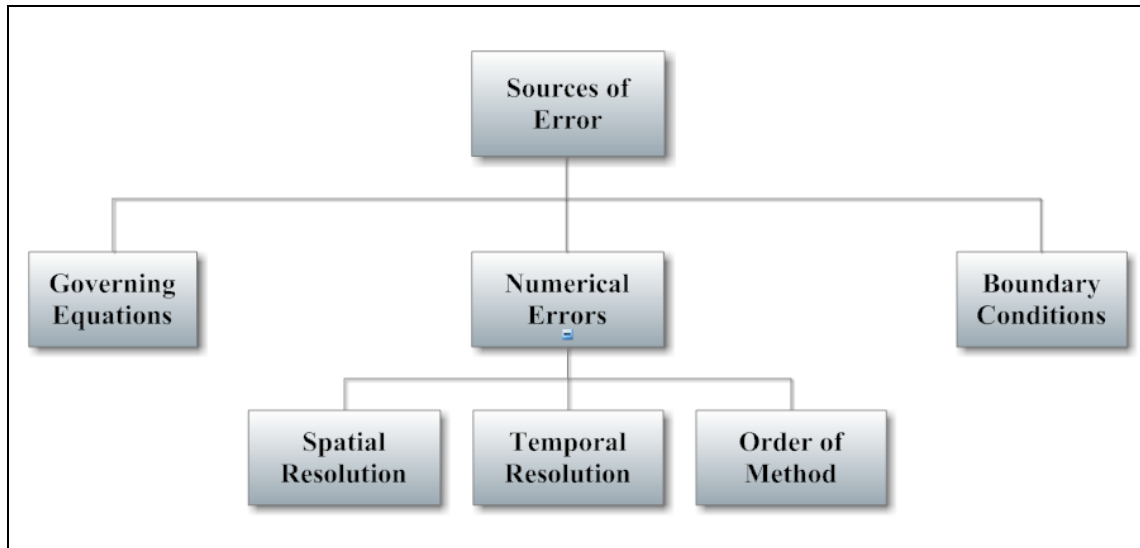


**Figure 2.9:** Flowchart of possible errors in the numerical code

resolution. The error caused due to the order of method is more predominant at peaks or discontinuities in the pressure profile.

Thus, spatial resolution, temporal resolution, and the order of method were chosen for the error analysis study. The selected values for spatial resolution were 5 mm, 2.5 mm, 1.25 mm, and 0.75 mm. For temporal resolution, the selected values for the CFL number were 0.45, 0.25, 0.15, and 0.08, and the orders of method used were first and second. A total tube length of 2.5 m and a LR of 2.4 were chosen for the analysis. The reason for choosing such a large LR was to allow reflected expansion waves to overtake the shock wave. The physical time of each simulation was 0.003 sec. To begin with, resolution, CFL, and order were chosen as indicated in Figure 2.10.

Figure 2.10 shows the progress of the shock wave down the tube at different snapshots in time. The time interval between two successive snapshots is equal. It is clear that after approximately 1.5 m, the peak pressure starts decreasing.

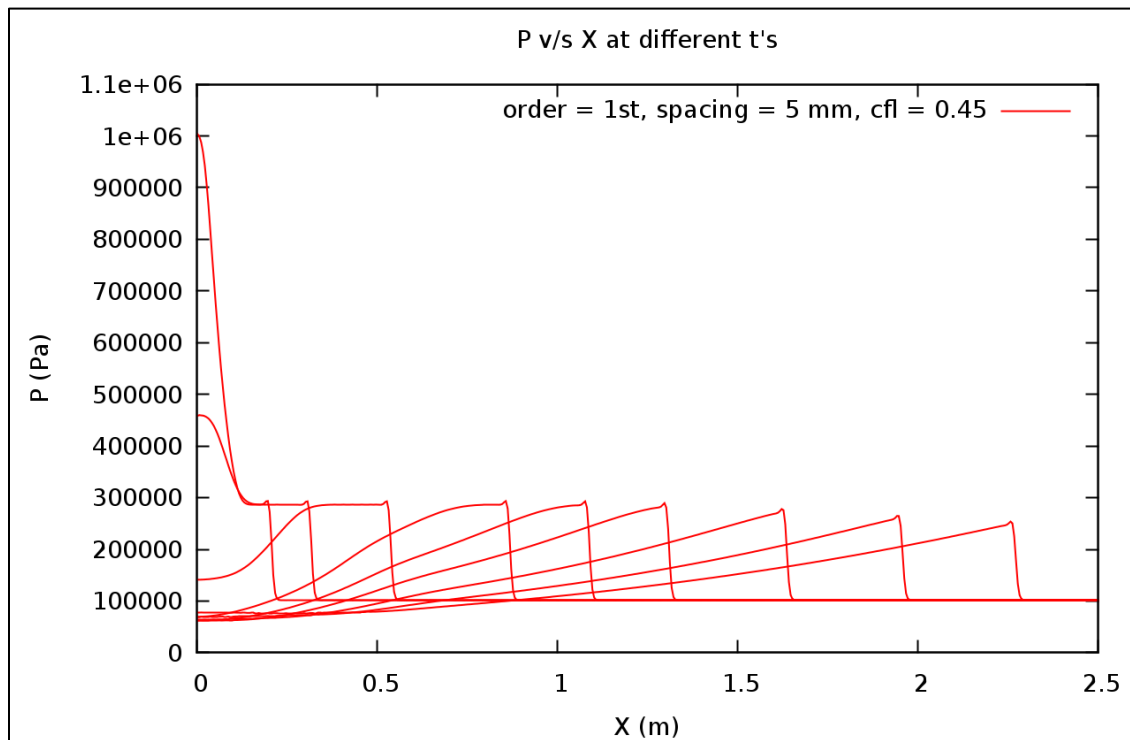


**Figure 2.10:** Pressure versus distance at different times

Considering the properties of ideal gas and the inviscid flow assumptions employed in the code, this is unexpected. This decay in the peak pressure over the distance can be attributed to either the error in the code or some physical phenomena that is not yet understood.

To investigate this further, spatial resolution and order of method were held constant while the CFL number was varied (Figure 2.11). As Figure 2.11 shows, there is a slight increase in the error between the two plots at the peak value over the time. However, in both cases, the pattern of decrement in the peak value along the length of the tube remains the same. Thus, the decrease in the peak pressure along the length of the tube is not dependent on the CFL number.

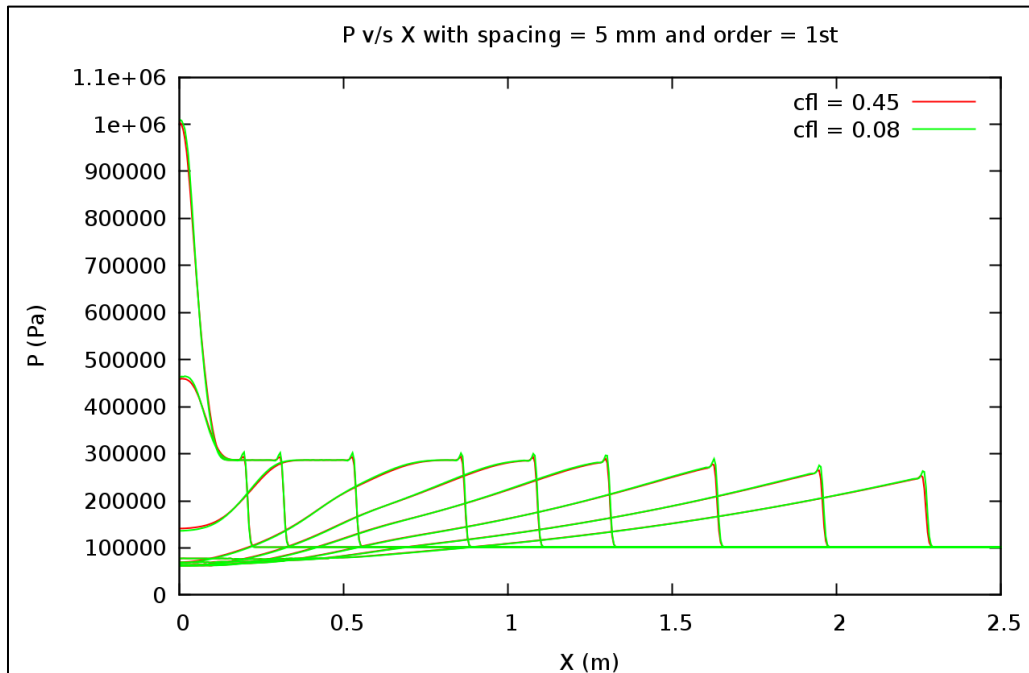


**Figure 2.11:** Pressure versus distance for different temporal resolutions

Next, the same order of method and CFL with different spatial resolution was chosen (Figure 2.12). As the figure shows, there is no appreciable change in the pressure profile due to the higher spatial resolution, except that the smoothness of the curve is reduced due to higher accuracy achieved by higher resolution. Even though there is a small increase in peak value, it does not change the pattern of decrease in pressure over time and distance. Thus, it can be safely concluded that resolution is not the cause for the reduction in peak pressure along the length of the tube.

Now, the same CFL and spatial resolution with different orders of method were chosen (Figure 2.13). Again, there is an overall slight increase in peak value but the pattern, of the decay of the peak pressure, remains the same.

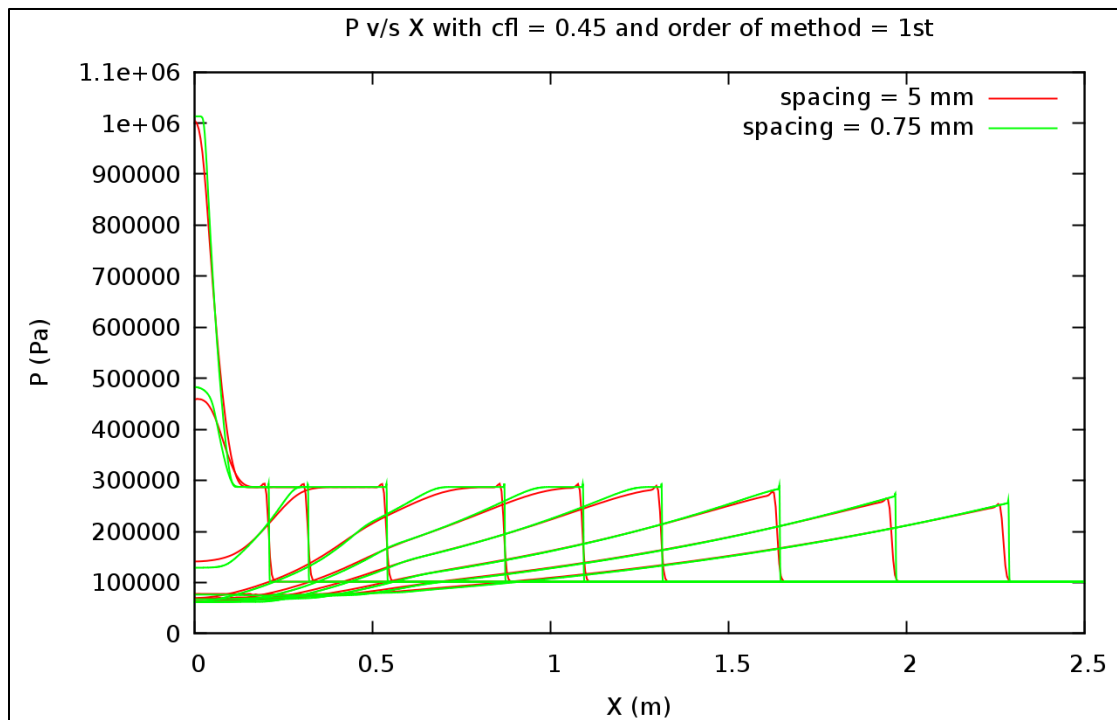


**Figure 2.12:** Pressure versus distance with different spatial resolutions

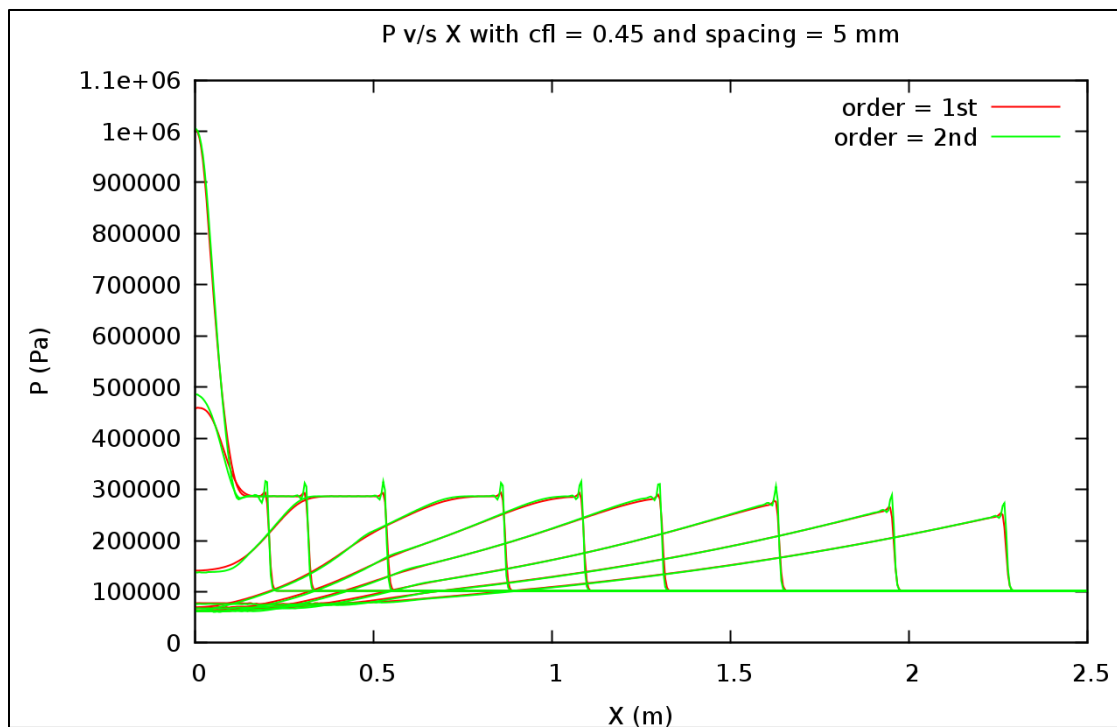


**Figure 2.13:** Pressure versus distance using different order of method

The increase of pressure only at the peaks is a fundamental error of dispersion [17] associated with using the second order of method. Therefore, error induced due to order of method used is not the cause of decrease in pressure along the distance.

Ultimately, it was decided to compare the accumulated errors caused by the three sources of errors. Figure 2.14 is the plot of comparison of two extreme conditions where all three parameters are different. It is shown that when the error due to all three parameters is combined, it is significant and can be clearly seen in Figure 2.14. However, even with a spatial resolution of 0.75 mm, second order and CFL of 0.08, the decrement in the peak value is still seen after the same distance of 1.5 m.

It can be concluded that coarse resolution, first order of method, and lesser timesteps do indeed induce error in the solution.

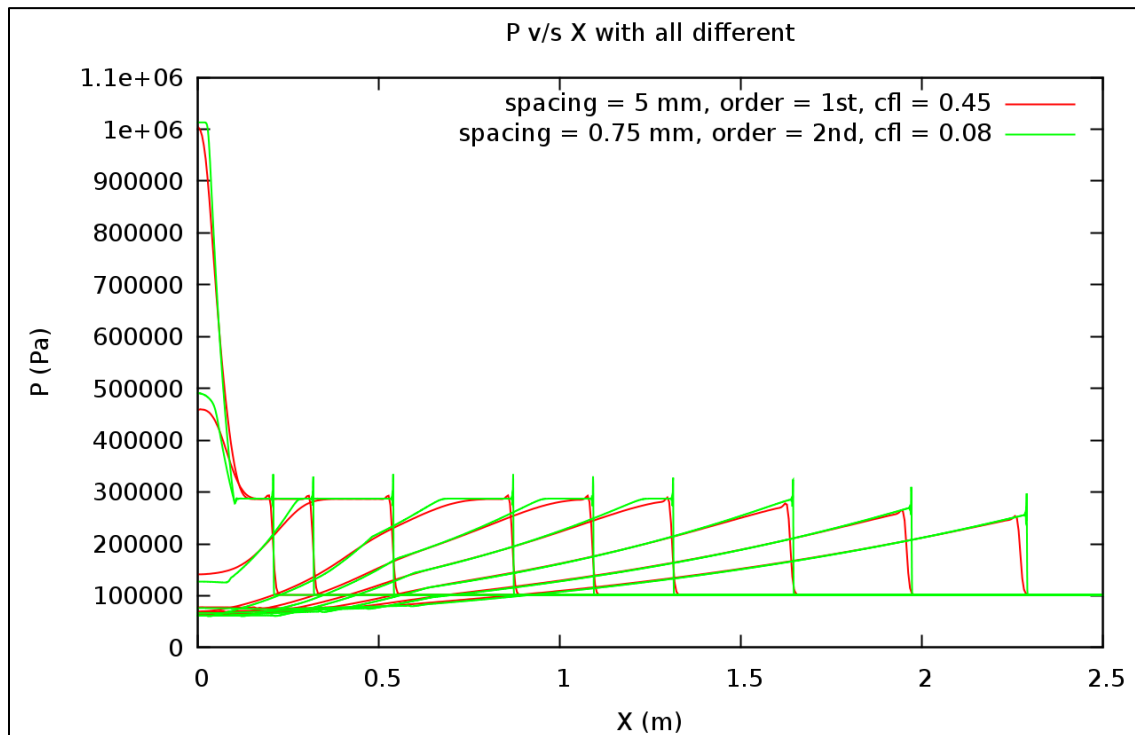


**Figure 2.14:** Pressure versus distance with all parameters different

This error becomes smaller and smaller with finer resolution, more timesteps, and use of higher orders of method, but it is clear that these parameters do not influence the demonstrated reduction in peak pressure.

As explained in Chapter 1, expansion waves overtake and degrade the shock wave, so further investigation was carried out to confirm that it is the physics of the shock tube which is reducing this peak over time (Figure 2.15). In Figure 2.15, there are flat portions behind the shock waves at different distances. Their lengths are noted by  $a_0$  to  $a_4$ . It can be seen here that,  $a_0 > a_1 > a_2 > a_3 > a_4$ . The flat portion  $a_4$  is very short, and the flat portion is eliminated altogether shortly after this point.

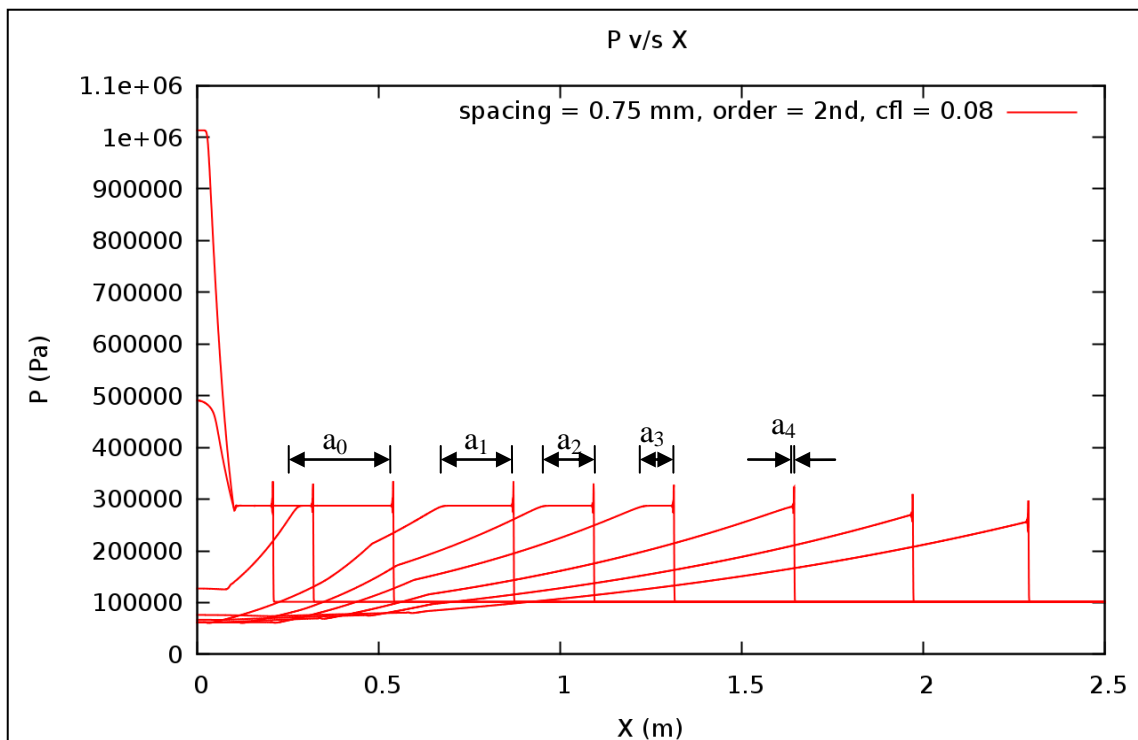


**Figure 2.15:** Shock wave in the shock tube at different instances in time

When the flat portion disappears, peak pressure starts decreasing. This is the point where the reflected expansion waves start overtaking the shock front. The continuous decrease in the length of the flat region is a result of the reflected expansion waves having velocities higher than the compression wave. The decrease in the peak value along the length of the tube is also the result of expansion waves overtaking the shock waves.

Referring back to Figure 2.8, it is now clear that the lower peaks corresponding to the shorter Driver length are due to the expansion waves. Expansion waves propagate in the direction opposite that of shock waves and reflect from the closed end of the tube. Lower Driver length offers expansion waves a smaller distance to travel and hence overtake the shock waves earlier, as shown in Figure 2.16. A few observations can be noted from Figure 2.16.

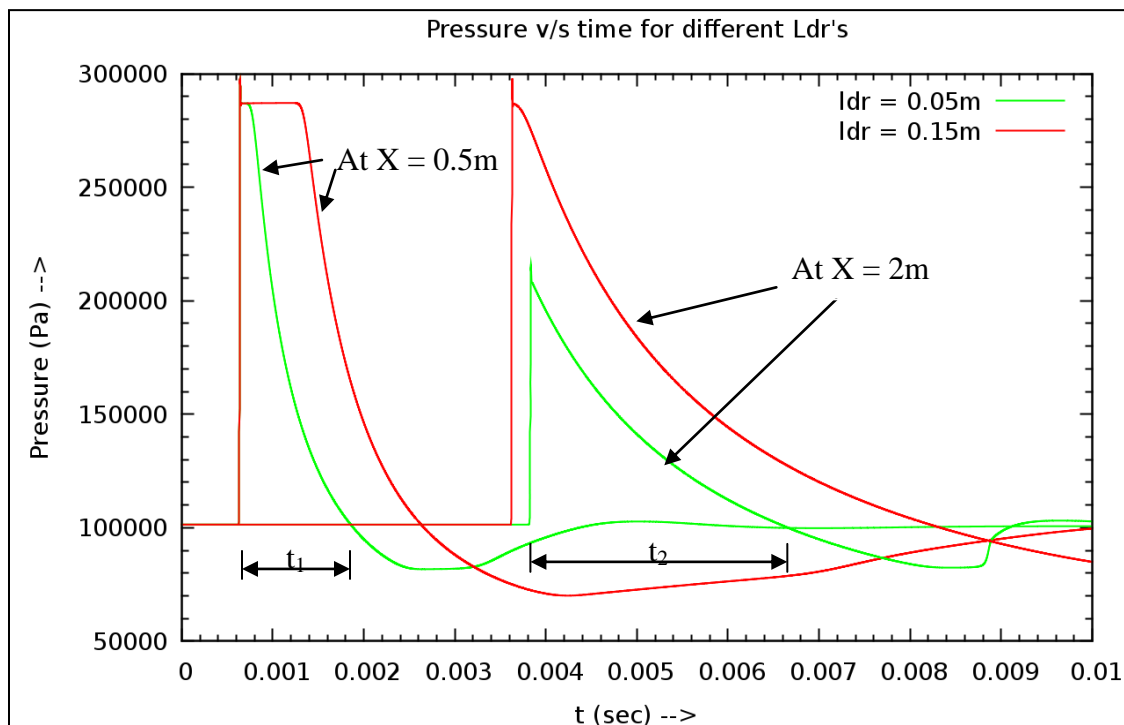


**Figure 2.16:** Pressure versus time at two different locations

At location  $x = 0.5$  m from the diaphragm, the arrival of the shock front for both of the driver lengths occur at the same time; the peaks are identical too, but at  $x = 2$  m from the diaphragm, the shock wave resulting from  $0.05$  m  $L_{dr}$  is overtaken by the expansion wave, and hence, slowed down. Ratios of these distances ( $0.5$  and  $2$  m) to Driver length are the instantaneous length ratios.

Also, the positive phase durations of the shock waves increased over time (e.g.  $t_2 > t_1$ ). At  $x = 0.5$  m, the positive impulse is dominated by the peak pressure while as the probe point is moved down the tube, the trend is changing where the impulse is dominated by the positive phase duration.

#### 2.8.3.2 Over-shoot error study

The preceding section makes it clear that the cause of the degradation of the peak value is expansion waves and not a numerical error. However, there is a significant error associated with the peak value in the numerical simulations. The Uintah computational framework currently has a bug that results in an error at discontinuities while solving a problem.

As explained in the first chapter, a shock is a discontinuous phenomenon, so the error influences the peak pressure value. A fix to this error has been programmed using MATLAB. Figures 2.17 and 2.18 compare the error in the numerical simulation with the applied fix for the first and second order of method, respectively.

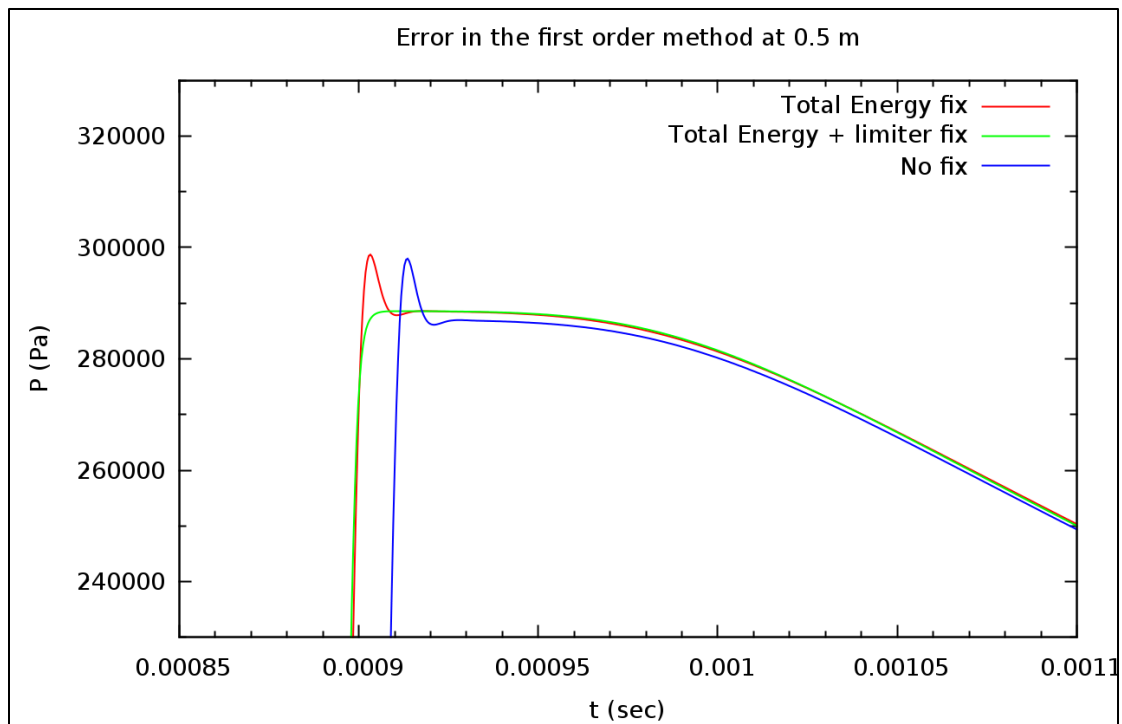


**Figure 2.17:** Comparison of the over-shoot error with its fix; first order

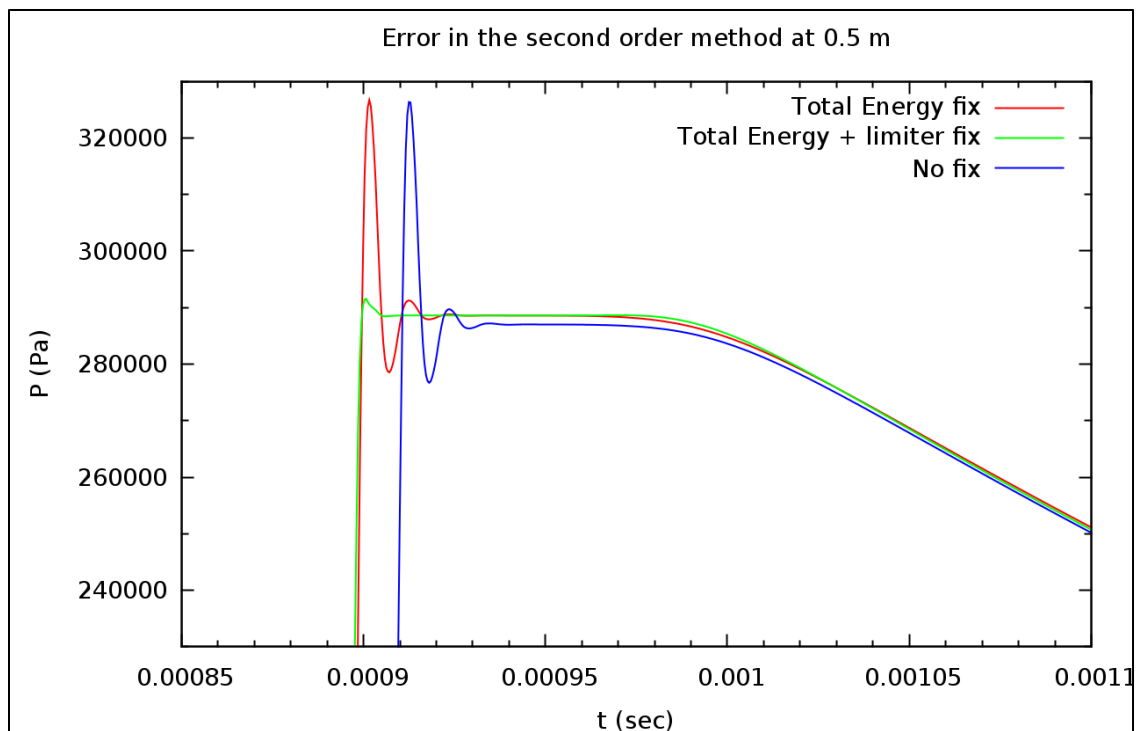


**Figure 2.18:** Comparison of the over-shoot error with its fix; second order

In both Figures 2.17 and 2.18, three plots are shown. The one captioned as “no fix” is plotted directly from the data-file generated by the simulation. Current implementation of ICE only considers internal energy ( $e$ ) and not the total energy. Total energy is the addition of internal energy and kinetic energy. The MATLAB code including the “total energy fix” considers the term related to kinetic energy, and accounts for the time difference between the peak with no fix and the peak with the total energy fix. The last fix applied is called the “limiter.” For discontinuous phenomena like shock, this fix applies limits. When the pressure value increases beyond the peak, it just cuts off the values above the limit. It can be observed from Figures 2.17 and 2.18 that the error is larger in the case of second order (11.93%) than first order (3.27%). Even though the fix has been programmed in MATLAB, it is not yet implemented into the production code ICE and thus, this error will be seen in the forthcoming chapters too.

## 2.9 Discussion of the 1D study

The intention of doing research on the 1D shock tube was to understand the characteristics of the shock wave inside of the tube and to develop intuition for variation in the shock tube parameters. The boundary conditions play a major role in any numerical simulation. However, as none of the available boundary conditions replicate the environment of the open end tube, we decided to use a longer tube with a simulation time short enough to eliminate contributions from the boundary. Results show that peak pressure increases linearly with the driver pressure. The graphs of positive and negative phase durations do not have linear relationship with the driver pressure throughout; these phenomena need more investigation. Nevertheless, the impulses generated for different

driver pressures are more or less the same. The nature of the shock or blast wave is highly dependent on the driver section length (or instantaneous length ratios) of the tube. Low LRs do not give the expansion wave sufficient time to overtake the shock wave. High LRs allow the expansion waves to overtake and degrade the shock, potentially to the point where it has lost much of its strength by the time it reaches its destination. An optimal LR is thus desired.

## **3 TWO-DIMENSIONAL SIMULATIONS**

### **3.1 Introduction**

In Chapter 2, the shock wave behavior inside the tube was characterized through 1D simulations. However, the area of interest for experimentation is outside the tube, where the shock expands axisymmetrically into 3D space. Because of this symmetry, the full 3D behavior could be modeled with a 2D code enforcing an axisymmetry condition. However, the code utilized for this study is currently not available in cylindrical coordinates. As a result, the problem was explored using the 2D code in rectangular coordinates, recognizing that results would not be quantitatively accurate but anticipating that trends could still be accurately simulated.

This chapter principally covers objectives (Sections 3.2), geometry and input parameters (Section 3.3), resolution study (Section 3.5), validation of the code (3.6), and finally, the results of the simulations (Section 3.8).

### **3.2 Objective of the 2D simulations**

In Chapter 2, the parameter study was carried out inside the shock tube. In this chapter, the focus is moved outside the end of the tube. The procedures followed for the parameter study are similar to those in the previous chapter. The purpose of generating a blast wave experimentally is to study its ability to produce brain injury in an animal model. In addition to the parameter study, another objective of 2D simulations is thus to

identify the appropriate region for testing outside the shock tube (Section 1.5). These objectives are discussed in the Results section of this chapter.

### 3.3 Defining geometry and input parameters

#### 3.3.1 Theoretical geometry of 2D shock tube

The theoretical 2D shock tube is similar to the theoretical 1D shock tube, except that it has a diametrical dimension, which results in a 2D computational space. Figure 3.1 is an illustration of the theoretical 2D shock tube. In Chapter 2, the characteristics of the shock were analyzed along the axis of the tube. In the 2D shock tube simulation, the area of interest is not along the axis of the tube but is, rather, at an off-axis position to prevent the target from being affected by the exhaust gas vent.

#### 3.3.2 Geometry defined in 2D simulations

Although the shock expands axisymmetrically outside the tube, the numerical shock tube is here modeled as being symmetric about its longitudinal axis (Figure 3.2). In the Figure,  $L_{dr}$  and  $L_{dn}$  are the driver and driven sections, respectively.  $L_{dr}$  is treated as a variable that changes from 4 to 10 cm in increments of 2 cm, while  $L_{dn}$  is fixed.

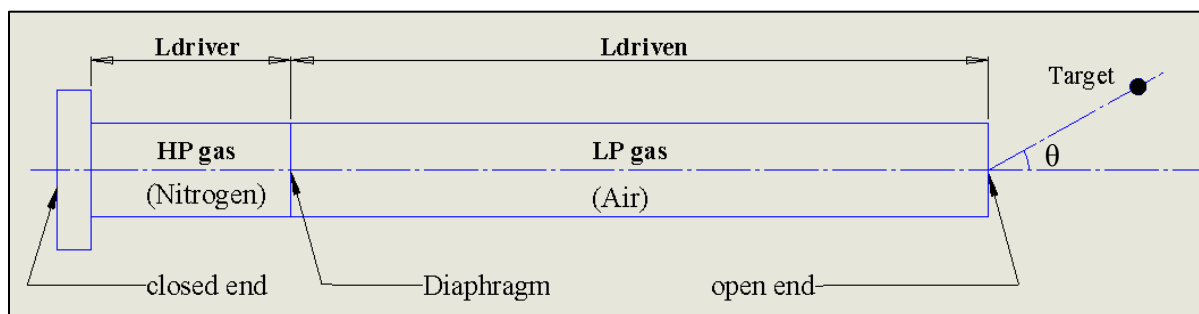


**Figure 3.1:** Theoretical geometry of 2D shock tube

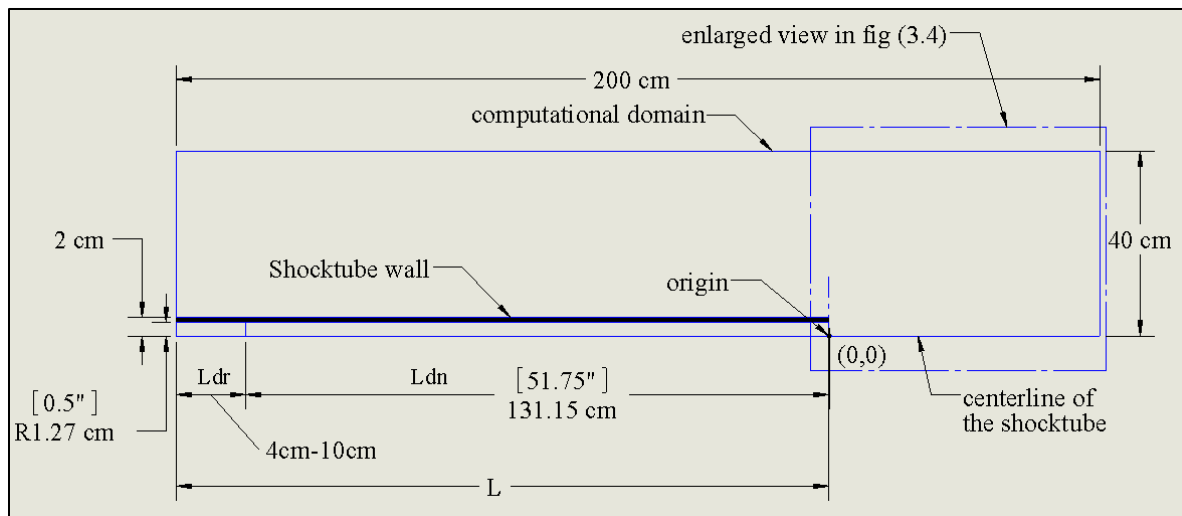


**Figure 3.2:** Geometry of shock tube defined in numerical simulation

The experimental shock tube has a diameter of 2.54 cm (or 1”) and a wall thickness of 7.3 mm. The shock tube wall is made of a rigid material, so there is no deformation of the shock tube wall despite the high pressure generated inside the tube. The origin of the coordinate system is chosen at the outlet of the tube, on the tube axis. The computational domain is a rectangular area of 200 cm x 40 cm, which is big enough to not affect the area of interest due to the reflection of the pressure wave from the boundaries.

An enlarged view of the box indicated in Figure 3.2 is shown in Figure 3.3. It shows the locations of the probe points placed outside the tube for data recording. As seen in Figure 3.3, the probe points are at angles  $30^{\circ}$ ,  $45^{\circ}$ ,  $60^{\circ}$ , and  $75^{\circ}$  with radii ranging from 2 to 14 cm in increments of 2 cm.

### 3.4 Governing equations

The governing equations used are the two-dimensional MPM-ICE equations as specified by Equations 1.8 – 1.10 in Chapter 1.

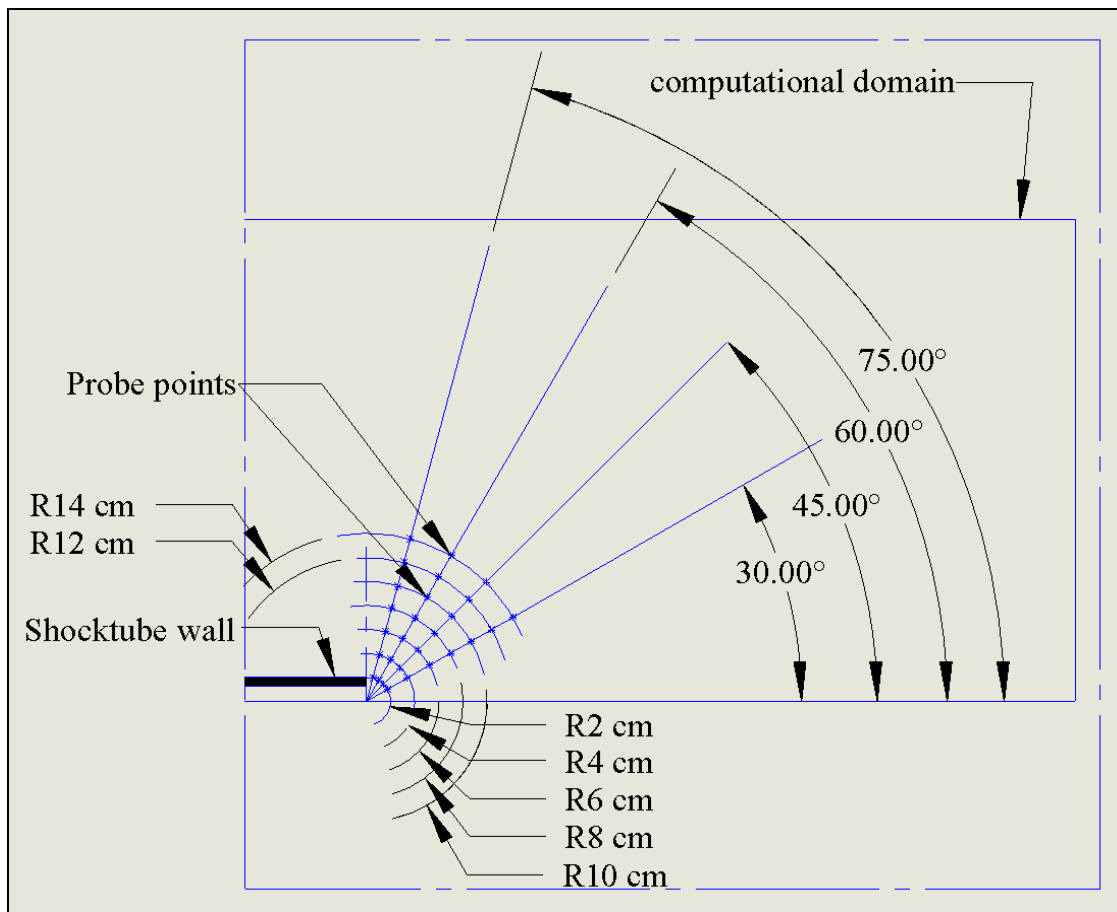


**Figure 3.3:** Probe points outside the tube

### 3.5 Resolution study

In this section, a study seeking the appropriate resolution for the 2D shock tube simulation is described. Because the major area of interest is outside the tube, the resolution study is carried out at the probe point of  $30^\circ$  and 5 cm. There is no specific reason for not choosing one of the radii mentioned in Figure 3.3. For the resolution study, as long as the chosen probe point is outside the tube, it does not make any difference what radius and angle it is at. Table 3.1 gives the input parameters used for this study.

**Table 3.1:** Input parameter declaration for the resolution study

Parameters	Values	Units
$L_{dr}$	0.1	m
$L_{dn}$	0.9	m
LR	9	-
Finest Resolution (cell spacing)	variable	mm
Density in HP region ( $\rho$ )	11.76	kg/m <sup>3</sup>
Density in LP region ( $\rho$ )	1.176	kg/m <sup>3</sup>
Temperature in HP region (T)	300	K
Temperature in LP region (T)	300	K
Specific heat ( $C_v$ )	716.4	J/kg-K
Specific heat ratio ( $\gamma$ )	1.4	-
Physical Time of the simulation (t)	0.00325	sec
Order of method	First	-
CFL	0.45	-

Out of the parameters displayed in Table 3.1, the density and temperature in both the high pressure and low pressure region are the same for all other simulations. Also, the specific heat ratio remains the same. In similar subsequent tables, only parameters that differ from those in Table 3.1 are displayed.

From Figure 3.4, it can be seen that as the spacing between cells decreases, the solution converges. For the spacing of 1.25 mm and 0.625 mm, pressure profiles almost overlap each other. Thus, spacing of 1.25 mm was chosen for further study.

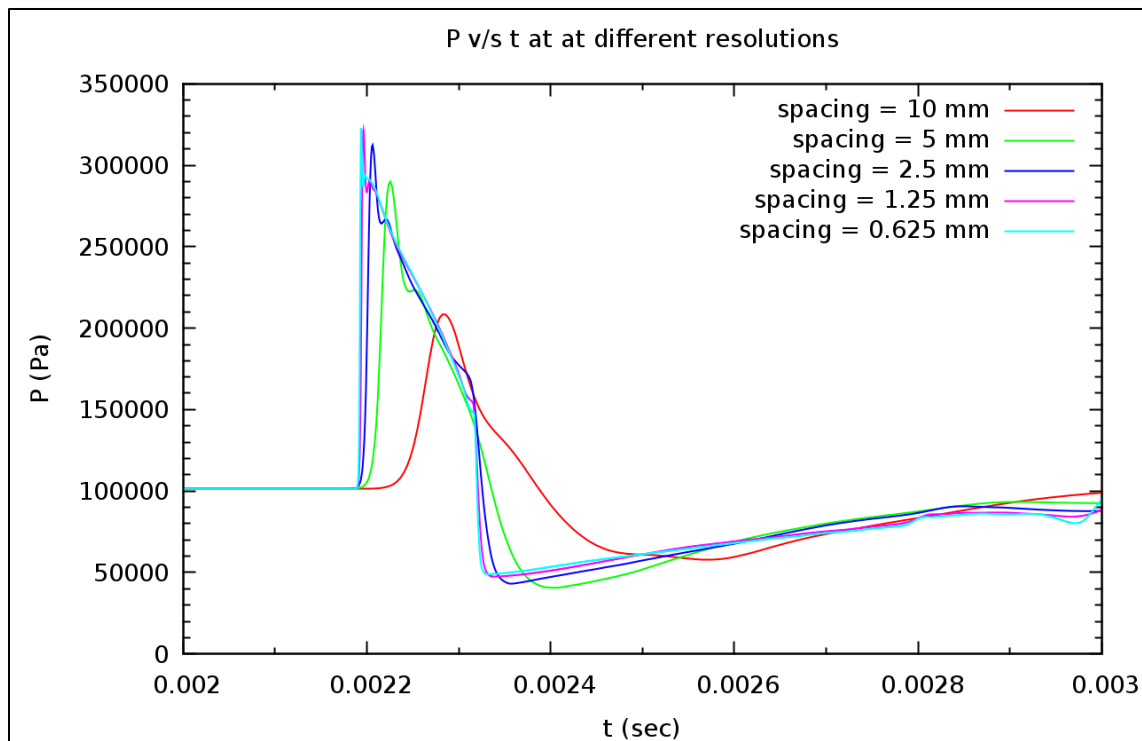


**Figure 3.4:** Results of the resolution study in 2D

As resolution is increased, simulation time naturally increases, and more computer memory is required. To help alleviate these effects, the AMR (Adaptive Mesh Refinement) feature available in the code was utilized. According to AMR, the grid would refine itself once pressure values increase beyond a threshold value. This threshold value is set in an input file of the simulation. In this way, only the cells on which the pressure value increases beyond the threshold value would refine and adopt the higher resolution. Three levels of resolution were defined. On the coarse level (level 0), the cell spacing was 20 mm. The ratio between successive levels was set at 4:1, yielding cell spacing for levels 1 and 2 equal to 5 and 1.25 mm, respectively.

### 3.6 Validation of the 2D code

Before using the code for further simulations, an important step of validating the code is necessary. The problem used for validating the code is different than the shock tube problem, though the code used for both problems is the same. The problem used is the explosion of a fireball in 2D.

#### 3.6.1 Description of the explosion problem

The geometry of the problem is shown in Figure 3.5. The circular region at the center of the domain, called the “fireball,” is at relatively high pressure and density at time  $t = 0$ .

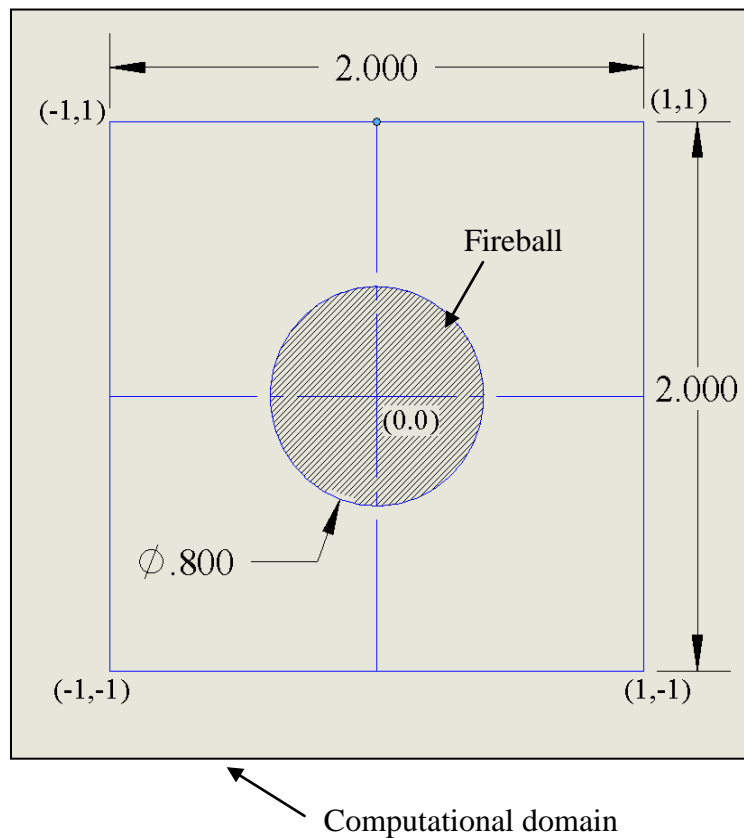


**Figure 3.5:** Geometry of the explosion problem

The computation domain is divided into two regions: a box of  $2 \times 2 \times 0.1$  and the fireball with a radius of 0.4. Any unit system can be used to specify the units of the physical or geometrical quantities. The initial conditions inside of the circular region are ( $p = 1$ ,  $\rho = 1$ ,  $u = 0$ ,  $v = 0$ ) and outside ( $p = 0.1$ ,  $\rho = 0.125$ ,  $u = 0$ ,  $v = 0$ ). Once the simulation begins, the expansion of the high-pressure gas forms a circular shock wave and a contact surface that expands axisymmetrically into the atmosphere. At the same time, a circular rarefaction wave travels towards the origin. The fluid is modeled as an ideal, inviscid, polytropic gas. Table 3.2 specifies the other initial parameters.

**Table 3.2:** Initial parameters for the explosion problem

Parameters	Values	Units
Fireball radius	0.4	units
Computational domain	$2 \times 2 \times 0.1$	units
Finest Resolution (Cell Spacing)	0.00125	units
Density in fireball ( $\rho$ )	1	units
Density in the box ( $\rho$ )	0.125	units
Temperature in HP region (T)	2.5	units
Temperature in LP region (T)	2.0	units
Specific heat ( $C_v$ )	1	units
Specific heat ratio ( $\gamma$ )	1.4	-
Physical Time of the simulation (t)	0.25	units
Order of method	second	-
CFL	0.4	-

### 3.6.2 Exact solution

In Figure 3.5, the explosion of the fireball is axisymmetric, and therefore, the Riemann problem is simplified to the 1D problem in cylindrical coordinates [18]. The exact solution of the explosion problem is solved using the HLLC Riemann solver [19].

### 3.6.3 Validation against the exact solution

Figure 3.6 is the plot of the exact solution against the numerical solution for the “explosion” problem. The x-axis is the perpendicular distance from the center of the fireball to the wall of the box. The data are presented for  $t = 0.25$ . The L-0, L-1, and L-2 are the different levels of the AMR grid, as explained in Section 3.5. The data on L-2, which is the level of finest resolution, match the exact solution reasonably well, so it is clear that the numerical code can safely be used for further study.

## 3.7 Data processing

The data files generated after running 2D simulations store the same variables as the data files of 1D simulations, so similar scripts were used to process the data. An example of the input file for the 2D shock tube problem is shown in Appendix A.3. In the case of the 2D problem, an additional approach for visualizing results was incorporated, using the tool called VISIT. VISIT is a visualization tool for the analysis of data defined on 2D and 3D structured meshes. In VISIT, the progress of physical parameters can be monitored in both space and time. It is a powerful tool for understanding intricate phenomena like the expansion of high pressure gases.

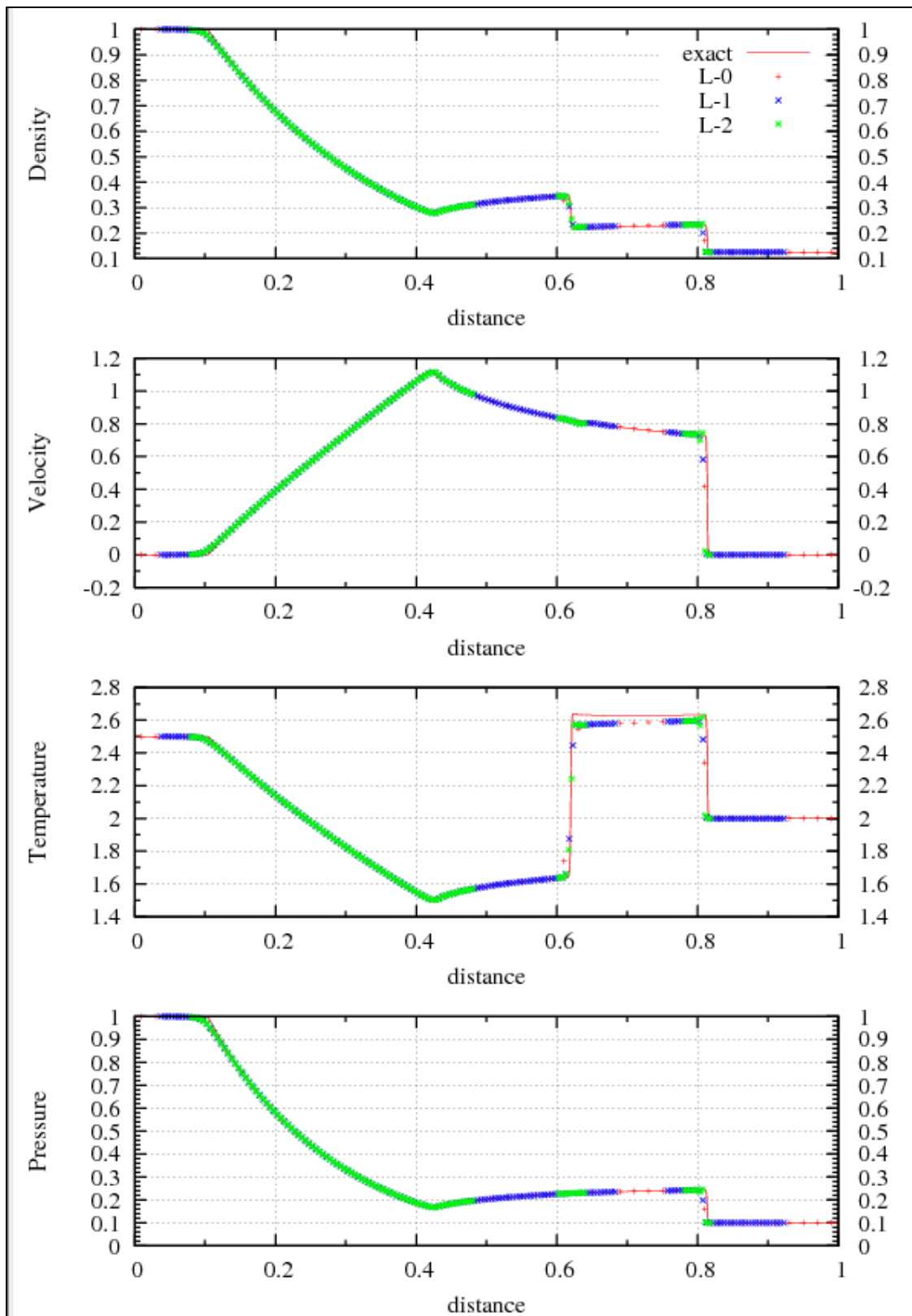


**Figure 3.6:** Comparison of the explosion problem with the exact solution ( $t = 0.25$  units)

## 3.8 Results

The objectives of these simulations are to prevent significant target interaction with venting gas and develop an intuition about the peak pressure, positive impulse, and negative impulse at a desired point in a space based on input parameters. The input parameters, here, refer to those parameters that are in control of the user, viz.  $L_{dr}$  and  $P_{dr}$ .

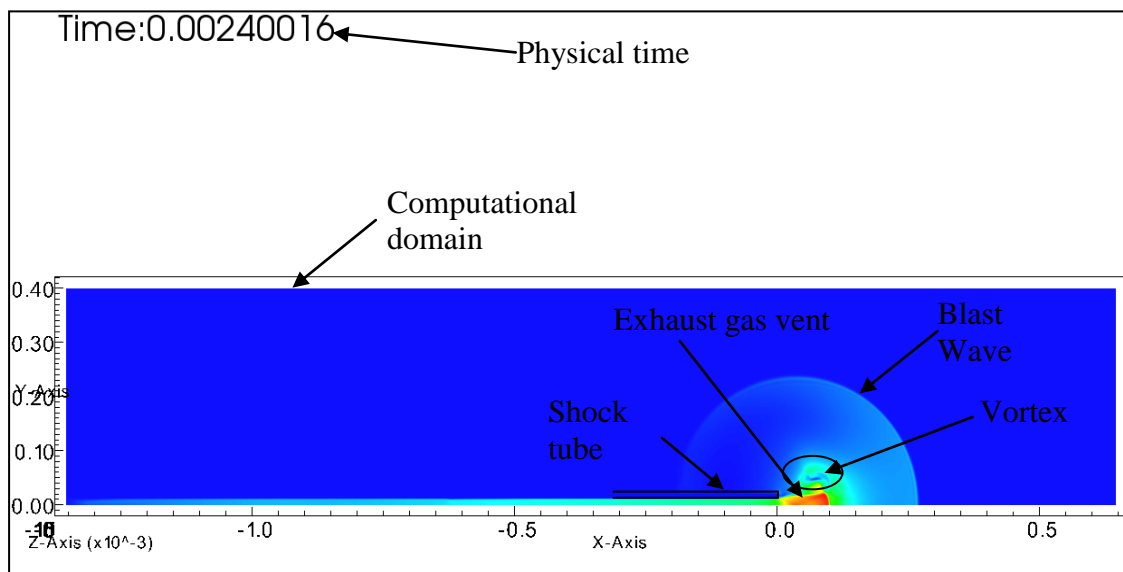
### 3.8.1 Quantifying an area where target is not affected by the exhaust gas vent

Figure 1.9 illustrates approximate boundaries for an appropriate testing region. This region is quantified in this section in detail. The initial parameters utilized for this research are displayed in Table 3.3. The gas in the driver section is Nitrogen and its Specific heat ( $C_v$ ) is 743.0 J/kg-K. The density in the HP region is denoted as 54.1311 kg/m<sup>3</sup>. Using the ideal gas law (Eq. 2.1), the pressure is 700 psi (4826.33 kPa). The value 700 psi (4826.33 kPa) is the most common driver pressure used currently in the experimental setup. Other parameters are listed in Table 3.3.

The appropriate region for placing the target was determined by evaluating pressure versus time at given locations and through the visualization of the velocity field outside the tube using VISIT. Figure 3.7 shows an example contour plot of the velocity field in the VISIT visualization window. This window shows the whole computational domain, similar to the one shown in Figure 3.2. This visualization of the velocity is a snapshot taken at the physical time of 0.00240016 sec. Velocity magnitudes are shown in different shades of colors, blue being the minimum velocity and red being the maximum velocity. The shock tube wall cannot be seen in VISIT, since the velocity of the wall is zero; hence, it is merged with the blue color outside.

**Table 3.3:** Initial parameter for quantifying the region for testing

Parameters	Values	Units
$L_{dr}$	4	cm
$L_{dn}$	131.45	cm
LR	32.8625	-
Finest Resolution (Cell Spacing)	1.25	mm
Density in HP region ( $\rho$ )	54.1311	kg/m <sup>3</sup>
Density in LP region ( $\rho$ )	1.176	kg/m <sup>3</sup>
Specific heat ( $C_v$ )	743	J/kg-K
Physical Time of the simulation (t)	0.003	sec
Order of method	Second	-
CFL	0.4	-

**Figure 3.7:** Visualization of the magnitude of the velocity field using VISIT

The part of wall is drawn using the drawing feature in MS Word. The scale along the X and Y axis is in meters.

It was mentioned earlier that the shock wave expands outside the tube axisymmetrically. In Figure 3.7, the velocity associated with the wave is shown. The red color area is the region of highest velocity and is the exhaust gas vent. As shown, a vortex is also generated. Figure 3.8 is the zoomed in view of the area outside the tube shown in Figure 3.7. It is clearly seen in Figure 3.8 that the region below the line at  $30^\circ$  is dominated by the exhaust gas vent. Above the exhaust gas vent, a circular vortex region generated. It has been observed that the center of the vortex is the area of lowest pressure, lowest density, and lowest velocity.

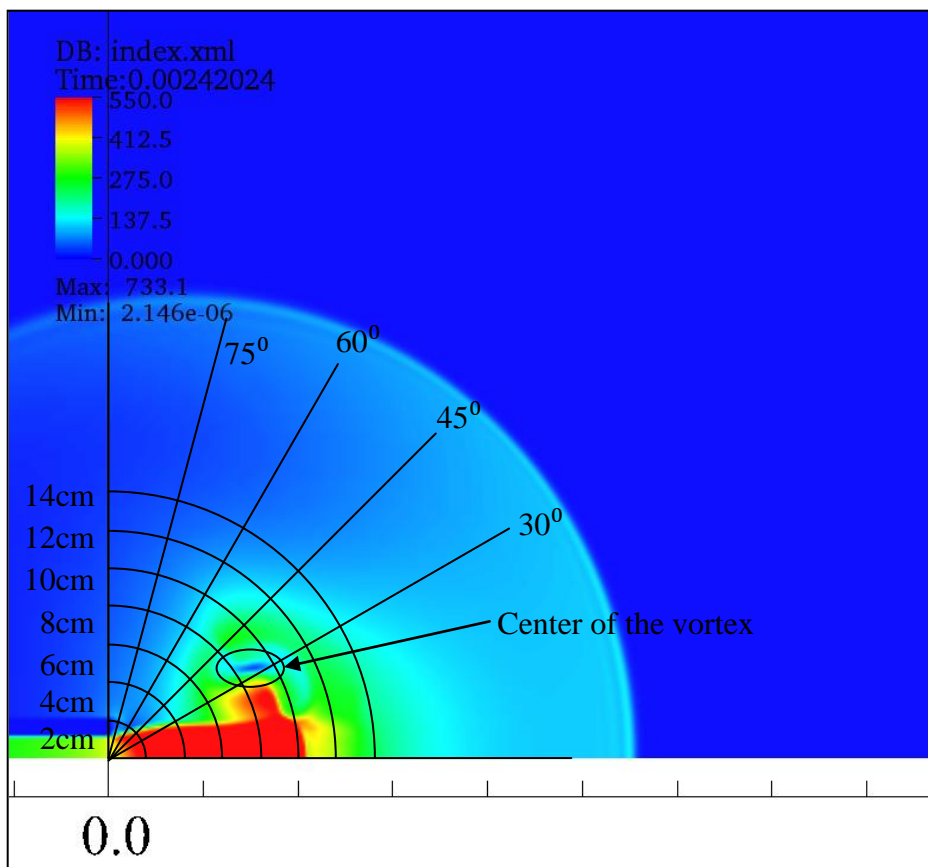


**Figure 3.8:** Zoomed view of Figure 3.7 with the geometry drawn

The vortex, when it forms, is not as significant as in Figure 3.8. Therefore, it is necessary to draw these contour plots at earlier times. Figure 3.9 shows the contour plot at  $t = 0.002$  sec. In Figure 3.9, at  $t = 0.002$  sec, and at radii of 2 cm and 4 cm, the area under the line at  $45^\circ$  is in the exhaust gas vent. In Figure 3.8, the exhaust gas vent has cleared of locations  $(4, 30)^\dagger$  and  $(4, 45)$ . The lines  $60^\circ$  and  $75^\circ$  are always clear of the exhaust gas vent, which seems therefore like a potential region for testing.

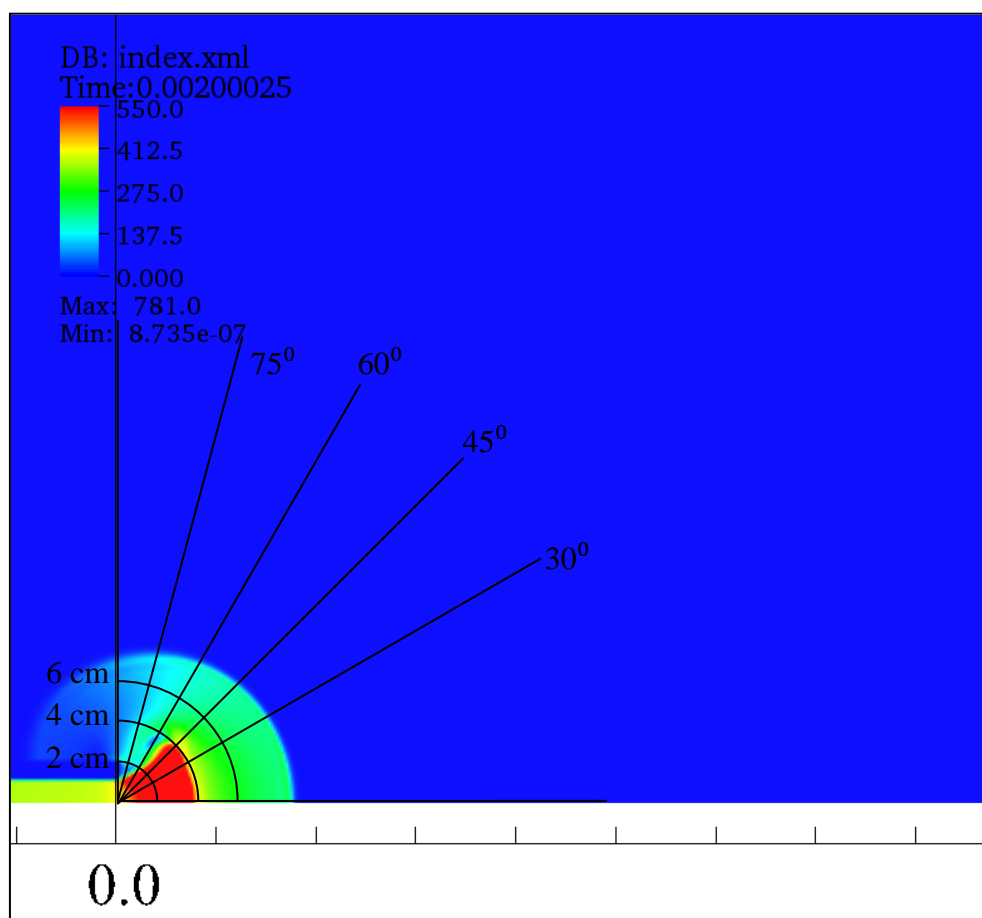


**Figure 3.9:** Contour plot of the magnitude of the velocity field at  $t = 0.002$  sec

---

<sup>1</sup> Locations specified here are in polar coordinates.  
 For example:  $(4, 30)$  implies radius of 4 cm at  $30^\circ$ .

The vortex formed at this time has no noteworthy influence on its surroundings compared to the one shown in Figure 3.8. Hence, in Figure 3.10, the contour plot of the magnitude of velocity field at  $t = 0.00212$  sec is shown.

It can be observed in Figure 3.10 that the region above the line at  $45^\circ$  is free of the highest gas velocities. Some of the region between lines at  $30^\circ$  and  $45^\circ$ , and the region beneath the line at  $30^\circ$ , are in the exhaust gas vent. So, it seems that the line at  $30^\circ$  is always in the exhaust gas vent, and hence, the target should not be placed in that region. The vortex has grown bigger compared to Figure 3.9, and some areas at  $45^\circ$  and  $60^\circ$  are in the vortex.

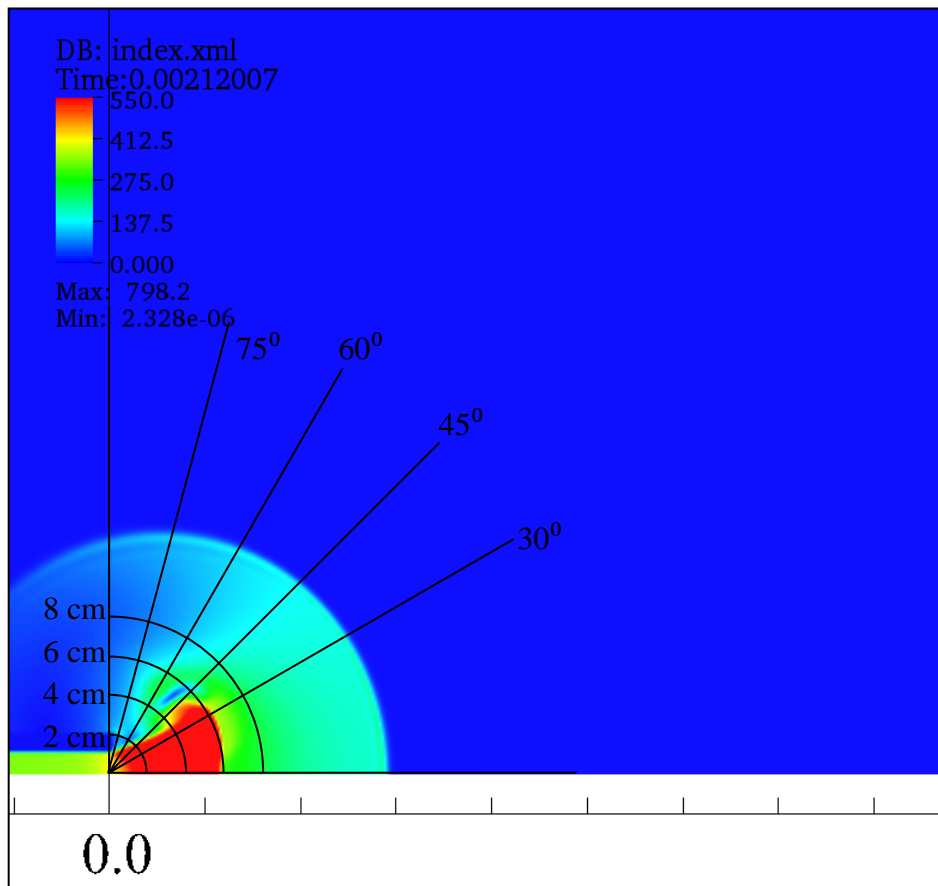


**Figure 3.10:** Contour plot of the magnitude of the velocity field at  $t = 0.00212$  sec

It is important to determine whether the vortex has any effect on the pressure profile desired in this research. Therefore, the pressure profile is studied in Figures 3.11 – 3.14. The pressure profiles at  $45^\circ$ ,  $60^\circ$ , and  $75^\circ$  exhibit desirable blast wave characteristics, with Friedlander-like positive and negative phases at all radii [4]. This area thus seems desirable for target placement. It can be clearly seen from the figures that as angle increases, the peak pressure and the phase durations decrease. Also, as the radial distance increases, peak pressure goes down.

In Figures 3.11 – 3.13, the region between the lines at  $0^\circ$  and  $30^\circ$  is dominated by the exhaust gas vent. In Figure 3.13, there are two pressure spikes indicated as  $P_1$  and  $P_2$ . Figure 3.15 offers an explanation.

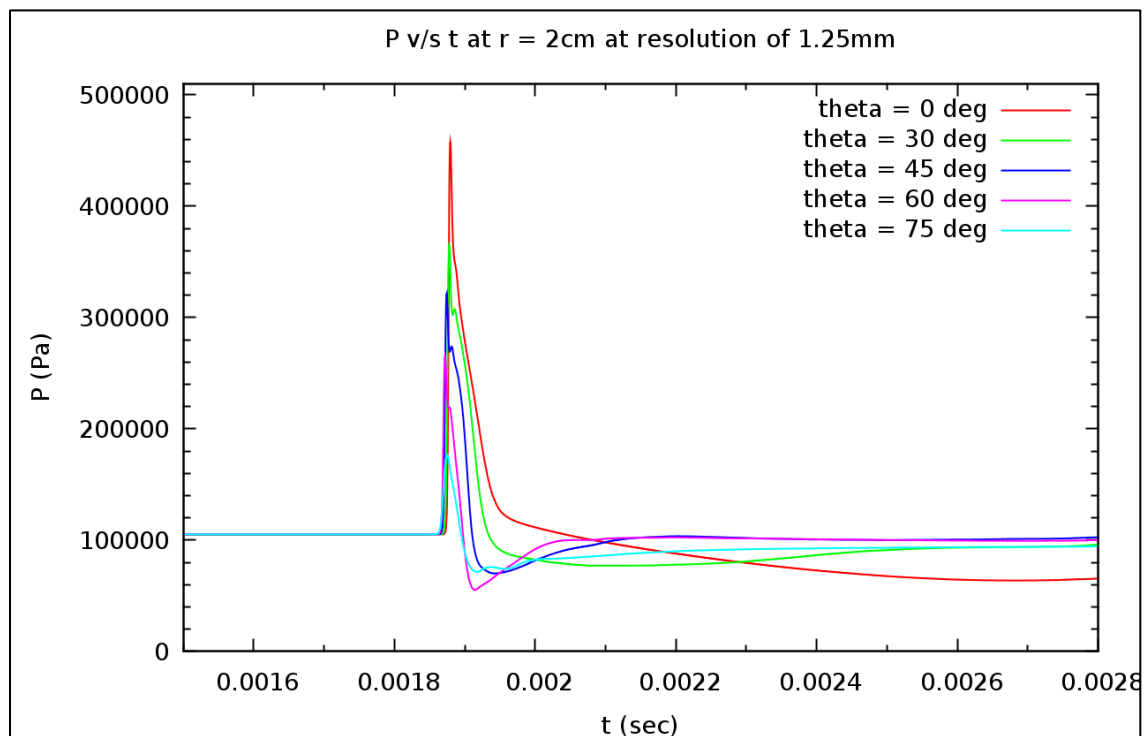


**Figure 3.11:** Pressure versus time at 2 cm outside the tube

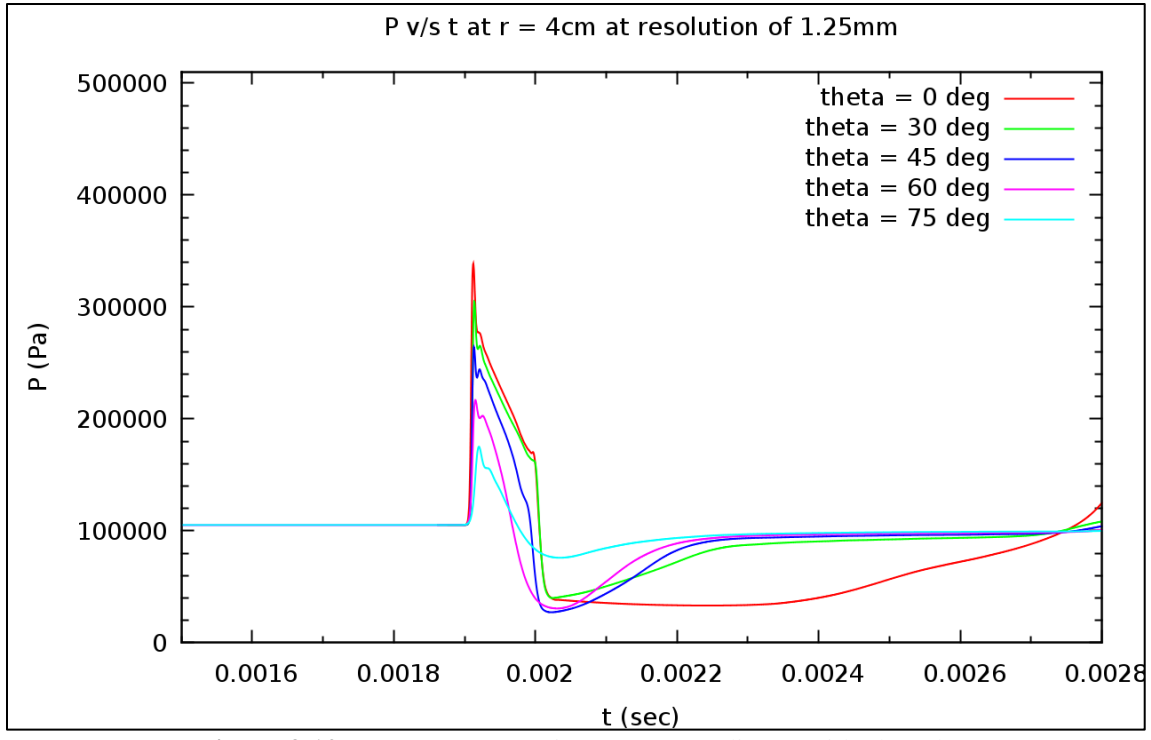


Figure 3.12: Pressure versus time at 4 cm radius outside the tube

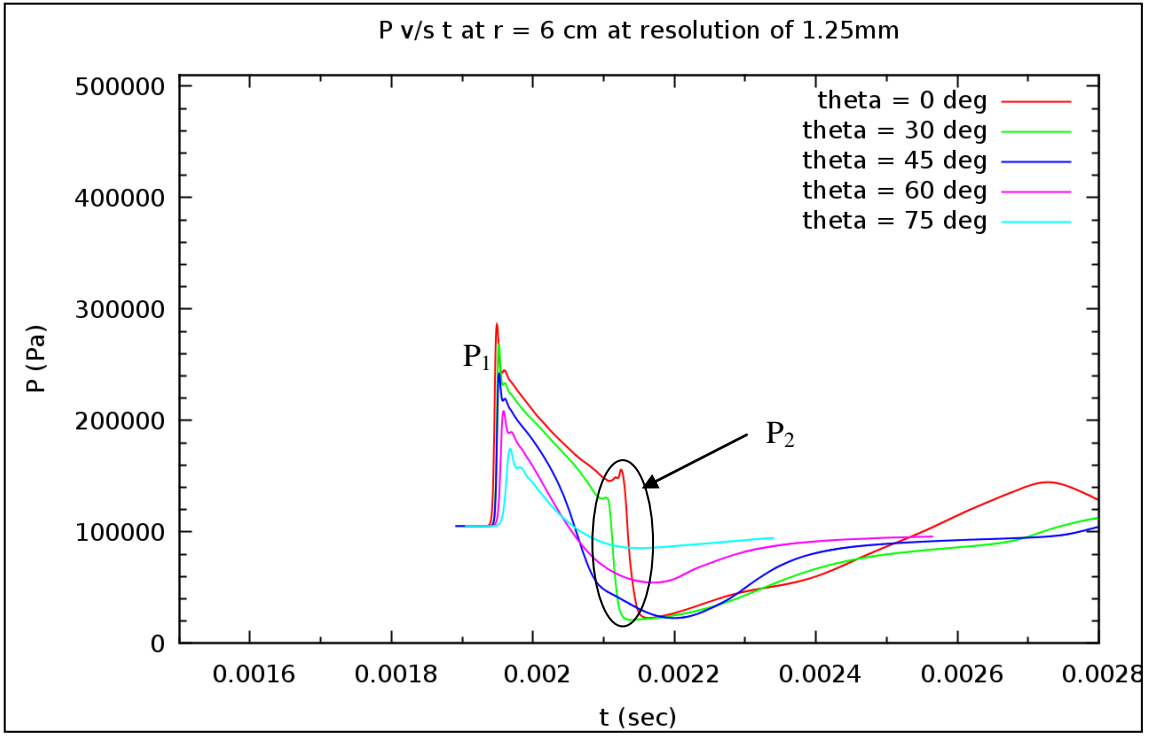
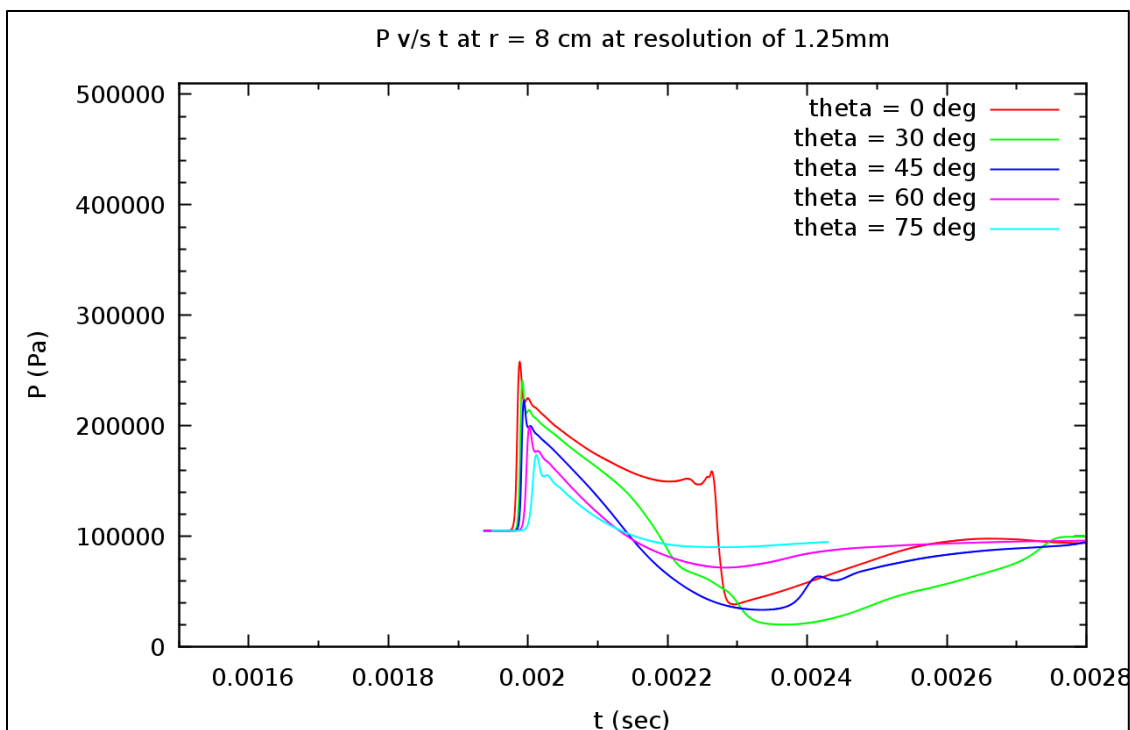


Figure 3.13: Pressure versus time at 6 cm radius outside the tube



**Figure 3.14:** Pressure versus time at 8 cm radius outside the tube

In Figure 3.15, it is clear that pressure peak  $P_1$  corresponds to the blast wave pressure. As the wave passes, the pressure at that location starts going down until it attains the value of  $P_2$ . Behind  $P_2$ , there is a high velocity exhaust gas vent. The fact to be noted here is that the exhaust gas vent has a very high velocity but a very low pressure. This pattern of two peaks actually starts at  $r = 4$  cm (see  $0^\circ$  and  $30^\circ$  plots in Figure 3.12).

In Figure 3.14, only one peak  $P_1$  is seen for (8, 30). The reason is that the angle of the gas vent continuously decreases and the region along the line at  $30^\circ$  is eventually clear of the exhaust gas vent. This is confirmed in Figure 3.8, where the line at  $30^\circ$  is completely cleared of the red area. As a result, the line at  $30^\circ$  would be appropriate for testing at farther locations, though the strength of the blast would be low.

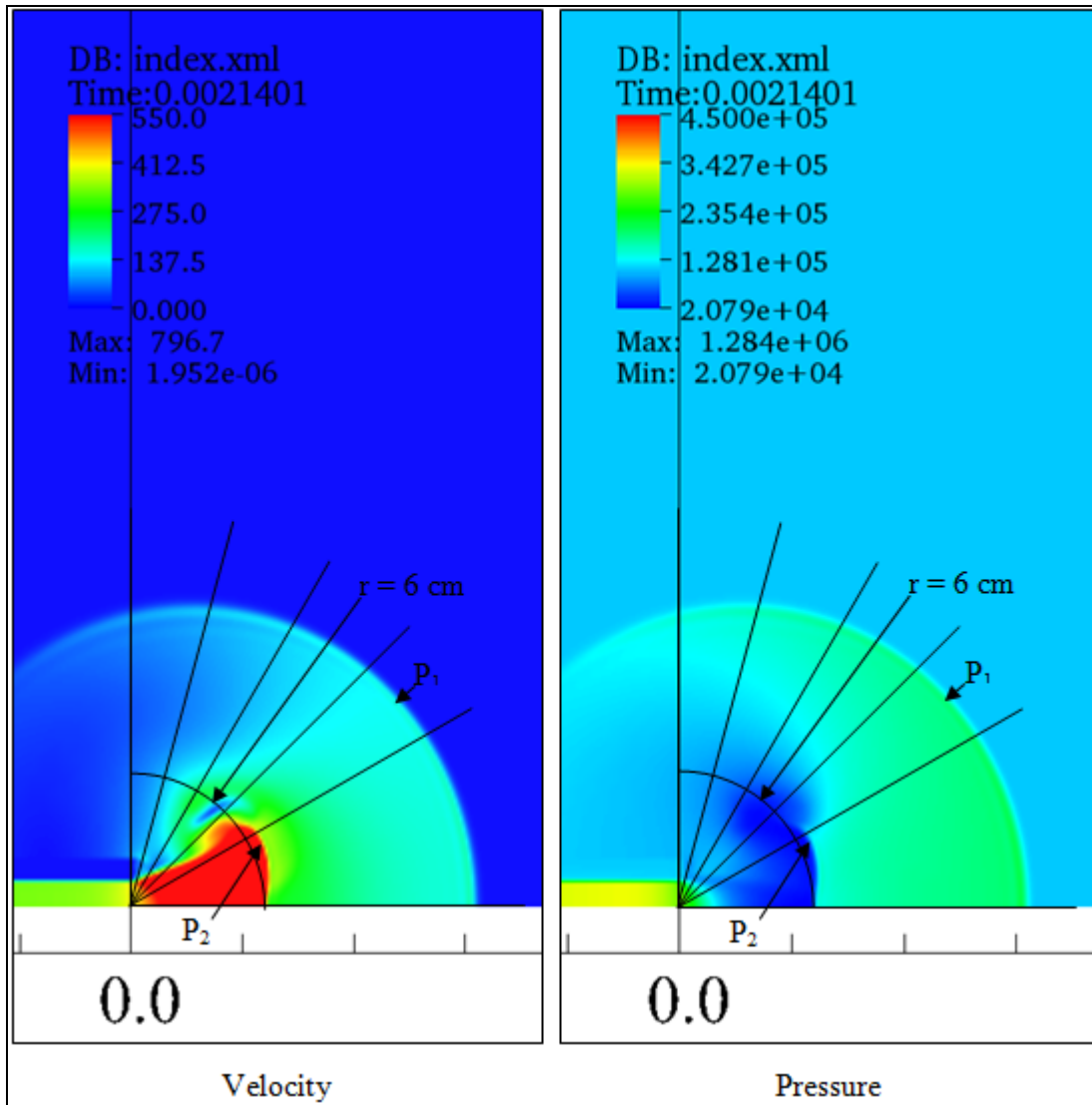


**Figure 3.15:** Visualization of velocity and pressure at  $t = 0.00214$  sec

The vortex does not have a large effect on the pressure profiles, except that the negative phase of the blast wave is perturbed in a small amount. Plots presented in this thesis show only a static pressure measurement. The stagnation pressure additionally considers the effects of kinetic energy. The small region around the vortex is at low pressure but high velocity, as seen in Figure 3.15. However, the velocity in that region is not as high as the velocity of the exhaust gas vent. Therefore, to understand the

phenomenon of the vortex better, the total energy approach is needed in future. Also, an experimental investigation is required to evaluate this region for testing.

From Figure 3.8 – 3.10, it can be observed that the probe points at (2, 30) and (2, 45) are always in the exhaust gas vent. Their pressure profiles in Figure 3.11, however, look very smooth. Despite this, the region below the line at  $45^{\circ}$  is not recommended for testing due to the presence of the vent. The probe points at (2, 60) and (2, 75) are very close to the tube and not in the exhaust gas vent, and hence, could be included in the potential testing region if higher peak pressures are desired.

#### 3.8.1.1 Conclusions

- For all radii greater than 2 cm, the region above the line at  $45^{\circ}$  is clear of the exhaust gas vent and is thus appropriate for testing.
- The region below the line at  $30^{\circ}$  is influenced by the exhaust gas vent at most times.
- Due to the reduction in the vent angle over time, the region along the line at  $30^{\circ}$  is eventually free of the exhaust gas vent at large radii (above 8 cm), but the strength of the blast wave is low at these larger distances.
- The vortex does not seem to be disturbing the pressure profile significantly, though the total energy approach is needed to understand the phenomena better.
- The recommended region for testing is shown in Figure 3.16

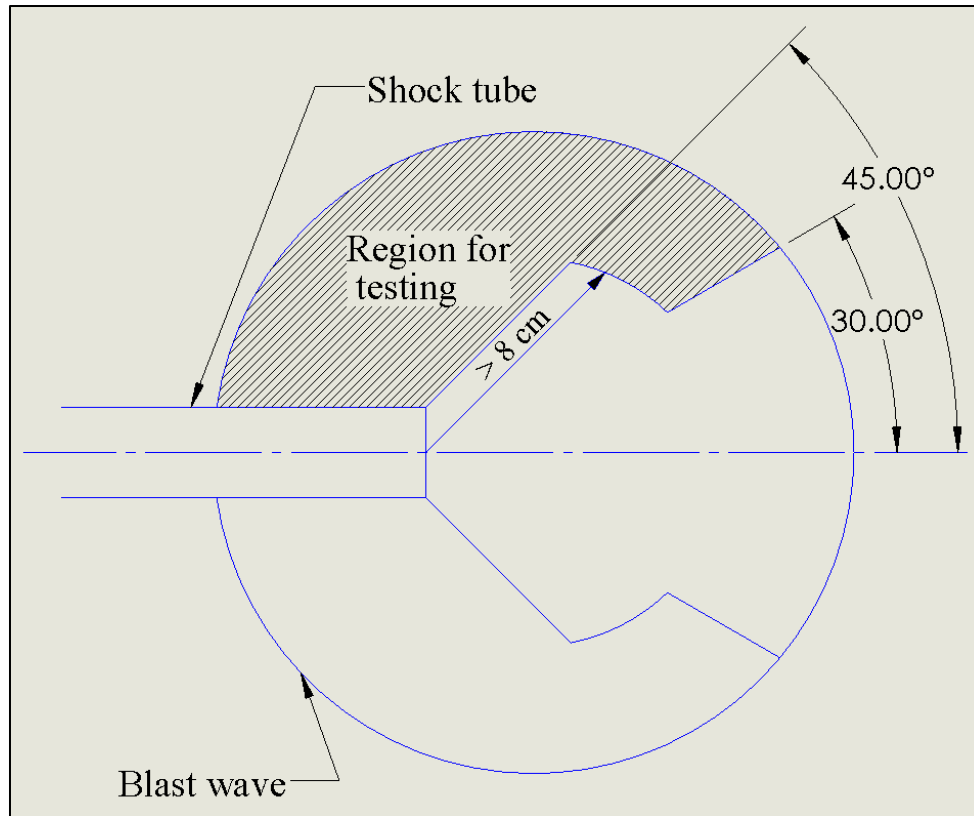


**Figure 3.16:** Quantified region for testing from 2D simulations

### 3.8.2 Parameter study

A parameter study is carried out taking into account the findings of the tube venting study, so only probe points along the lines at  $45^{\circ}$ ,  $60^{\circ}$ , and  $75^{\circ}$  are considered.

The parameter study is divided into the following three types.

- Choosing one driver length and driver pressure, and then observing the change in the blast wave over the entire field outside the tube.
- Choosing one point in space and observing the characteristics of the blast wave at that point for different driver lengths.
- Choosing one point in space and observing the characteristics of the blast wave at that point for different driver pressures.

Dependent variables studied were peak pressure and positive phase duration. The negative phase duration was not studied because it is perturbed by the vortex, and hence, not smooth (Figures 3.11 – 3.14).

### 3.8.2.1 Study over the entire field

The entire field here refers to the region between the line at  $45^\circ$  and  $75^\circ$  for all radii. Table 3.3 indicates the initial parameters chosen for this study. It can be observed from Figures 3.11 – 3.14 that as the probe point is moved farther from the origin of the tube, peak pressure goes down. Also, as angle increases, peak pressure goes down. These are the intuitive observations from Figures 3.11 – 3.14. Figures 3.17 – 3.18 are the contour plots of pressure in the field outside the tube for the radii 4 cm and 8 cm, respectively. These plots help illustrate trends in peak pressure over the entire field. Pressure contours for other Driver length are shown in Appendix A.2.

The positive impulse carried by the blast wave is a function of both peak pressure and positive phase duration. Figure 3.19 shows that positive phase duration increases with radius, even though the peak pressure goes down with it. As described in Section 2.8, the wave speed decreases with distance from the origin due to the expansion waves catching the shock front. This increases the positive phase duration of the wave. Figure 3.20 shows a contour plot of the positive phase duration over the region for testing. As positive impulse is proportional to the product of the peak pressure and positive phase duration, the results obtained from Figure 3.17 and Figure 3.20 infer that different combinations of peak pressure and positive phase duration can be used to obtain different and/or similar impulses dominated by either peak pressure or positive phase duration, or both, during experiments.

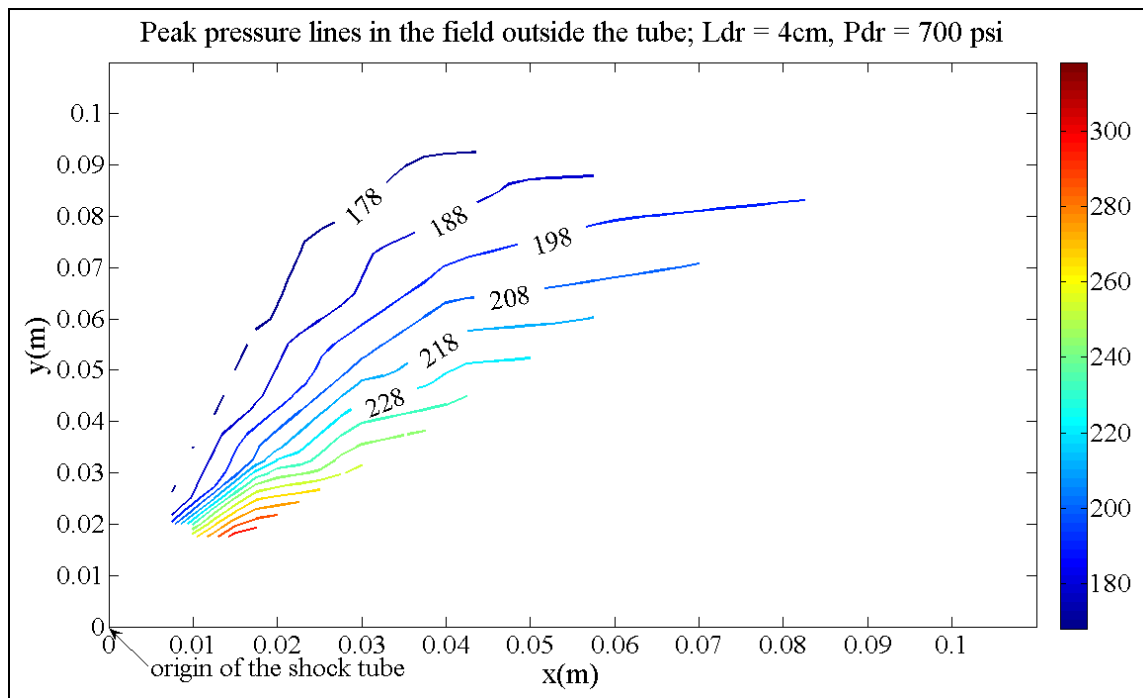


**Figure 3.17:** Contour plot of the peak pressure in the field outside the tube;  $L_{dr} = 4\text{ cm}$

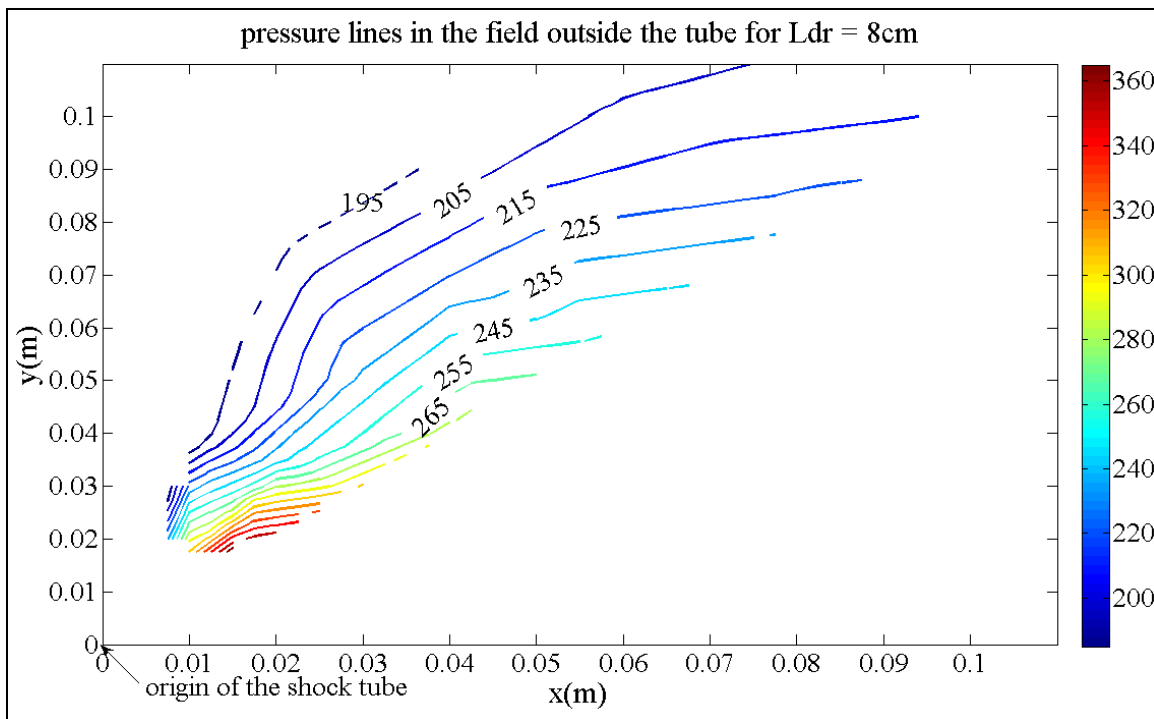


**Figure 3.18:** Contour plot of pressure in the field outside the tube;  $L_{dr} = 8\text{ cm}$

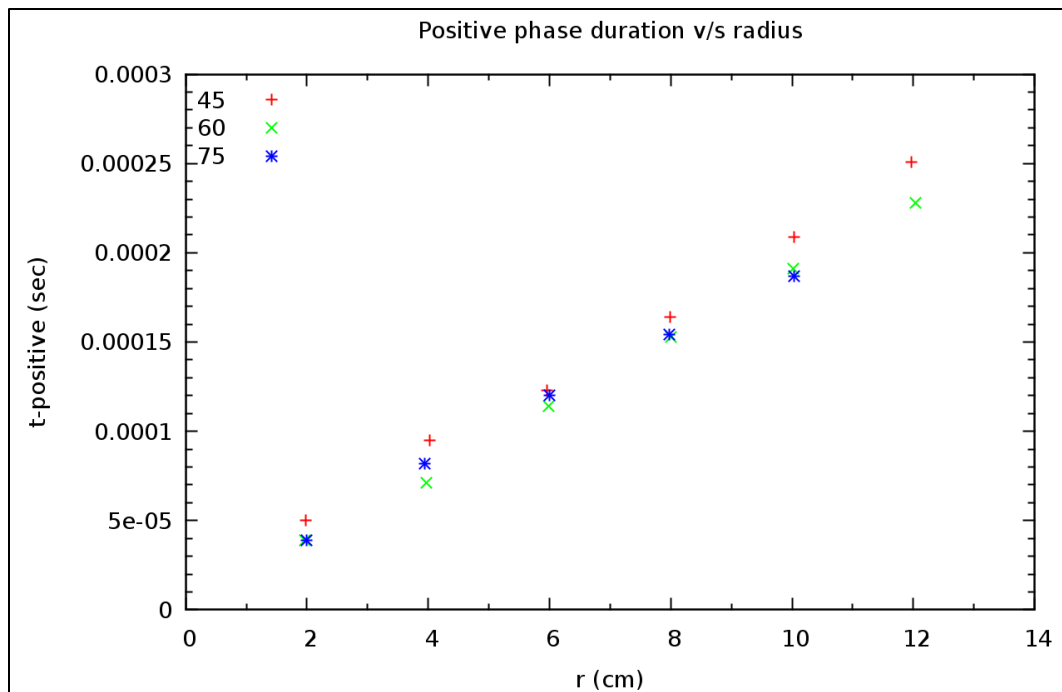


**Figure 3.19:** Positive phase duration versus radius at different angles

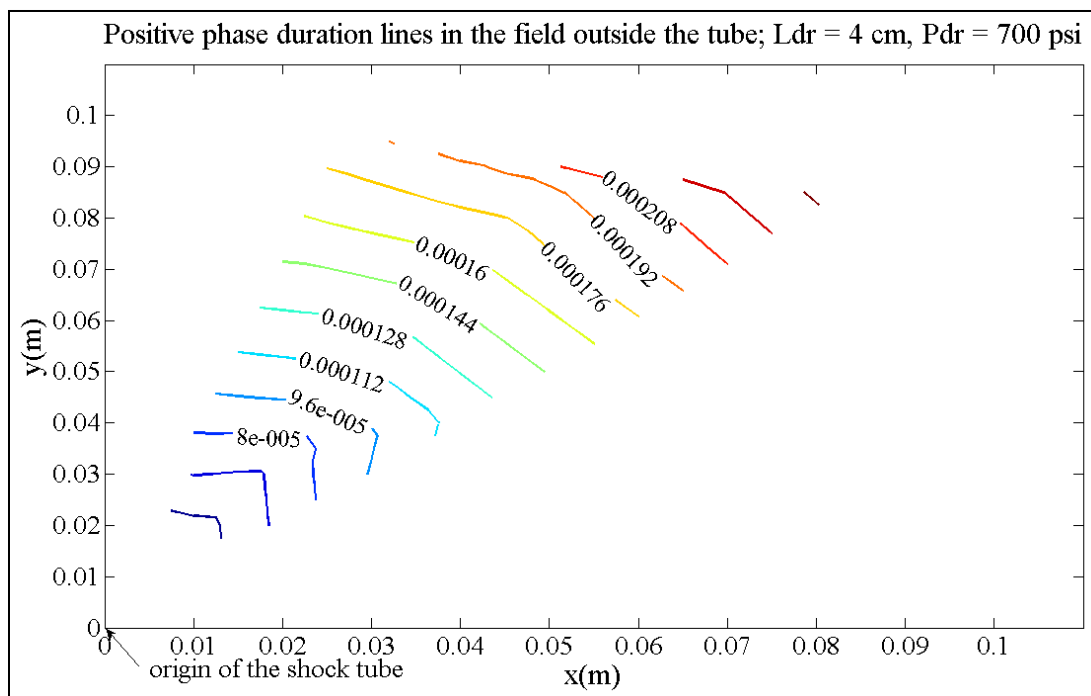


**Figure 3.20:** Positive phase duration (sec) in the field

### 3.8.2.2 Parameter study with different driver lengths

The driver section length is one of the independent variables that are under experimental user control. Input parameters for this study were the same as those presented in Table 3.3, with  $L_{dr}$  being the variable. The probe point chosen for the study is (4, 60).

Figures 3.21 – 3.22 show the variation of peak pressure and positive phase duration with  $L_{dr}$ . These two plots are practically mirror images of each other. The driver length with the lowest peak pressure has the highest positive phase duration. As discussed in Section 2.8, this can be attributed to expansion waves more rapidly overtaking the shock wave in cases with lower  $L_{dr}$ . Hence, the peak value is lowest for  $L_{dr} = 4$  cm, but the t-positive corresponding to the same  $L_{dr}$  is highest for the same reason. However, both peak pressure and positive phase duration are unchanged for  $L_{dr}$  of 8 and 10 cm. The reason for this is that the expansion waves have not yet overtaken the shock front in either case.

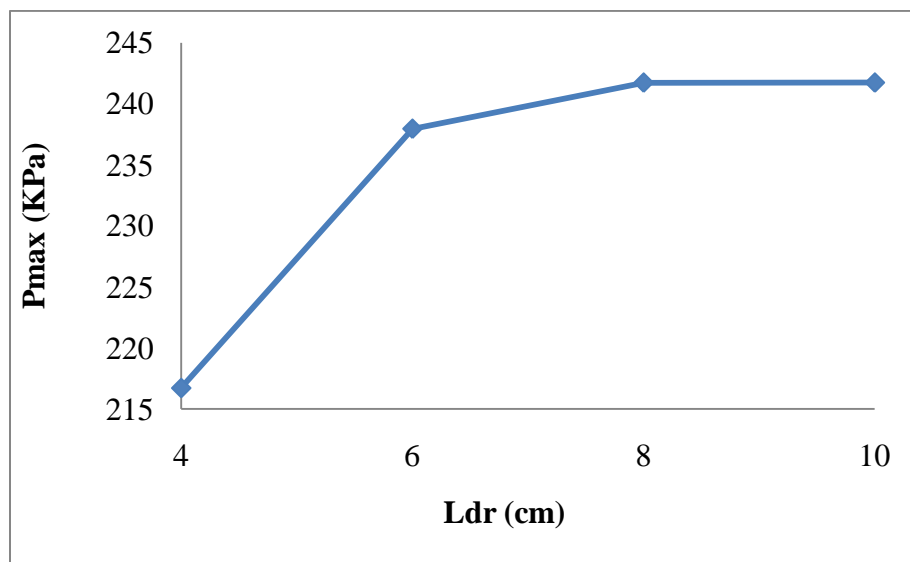


**Figure 3.21:** Peak pressure versus the driver length at (4, 60)

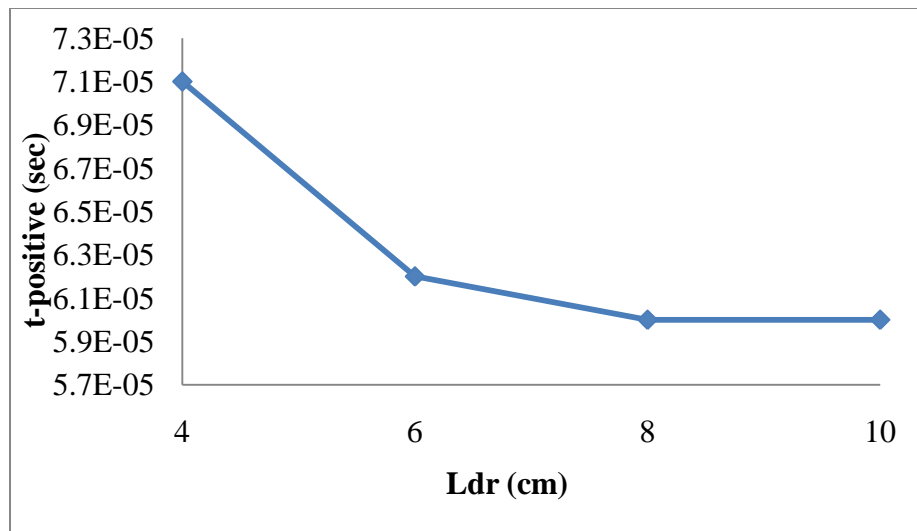


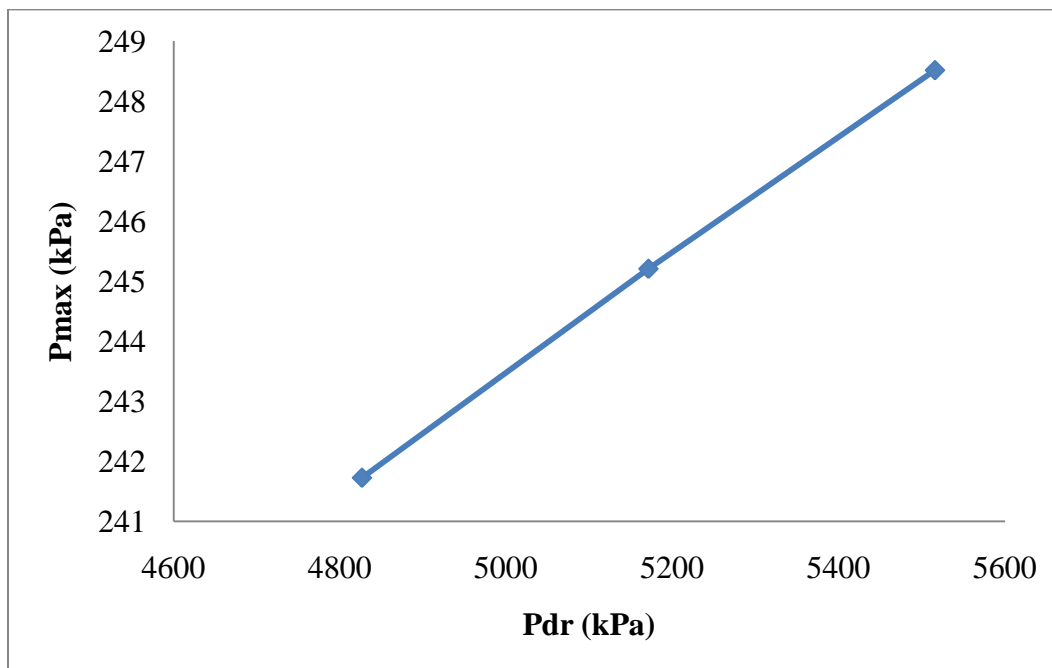
**Figure 3.22:** Positive phase duration versus the driver length at (4, 60)

### 3.8.2.3 Parameter study with different driver pressure

Another controllable variable is the driver pressure. Table 3.4 shows the initial parameters to study the influence of this variable. Peak pressure ( $P_{\max}$ ) increases linearly with driver pressure ( $P_{\text{dr}}$ ) (Figure 3.23), while positive phase duration decreases with the same (Figure 3.24). As shown, the decrement in the positive phase duration, with respect to the  $P_{\text{dr}}$ , is small. For an increase in 50 psi (344.7 kPa), the reduction in the positive phase duration is 0.001 ms. The time axis scales in Figure 3.22 and Figure 3.24 are intentionally the same to compare the influence of  $L_{\text{dr}}$  and  $P_{\text{dr}}$  on positive phase duration.

**Table 3.4:** Initial parameter declaration for the variable  $P_{dr}$  study

Parameters	Values	Units
$L_{dr}$	8	cm
$L_{dn}$	131.45	cm
LR	16.43	-
Finest Resolution (Cell Spacing)	1.25	mm
Density in HP region ( $\rho$ )	variable	$\text{kg/m}^3$
Specific heat ( $C_v$ )	743	J/kg-K
Physical Time of the simulation (t)	0.003	sec
Order of method	second	-
CFL	0.4	-

**Figure 3.23:** Peak pressure versus the driver pressure

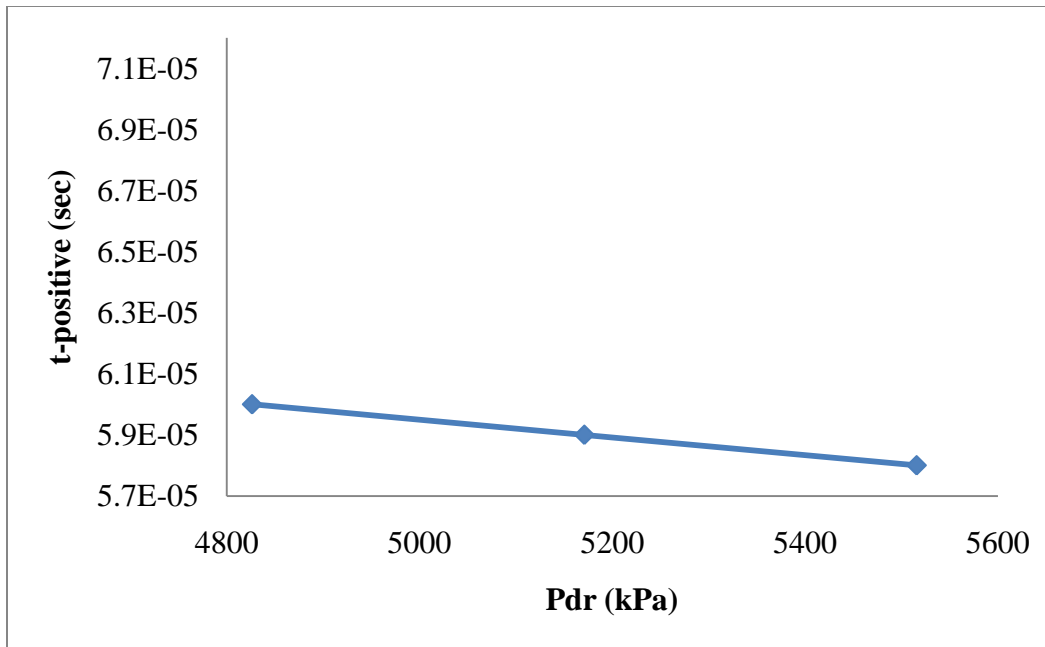


**Figure 3.24:** Positive phase duration versus the driver pressure

### 3.9 Conclusions

- The region above the line at  $45^\circ$  is the recommended region for testing.
- As shown in the results, the region below the line at  $30^\circ$  is in the exhaust gas vent, so it is recommended to avoid that region. At more distant locations, the exhaust gas vent does not influence the region along the line at  $30^\circ$ , but the strength in the blast wave is decreased.
- Increasing the driver pressure increases the strength of the blast wave by increasing the peak pressure.
- Lower driver length results in longer positive phase durations and lower peak pressures, while higher  $P_{dr}$  results in higher peak pressures. Using combinations of both  $L_{dr}$  and  $P_{dr}$ , different impulses can be obtained.

## **4 INTRODUCTION TO 3D SOLUTION**

### **4.1 Introduction**

While the 1D simulations described in Chapter 2 produced an exact solution for shock wave phenomena inside the tube, it is clear that 2D simulations of a wave exiting the tube, described in Chapter 3, could not be expected to produce quantitatively accurate results for a naturally 3D problem. As previously stated, however, it was determined that an understanding of general trends could be accurately and more efficiently explored using the 2D simulations. In order to define the magnitude of error associated with the 2D simulations, 3D simulations were briefly investigated. This chapter gives only a brief introduction to the 3D approach and recommends some ideas for future implementation. Equations 1.8 – 1.10 are the governing equations utilized for the 3D shock tube problem. Input parameters used for both 2D and 3D simulations are almost the same as listed in Table 3.3. except that the value of driver length chosen is 6 cm.

### **4.2 Comparisons between 2D and 3D simulations**

#### **4.2.1 Comparison between 2D and 3D geometry**

In Figure 4.1, the geometry of the 2D and 3D problems is shown in the YZ plane where the X axis, the axis of the shock tube, is perpendicular to the paper. The 2D shock tube is limited to the XY plane; the thickness in the Z direction shown in the 2D portion

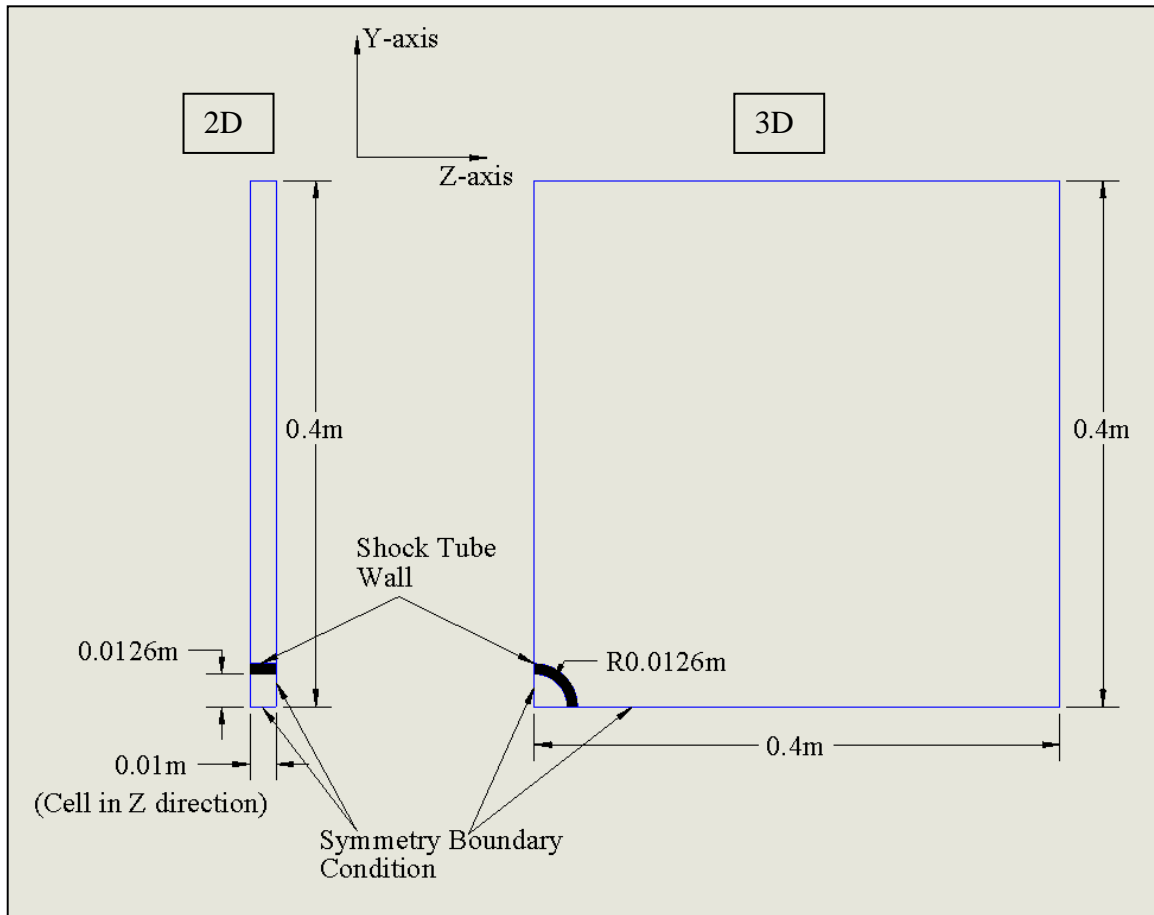
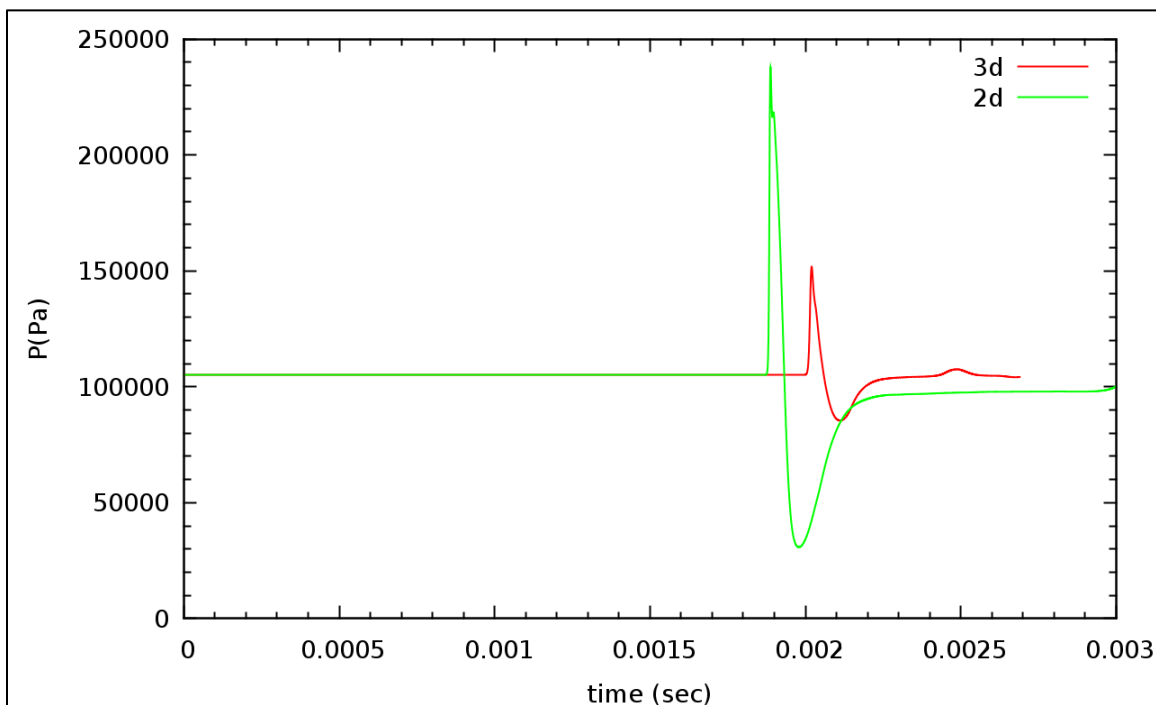


**Figure 4.1:** Geometry comparison of 2D and 3D shock tube problem

of Figure 4.1 is the width of a single cell. The Uintah computational framework is programmed in such a manner that cells need to have all three dimensions regardless of the dimension of the problem. With just one cell in the Z direction for the 2D case, there is no transport of any fluid property in the Z direction and the problem remains 2D. In the case of 3D, one quarter of the cylindrical shock tube is defined, with symmetry boundary conditions on the Y- and Z- faces as it can be seen in Figure 4.1.

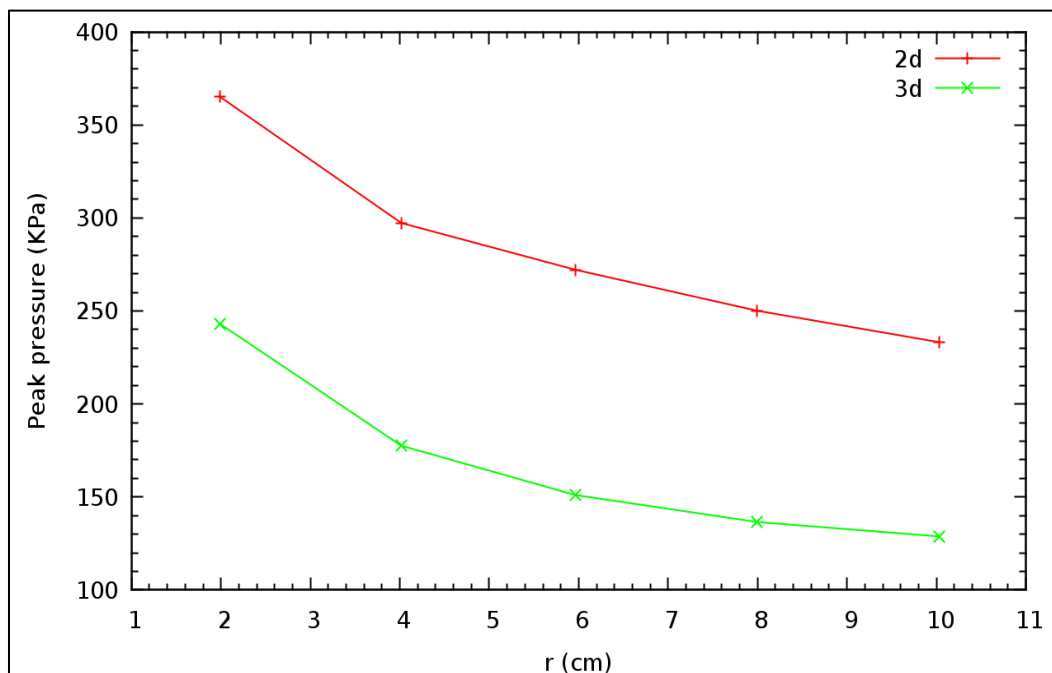
#### 4.2.2 Comparison between 2D and 3D results

Figure 4.2 shows a comparison of pressure profiles at a location of 4 cm and  $60^\circ$  from the origin of the tube for the 2D and 3D simulations. There is clearly a large difference between the peak pressures. Also, the pressure profile for the 3D case lags that of the 2D. Referring to Figure 4.1, the region available outside the tube for the expansion of high pressure gases is obviously different in 3D than in 2D. The volume through which the pressure wave passes is greater in 3D than in 2D for the same radial location outside the tube. Hence, the expansion in 3D space occurs more rapidly than in 2D space, which reduces peak pressure and wave velocity.



**Figure 4.2:** Comparison of pressure profiles from 2D and 3D models at a location 4 cm and  $60^\circ$  from the end of the tube

While a difference in quantitative results was expected, further comparison was performed to determine whether the trends, identified using the 2D model, were appreciable. Figure 4.3 and Figure 4.4 show plots of peak pressure and positive phase duration against the radius along the  $45^\circ$  line, respectively. In Figure 4.3, a nearly constant offset is seen in the peak pressures obtained from 2D and 3D simulations. A similar plot along the  $60^\circ$  line is shown in Appendix A.2. Figure 4.4 shows that there is also a significant difference in positive phase duration between 2D and 3D simulations. In 2D, the relationship between positive phase duration and radius is approximately linear while in 3D, it is nonlinear. It is encouraging, however, to note that overall trends for both peak pressure and positive phase duration, as a function of radius, are similar for both simulation approaches. Trends of positive phase duration in the 3D simulations are shown in Figure 4.5.



**Figure 4.3:** Peak pressure versus radius at  $45^\circ$ ; 2D versus 3D results

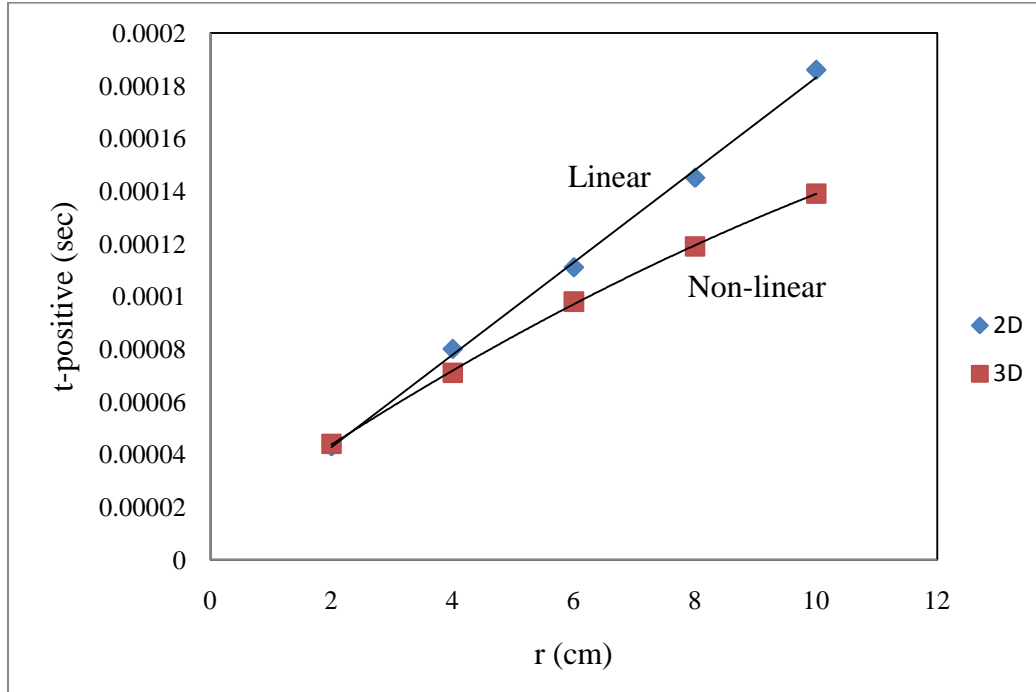


**Figure 4.4:** Positive phase duration versus radius at  $45^\circ$ ; 2D versus 3D results

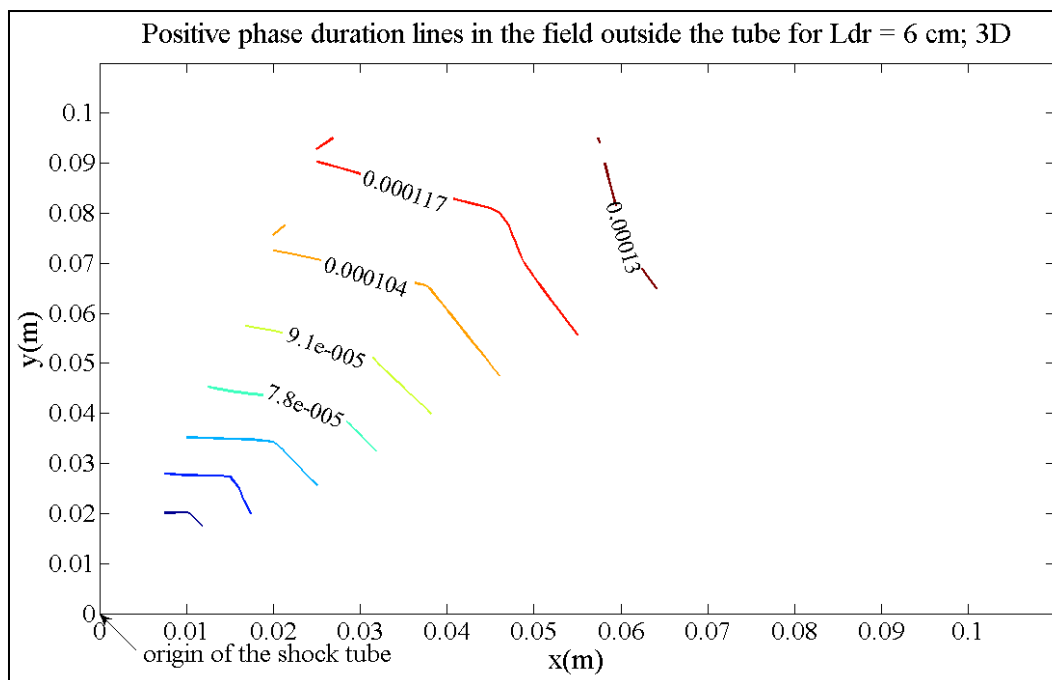


**Figure 4.5:** Positive phase duration (sec) in the field

Further evaluation of 3D results shows that the region-for-testing identified in Chapter 3 is reasonable because the exhaust gas vent similarly expands in the form of a conical jet. Figures 4.6 – 4.7 show 2D and 3D contour plots of the velocity magnitude at nearly the same simulation time. In the case of 2D, the velocities of the pressure wave and the exhaust gas vent are both higher than in the 3D simulations. The shape of the exhaust gas vent in both cases is conical, but the angle the jet makes with the horizontal is smaller in the case of 3D than 2D. This indicates that the region for testing is actually wider in reality, including more area closer to the tube axis, than what is predicted by 2D simulations, so the earlier recommendations can be considered conservative. The lines at  $45^\circ$ ,  $60^\circ$ , and  $75^\circ$  were already recommended for testing. Future work should investigate the line at  $30^\circ$  for reasonable inclusion into the testing region.

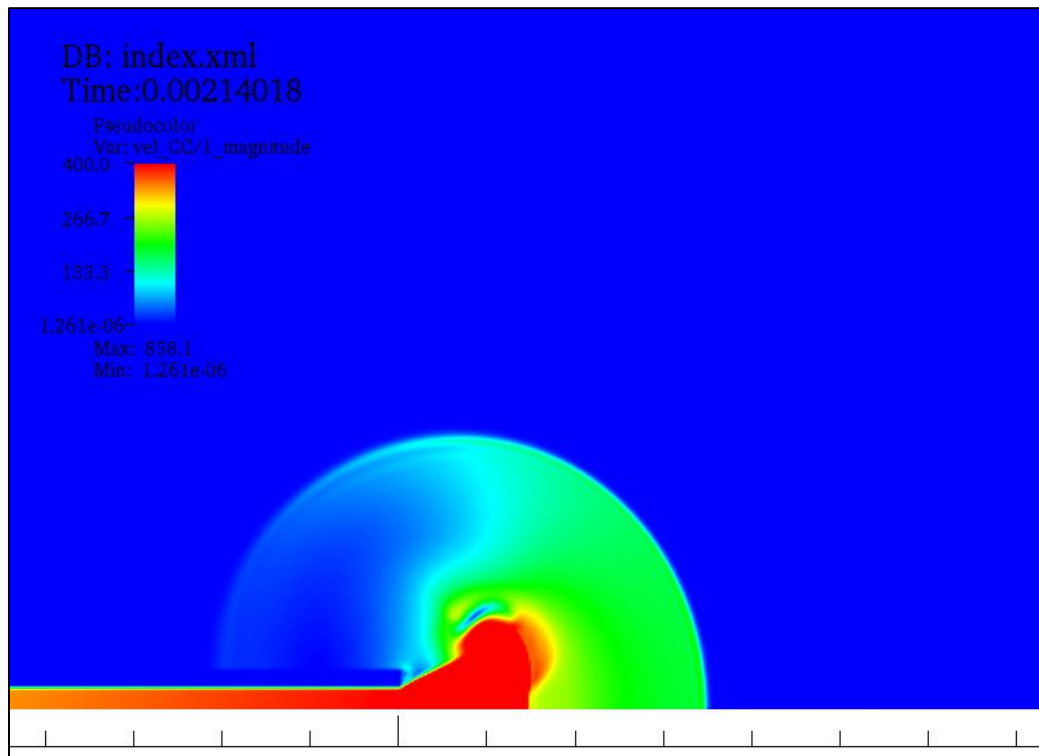


**Figure 4.6:** Magnitude of velocity in 2D simulation

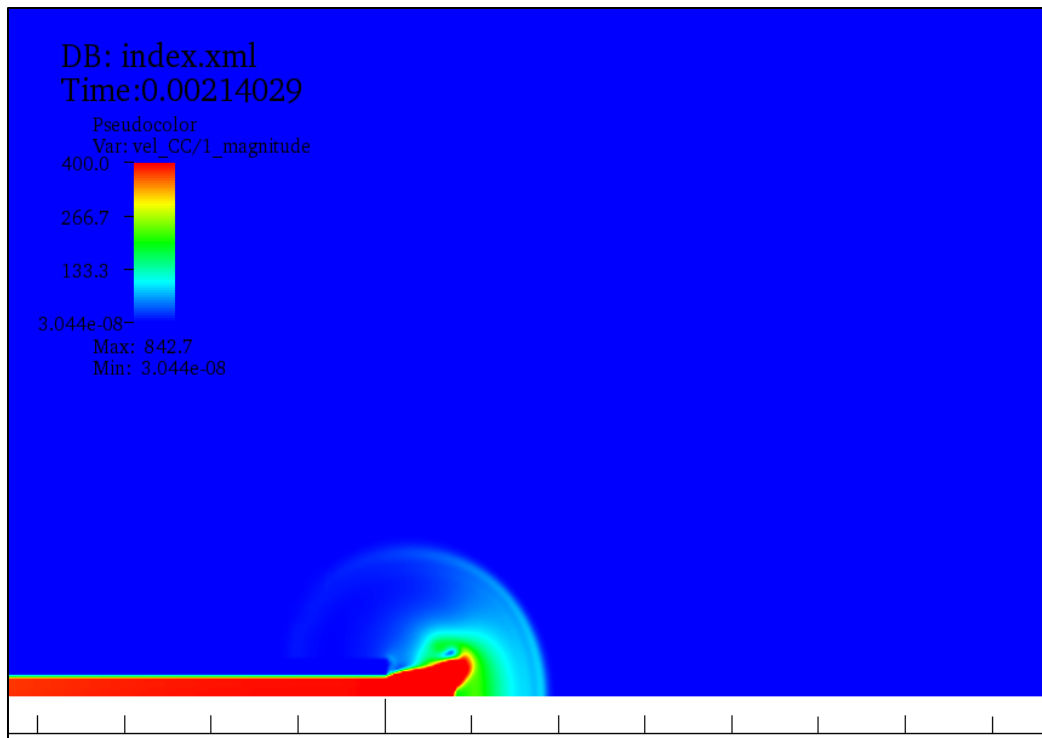


**Figure 4.7:** Magnitude of velocity in 3D simulation

### 4.3 Additional results from 3D simulations

While 3D results have already been discussed in comparison with 2D results, some additional discussion of 3D findings is helpful. Figure 4.8 shows a contour plot of pressure over the whole 3D domain at the time 0.00214 sec. The thick line is the shock tube wall. The vertical slab downstream of and perpendicular to the tube axis is a slice taken to facilitate further visualization of the phenomena outside the tube. Figure 4.9 shows the pressure values on this slice.

The blast wave, exhaust gas vent, and shock tube wall are indicated in Figure 4.9. The blast wave shown in Figure 4.9 appears to be axisymmetric about the x-axis, meaning that the pressure profile does not change about the x-axis of the tube. It thus can be concluded that the imposed symmetry boundary conditions are performing accurately.

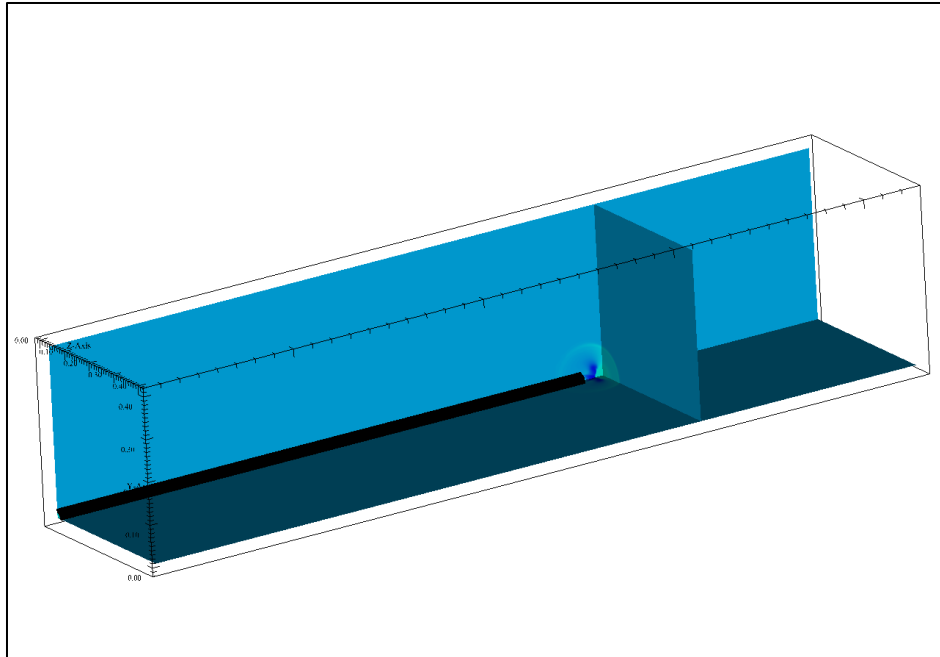


**Figure 4.8:** Contour plot of pressure in 3D at 0.00214029 sec

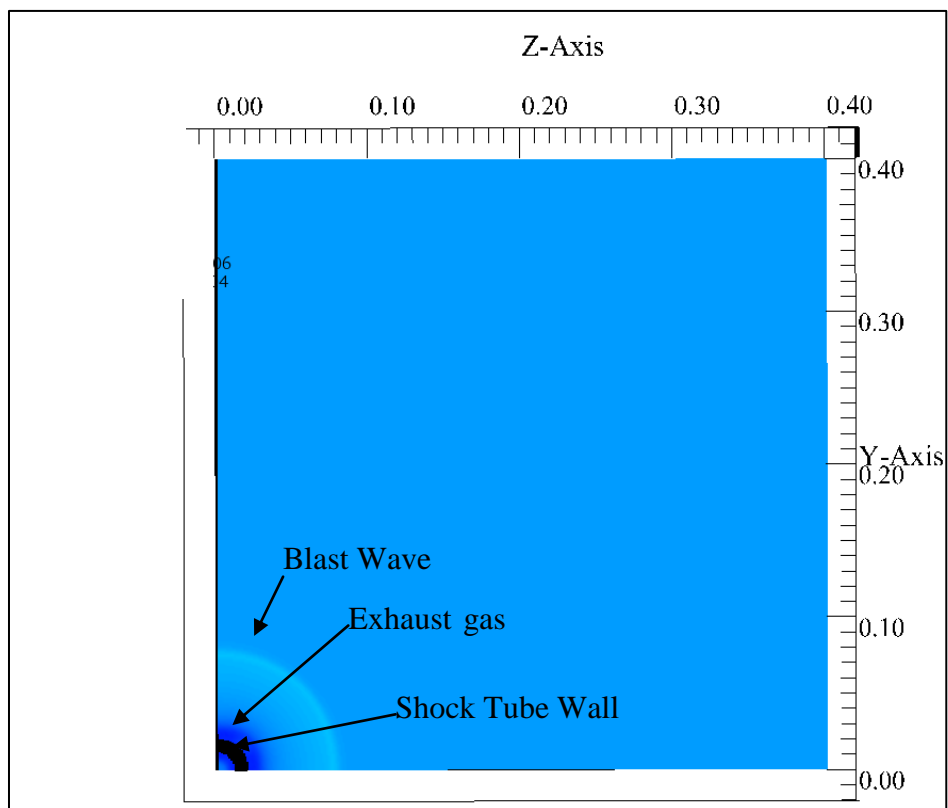


**Figure 4.9:** Projection on the slice indicated in Figure 4.8

#### **4.4 Discussion**

Considering the code is free of bugs, the 3D approach simulates reality more accurately than the 2D approach. However, research carried out with the 2D approach is useful for understanding the physical phenomena of the tube because it provides a reasonable estimate of variable relationships and behavior.

## **5 SUMMARY, CONCLUSIONS, AND FUTURE WORK**

The preceding chapters present results from computational models simulating flow of high pressure gas inside and outside of a compressed gas-driven shock tube. A summary of results, conclusions, and recommendations for the continuation and advancement of this research are given in the present chapter.

### **5.1 Summary**

This research on shock tubes stems from rising concern about blast-induced traumatic brain injury (TBI). It has been hypothesized that brain tissue is damaged by the pressure wave generated during a blast, but the mechanism of tissue injury is unknown. The pressure wave produced by a typical explosion includes a peak pressure, or overpressure, and positive and negative pressure phases; each component of this blast wave may make a unique contribution to injury. A simple device called a shock tube is capable of generating the characteristics associated with the blast wave. A computational model of a shock tube is helpful in experiment design and interpretation.

The formation and advancement of a shock wave inside a tube is characterized using a 1D shock tube simulation, described in Chapter 2, while the expansion of the shock wave outside the tube is characterized using 2D simulation, described in Chapter 3. These simulations are helpful in understanding the influence of experimentally-controllable parameters on peak pressure, positive impulse, and negative impulse of the

resulting pressure wave. In the experimental shock tube, driver pressure and driver length may be varied. Different impulses can be obtained by varying these two parameters and by changing the location of the target in the field. The 2D shock tube simulation is investigated for another significant purpose – to explore the influence of primary blast injury, due to the high pressure wave alone, in the absence of other forces. It was thus important to estimate a region-for-testing that is clear of exhaust gas venting from the tube after passage of the pressure wave.

Two-dimensional simulations were carried out to understand the general trends of the blast wave characteristics for a naturally 3D problem. Hence, the accuracy of 2D simulation results was tested by comparing it with one 3D simulation. Results were presented in Chapter 4.

## 5.2 Conclusions

- The approximate region for testing was quantified in Chapter 2. The region above the line at  $45^{\circ}$  is the recommended region for testing. Below the line at  $45^{\circ}$ , the exhaust gas vent complicates the loading conditions. The exhaust gas vent expands outside the tube in a conical shape. The angle of the cone with the horizontal continuously decreases as it progresses in open space. At later times, the vent clears of the line at  $30^{\circ}$  and so at the distance from 8 cm onwards from the origin of the shock tube, a testing sample can be placed along the line at  $30^{\circ}$ . However, in the case of 3D simulations, the usable area is actually wider, including some of the region below the line at  $45^{\circ}$ .

- Peak pressure increases linearly with driver pressure both inside and outside the tube.
- For very low length ratios (less than 5), the shock exits the tube before the expansion waves overtake the shock front, while for very high length ratios (above 25), expansion waves overtake and degrade the shock, potentially to the point where it has lost much of its strength by the time it reaches its destination.
- Once the expansion waves overtake the shock front, peak pressure starts decreasing but positive phase duration increases. As a result, if a target is placed near the tube, it will experience a relatively high peak pressure over a relatively short duration. If the target is placed at a longer distance from the tube, it will experience a relatively low peak pressure over a relatively long duration. The same positive impulse can be achieved at both locations. The trauma experienced in both locations can then be compared to see which combination is more injurious. High peak pressure can be achieved with high driver pressure while longer positive phase duration can be achieved with shorter driver section lengths.
- The relationship between the dependent and independent variables in 2D and 3D simulations is the same. Three-dimensional simulations quantify the results more accurately than 2D simulations.
- None of three possible boundary condition formulations was accurate in modeling conditions at the outlet boundary of the 1D shock tube simulation. Alternatives to seeking an appropriate boundary condition for this problem include using a longer computational domain and/or stopping the simulation before the shock front reaches the end of the domain to avoid contributions from boundary behavior.

### 5.3 Future work

The work presented in this thesis results mainly from 1D and 2D simulations. However, the 3D simulation naturally simulates reality more accurately than the 2D approach. At the same time, the 2D simulation runs faster than the 3D simulation and demands less computer memory and storage space. Future work could involve combining the advantages of both. One solution would be to convert the Cartesian coordinate system of the Uintah computational framework into the cylindrical coordinate system and then to model the 3D problem as a 2D wedge with axisymmetry about the tube axis.

As discussed already in Chapter 3, the phenomenon of vortex needs more investigation by comparing the static and total energies in the region around the vortex. Also, to see its influence on an actual target, an experimental approach should be adopted.

As discussed in Chapter 1, inside the tube, the variation of the positive and negative phase duration with the driver pressure is bilinear, so more investigation is needed in future to explore this phenomenon.

The ultimate goal of this research on traumatic brain injury is to study the impact of a blast wave on an animal or biological tissue. This thesis is concerned only with characterizing the blast tube system. In the future, fluid-structure interaction can be implemented to simulate deformation of a target.

## APPENDIX

### A.1 Study of boundary conditions

#### A.1.1 Introduction

Every 3D computational domain has 6 faces; they are  $x^-$ ,  $x^+$ ,  $y^-$ ,  $y^+$ , and  $z^-$ ,  $z^+$ . The 1D problem defined is symmetric about the Y and Z axes. In the Uintah computational framework, the application of boundary conditions on each of the six faces is required, irrespective of the dimension of the problem. Hence the “symmetry” boundary condition was applied on all the y and z faces. The remaining faces are  $x^-$  and  $x^+$ . The  $x^-$  face is at the left side of the high pressure region, while the  $x^+$  face is open to the atmosphere.

There are four main fluid properties that need to be defined on the boundary, namely, pressure, temperature, velocity, and density of the gas. These parameters are defined on the boundaries using one of the following three boundary conditions: Dirichlet, Neumann, and Local One Dimensional Inviscid (LODI).

##### A.1.1.1 Dirichlet boundary condition

This boundary condition was named after Johann Peter Gustav Lejeune Dirichlet. It specifies the value a solution takes on the boundary. Thus, if Q is any of the fluid properties mentioned above, according to the Dirichlet boundary condition,

$$Q=C \quad (\text{A.1})$$

where  $C$  is a prescribed constant. In other words, it is a “fixed” boundary condition.

#### A.1.1.2 Neumann boundary condition

This boundary condition is named after Carl Neumann. When imposed on any boundary, it specifies the value of the derivative of the solution. Thus, if  $Q$  is any fluid property, then the Neumann boundary condition states that

$$\frac{dQ}{dx} = C \quad (\text{A.2})$$

where  $C$  is the value of the derivative of  $Q$  with respect to  $x$ . In other words, it's a gradient boundary condition.

#### A.1.1.3 Local One-dimensional Inviscid (LODI)

boundary condition [20]

One-dimensional Navier-Stokes equations near a boundary can be written in terms of the amplitudes ( $L_i$ ) of characteristic waves associated with each characteristic velocity  $\lambda_i$ . For values of  $\lambda_i$ , refer to Equation 9.14 in Poinso's book [20]. These equations are formed by neglecting transverse, viscous, and reaction terms and are hence called one-dimensional inviscid equations. Relations obtained by this method have no physical significance but are used to specify the amplitudes of the waves crossing the boundary.

$$\frac{\partial \rho}{\partial t} + \frac{1}{c^2} \left[ L_2 + \frac{1}{2} (L_5 + L_1) \right] = 0 \quad (\text{A.3a})$$

$$\frac{\partial p}{\partial t} + \frac{1}{2} (L_5 + L_1) = 0 \quad (\text{A.3b})$$

$$\frac{\partial u_1}{\partial t} + \frac{1}{2\rho c} (L_5 - L_1) = 0 \quad (\text{A.3c})$$

$$\frac{\partial u_2}{\partial t} + L_3 = 0 \quad (\text{A.3d})$$

$$\frac{\partial u_3}{\partial t} + L_4 = 0 \quad (\text{A.3e})$$

$$\frac{\partial Y_k}{\partial t} + L_{5+k} = 0 \quad (\text{A.3f})$$

where,  $u_1, u_2, u_3$  are the velocity components in three perpendicular directions and  $Y_k$  is the mass fraction of the  $k^{\text{th}}$  species. By setting different values to  $L_i$  in Equations A.3a – A.3f, nonreflecting boundary condition can be obtained. For more information, please refer to Poinot's book [20].

### A.1.2 Boundary conditions on the left boundary (x- face)

As is mentioned above, the computational domain for the 1D shock tube problem is bounded by x- and x+ faces. Table A.1 represents the boundary conditions that are applied on the x- face. This is a closed inlet boundary problem. This is modeled by setting velocity equal to zero on the inlet boundary using the Dirichlet boundary condition. For the other fluid properties, the Neumann boundary condition is used. Due to the wall, the gradients of both density and pressure set to zero. The gradient of temperature becomes zero due to the inviscid flow assumption.

**Table A.1:** Boundary conditions on the x- face

Fluid Property	BC	Value	Units
Pressure	Neumann	0	Pa
Temperature	Neumann	0	K
Velocity	Dirichlet	0	m/s
Density	Neumann	0	kg/m <sup>3</sup>

### A.1.3 Boundary conditions on the outlet boundary (x+ face)

Boundary conditions for the x+ face were defined as shown in Table A.2. The appropriate boundary condition for pressure was not obvious. As a result, all three possibilities were investigated further. In the case of the Dirichlet boundary condition, the pressure on the x+ face was set to the atmospheric value since the shock tube used for this research is open to the atmosphere. The Neumann boundary condition was defined with the gradient of pressure across the boundary equal to zero. Table A.3 displays the input file parameter settings for the boundary condition simulations.

**Table A.2:** Boundary conditions on the x+ face

Fluid Property	BC	Value	Units
Pressure	Neu/Dir/LODI	Variable	Pa
Temperature	Neumann	0	K
Velocity	Neumann	0	m/s
Density	Neumann	0	kg/m <sup>3</sup>

**Table A.3:** Input parameter declaration to study boundary conditions

Parameters	Values	Units
$L_{dr}$	0.2	m
$L_{dn}$	0.8	m
LR	4	-
Resolution (size of each cell)	1.25	mm
Physical time of the simulation (t)	0.015	sec
Order of method	First	-
CFL	0.4	-

#### A.1.4 Results of the boundary condition study on the x+ face

Figure Figures A.1 and A.2 are the pressure-time plots for all three boundary conditions. In the figures, the pressure-time curves for all three boundary conditions are identical for a short period of time and then separate. This separation is due to the reflected wave from the x+ boundary. Once the wave hits the boundary, it reflects back, and the nature of the reflected wave is different for different boundary conditions. Also, the profiles seem to separate earlier in Figure A.1 (approximately  $t = 0.0034$  sec) than in Figure A.2 (approximately  $t = 0.0046$  sec). This is because for the reflected wave, the probe point at 0.7 m is nearer than the probe point at 0.5 m. To study the pressure wave characteristics, a pure incident shock that is not affected by the reflected wave is required. Hence, the performance of the boundary conditions needs to be evaluated.

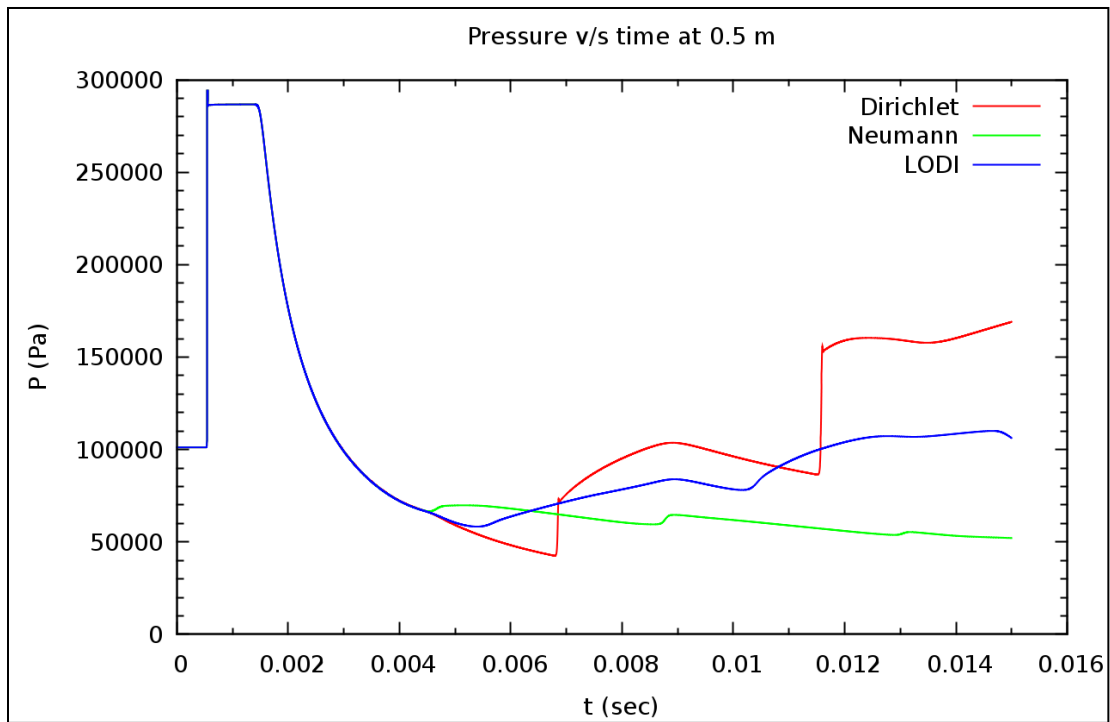


**Figure A.1:** P versus t at  $x = 0.5$  m

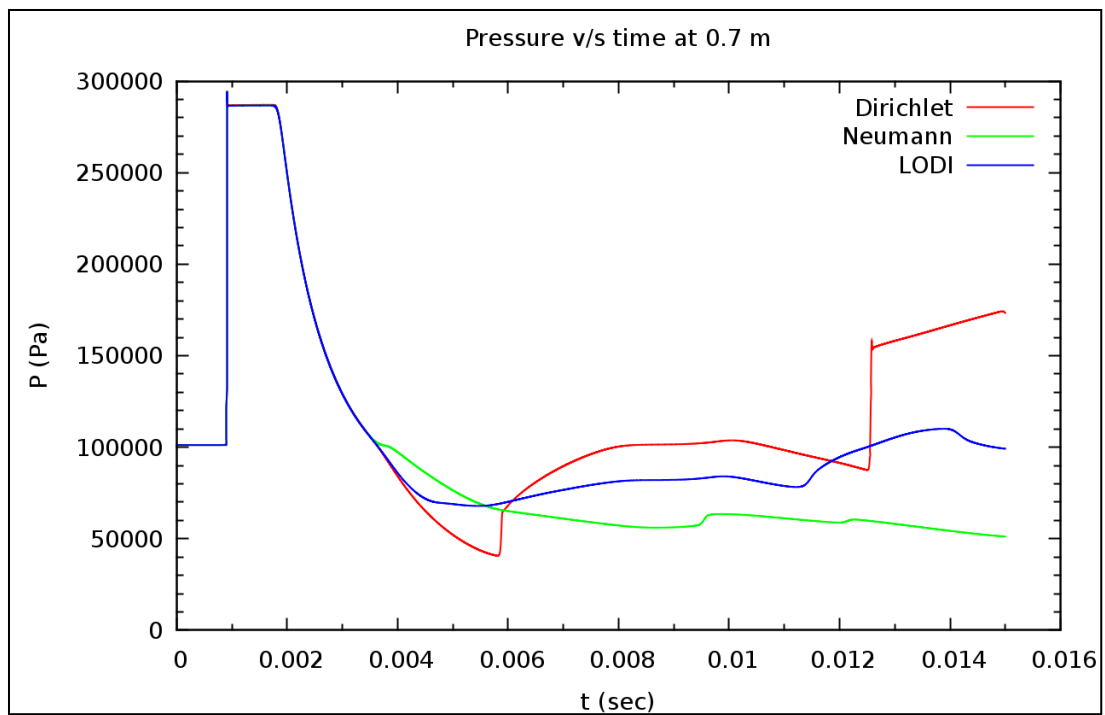


**Figure A.2:** P versus t at  $x = 0.7$  m

Figures A.3 – A.5 show the pressure profile inside the tube at different times. In Figure A.3, as the wave strikes the boundary, reflected waves are generated in a continuous manner and the pressure wave never settles to the atmospheric boundary value. So, the choice of applying the Dirichlet boundary condition on the  $x+$  face was rejected. In Figures A.4 and A.5, after the shock wave reaches the boundary, the pressure at the boundary decreases with time, as expected. Both cases seem reasonable initially, but at later times, due to the Neumann boundary condition, pressure never recovers to the atmospheric value, as can be seen in Figures A.1, A.2, and A.4. The LODI boundary condition, which is described as the nonreflective boundary condition, seems to be the most favorable choice here. Even though it is described as the nonreflective boundary condition, a validation of the same is essential by comparing against the 2D results.

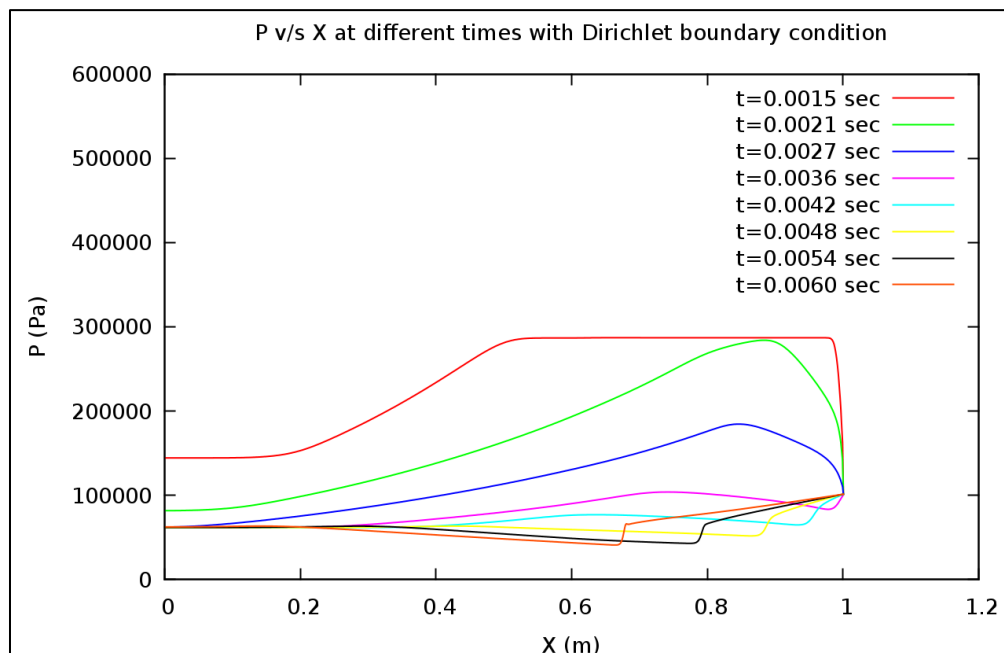


**Figure A.3:** P versus x at different times when Dirichlet BC is imposed

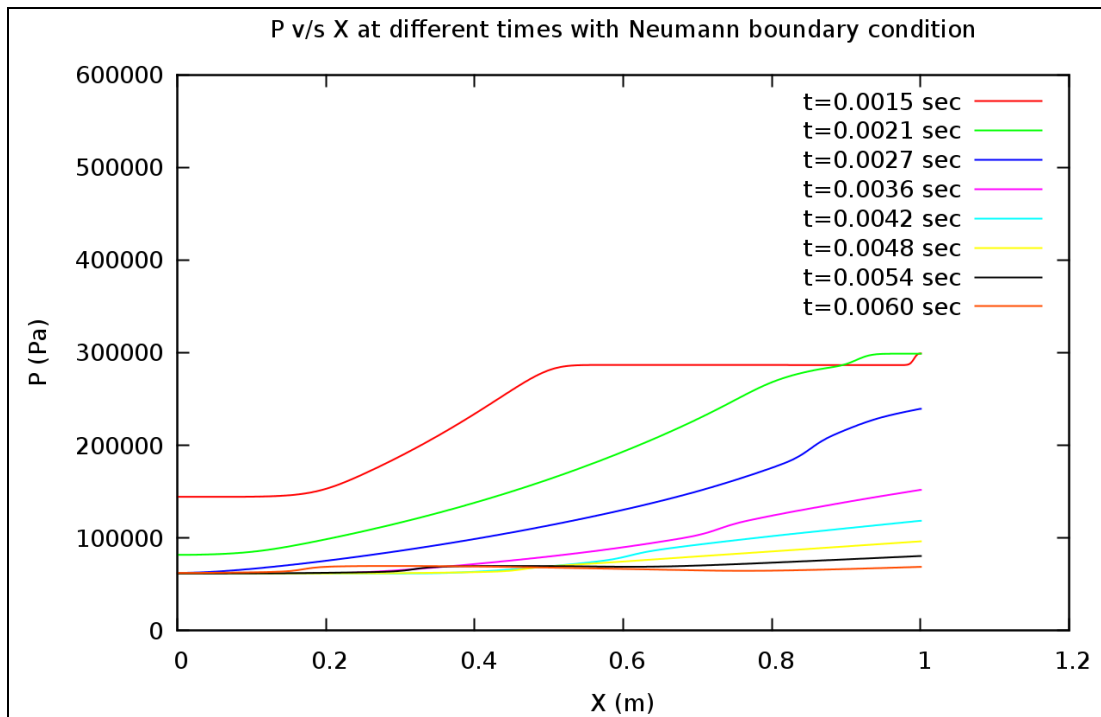


**Figure A.4:** P versus x at different times when Neumann BC is imposed

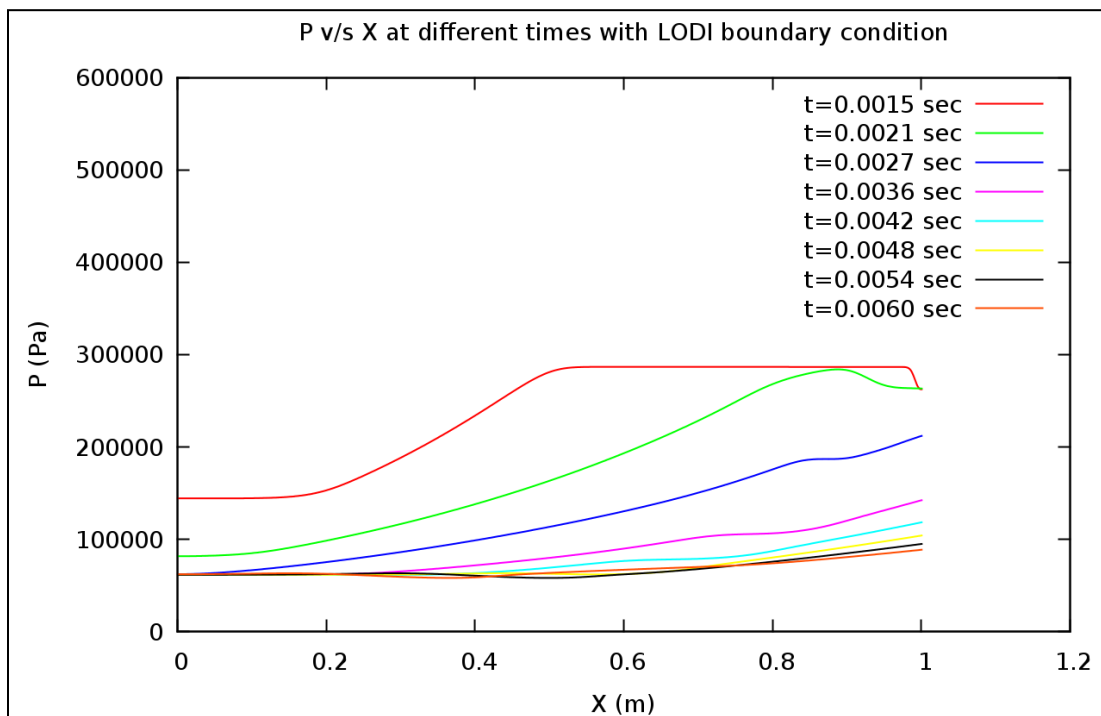


**Figure A.5:** P versus x at different times when LODI BC is imposed

### A.1.5 Comparison of 1D and 2D pressure profiles

The only additional geometrical parameter in the 2D shock tube simulation is the diameter of the tube, and the pressure profile of the shock wave is not dependent on the diametrical dimension of the shock tube (see Equation 1.4). Thus, inside the tube, both 1D and 2D simulations should properly model the wave behavior. The boundary conditions are always applied on the boundaries of the computational domain and the boundaries of the 2D computational domain are extended outside the shock tube exit. Figure A.6 explains the phenomenon more clearly. As shown, the computational domain of the 2D shock tube is far enough from the end of the shock tube that the reflected waves do not affect the pressure profile at the selected probe point; that means it reflects the phenomena of no boundary condition. Figure A.7 shows the comparison of the previously plotted 1D (minus the Dirichlet results) and 2D pressure profiles at  $x = 0.7$  m. From Figure A.7, it is clear that the pressure profile is the same for all three cases before the wave reaches the boundary. The pressure profiles separate once the shock wave, in the 1D case, reaches the boundary. After the comparison with the 2D results, it was observed that none of the boundary conditions replicate the nonreflecting behavior of the shock wave; thus, it was decided to use a longer tube or a shorter duration time to avoid the reflections from the boundary.

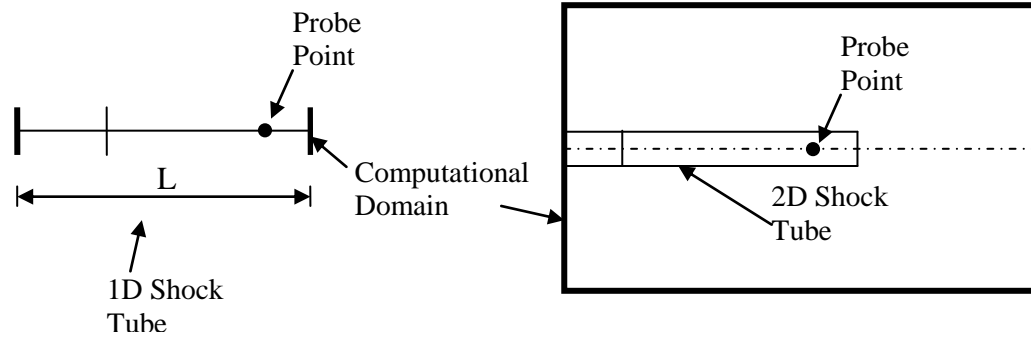


**Figure A.6:** Difference between the computational domain of 1D and 2D shock tubes

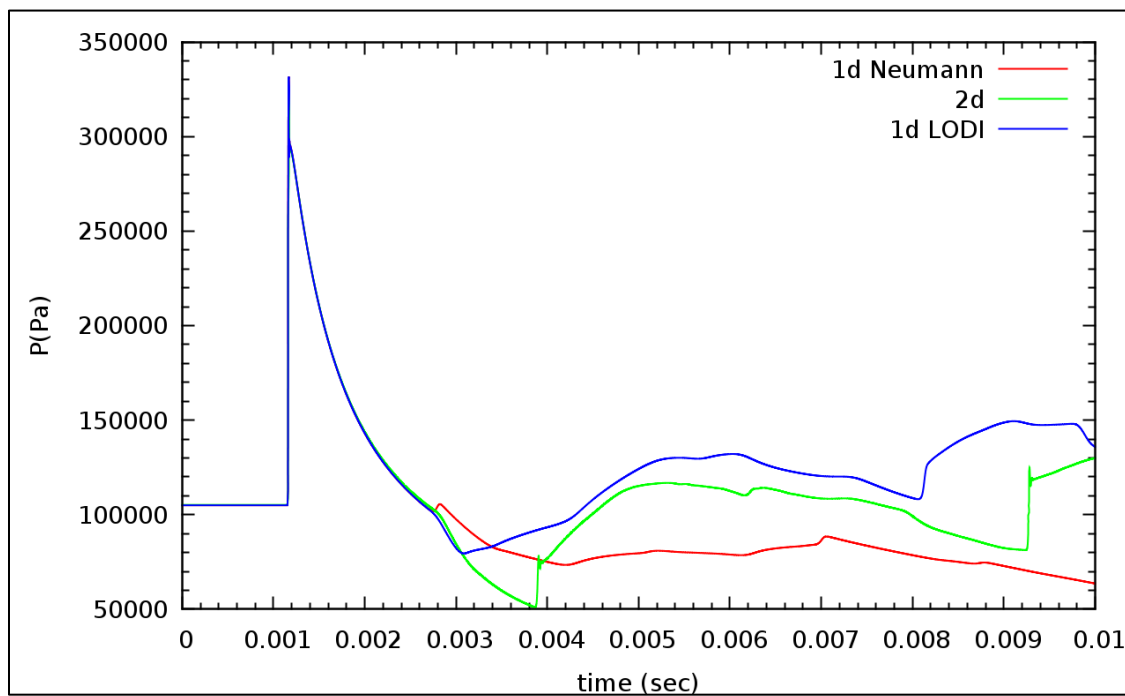


**Figure A.7:** Comparison of the pressure profiles of 1D and 2D at 0.7 m

## A.2 Additional plots

### A.2.1 Pressure contour in the field outside the tube at $L_{dr} = 6$ cm

In Section 3.8.2, the pressure contours for 4 cm and 8 cm driver section length are shown. The initial conditions are listed in Table 3.3 except the in this case,  $L_{dr}$  is 6 cm. Figure A.8 shows the contour plot of peak pressure lines at  $L_{dr}$  of 6 cm.

### A.2.2 Comparison between peak pressures of 2D and 3D

In Section 4.2, the comparison between the peak pressures of 2D and 3D at  $45^\circ$  line is shown. Figure A.9 shows the comparison between peak pressures of 2D and 3D results along the  $60^\circ$  line at all radii.

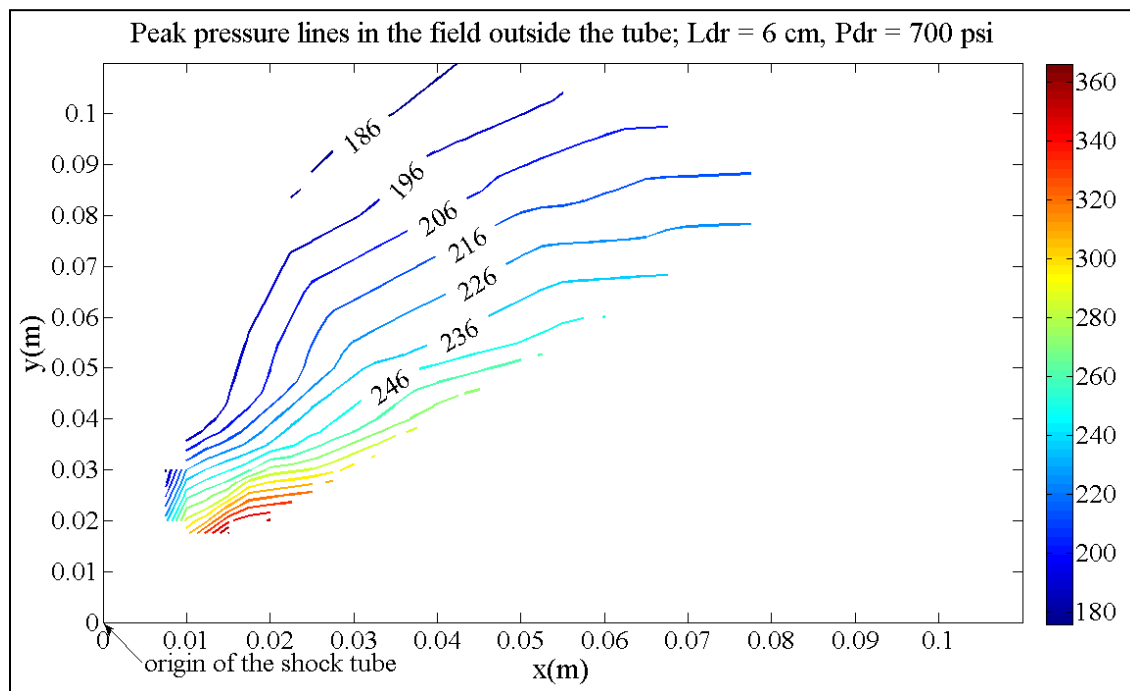


**Figure A.8:** Contour plot of pressure in the field outside the tube;  $L_{dr} = 6$  cm

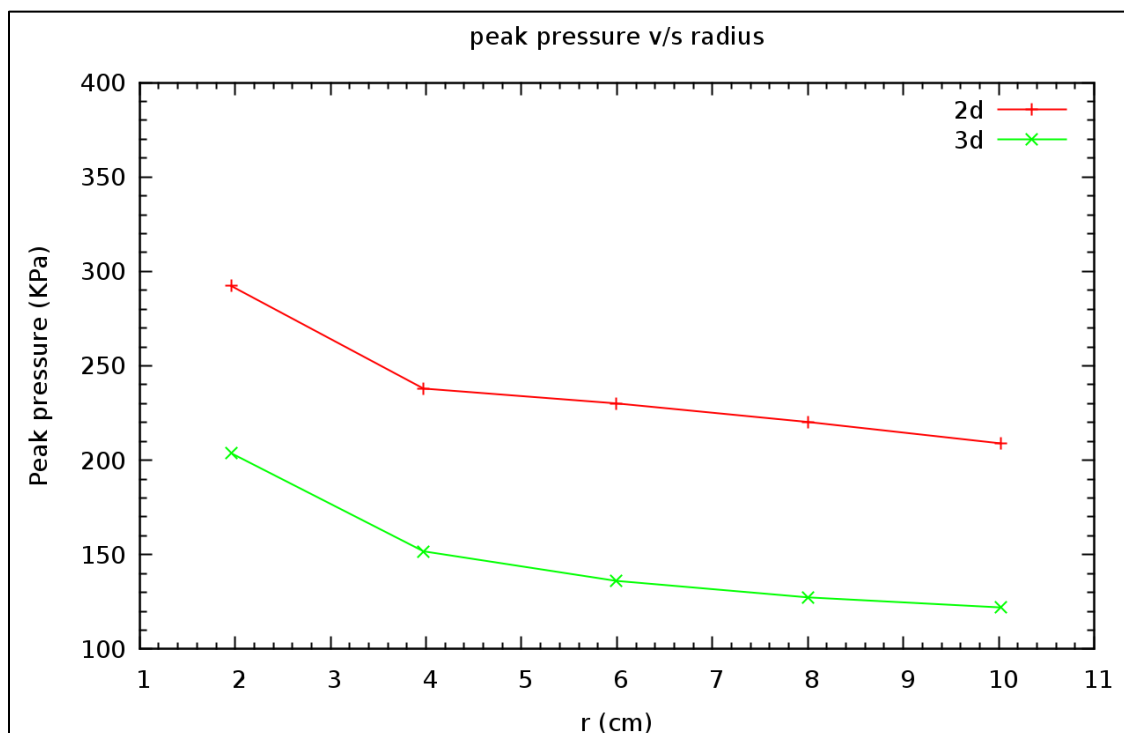


**Figure A.9:** Peak pressure versus radius at  $60^\circ$ ; 2D versus 3D results

### A.2.3 Comparison between the positive phase durations

#### of 2D and 3D results along the $60^\circ$ line

In Section 4.2, the comparison between the positive phase durations of 2D and 3D at  $60^\circ$  line is shown. Figure A.10 shows the comparison between positive phase durations of 2D and 3D results along the  $60^\circ$  line at all radii.

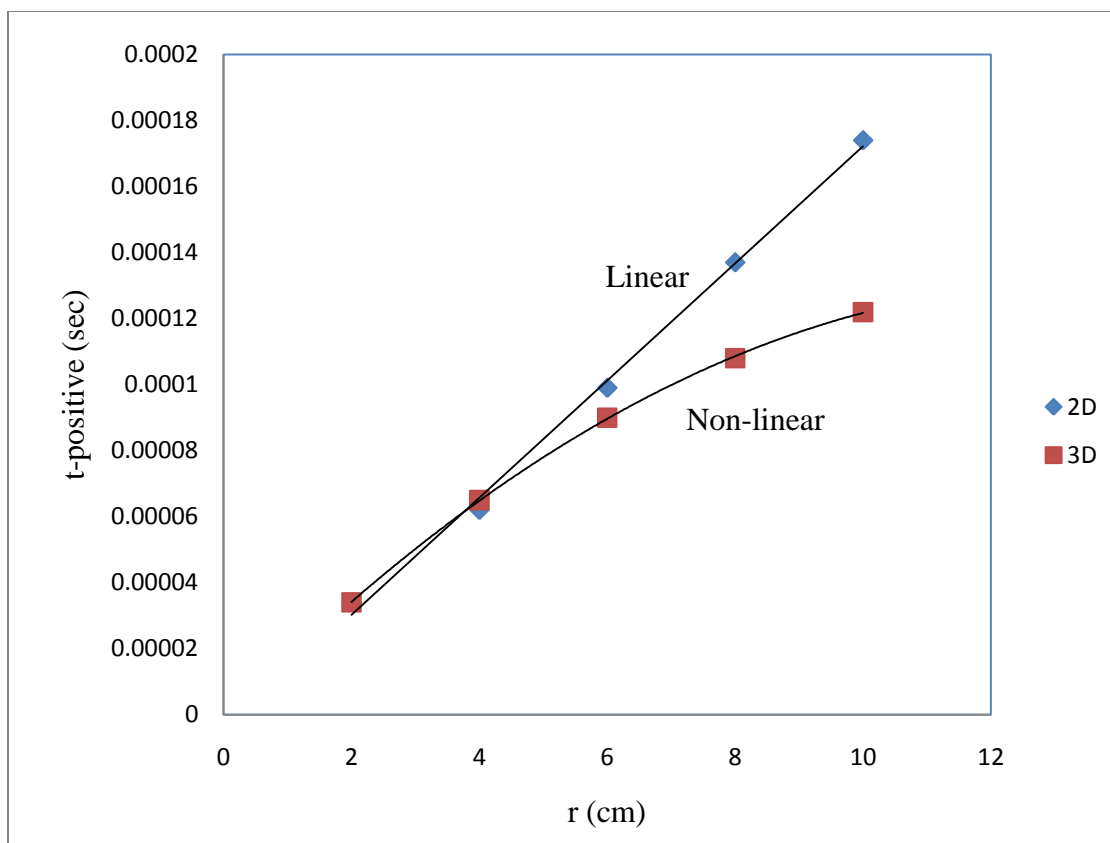


**Figure A.10:** Positive phase duration versus radius at  $60^\circ$ ; 2D versus 3D results

## A.3 Input files

### A.3.1 Input file – 1D shock tube problem

```
<?xml version="1.0" encoding="UTF-8"?>
<Uintah_specification>
  <!--Please use a consistent set of units, (mks, cgs,...)-->
  <Meta>
    <title>Advection test</title>
  </Meta>
  <SimulationComponent type="ice"/>
  <!--
----->
  <!--      T I M E      V A R I A B L E S
-->
  <!--
----->
  <Time>
    <maxTime>          0.01          </maxTime>
    <initTime>         0.0           </initTime>
    <delt_min>         0.0           </delt_min>
    <delt_max>         1.0           </delt_max>
    <delt_init>        1.0e-6        </delt_init>
    <timestep_multiplier>1.0         </timestep_multiplier>
  </Time>
  <!--
----->
  <!--      G R I D      V A R I A B L E S
-->
  <!--
----->
  <Grid>
    <BoundaryConditions>
      <LODI>
        <press_infinity> 1.0132500000010138e+05 </press_infinity>
        <sigma>          0.27             </sigma>
        <ice_material_index> 0           </ice_material_index>
      </LODI>
      <Face side="x-">
        <BCType id="0" label="Pressure" var="Neumann">
          <value> 0. </value>
        </BCType>
        <BCType id="0" label="Velocity" var="Dirichlet">
          <value> [0.,0.,0.] </value>
        </BCType>
        <BCType id="0" label="Temperature" var="Neumann">
          <value> 0. </value>
        </BCType>
        <BCType id="0" label="Density" var="Neumann">
          <value> 0 </value>
        </BCType>
        <BCType id="0" label="SpecificVol" var="computeFromDensity">

```

```

    <value> 0.0 </value>
  </BCType>
</Face>
<Face side="x+">
  <BCType id="0" label="Pressure" var="LODI">
    <value> 0.0 </value>
  </BCType>
  <BCType id="0" label="Velocity" var="Neumann">
    <value> [0.,0.,0.] </value>
  </BCType>
  <BCType id="0" label="Temperature" var="Neumann">
    <value> 0.0 </value>
  </BCType>
  <BCType id="0" label="Density" var="Neumann">
    <value> 0.0 </value>
  </BCType>
  <BCType id="0" label="SpecificVol" var="computeFromDensity">
    <value> 0.0 </value>
  </BCType>
</Face>
<Face side="y-">
  <BCType id="0" label="Symmetric" var="symmetry">
    </BCType>
</Face>
<Face side="y+">
  <BCType id="0" label="Symmetric" var="symmetry">
    </BCType>
</Face>
<Face side="z-">
  <BCType id="0" label="Symmetric" var="symmetry">
    </BCType>
</Face>
<Face side="z+">
  <BCType id="0" label="Symmetric" var="symmetry">
    </BCType>
</Face>
</BoundaryConditions>
<Level>
  <Box label="1">
    <lower> [0,0,0] </lower>
    <upper> [5,1,1] </upper>
    <extraCells> [1,1,1] </extraCells>
    <patches> [80,1,1] </patches>
    <resolution> [4000,1,1] </resolution>
  </Box>
  <periodic>[0, 0, 0]</periodic>
</Level>
</Grid>
<!-- _____ -->
<!-- O U P U T V A R I A B L E S -->
<!-- _____ -->
<DataArchiver>
  <filebase>shockTube.uda</filebase>
  <outputInterval>.0002</outputInterval>
  <save label="press_equil_CC"/>
  <save label="uvel_FCME"/>

```

```

<save label="vvel_FCME"/>
<save label="wvel_FCME"/>
<save label="delP_Dilatate"/>
<save label="press_CC"/>
<save label="mom_L_ME_CC"/>
<save label="rho_CC"/>
<save label="vel_CC"/>
<save label="temp_CC"/>
<save label="sp_vol_CC"/>
<!-- needed for regression tester dat comparisons -->
<save label="KineticEnergy"/>
<save label="TotalIntEng"/>
<checkpoint interval="0.0005" cycle="2"/>
</DataArchiver>
<!-- _____ -->
<!-- I C E P A R A M E T E R S -->
<!-- _____ -->
<CFD>
  <cf1>0.25</cf1>
  <ICE>
    <advection type="FirstOrder"/>
  </ICE>
</CFD>
<!-- _____ -->
<!-- P H Y S I C A L C O N S T A N T S -->
<!-- _____ -->
<PhysicalConstants>
  <gravity> [0,0,0] </gravity>
  <reference_pressure> 101325.0 </reference_pressure>
</PhysicalConstants>
<!-- _____ -->
<!-- Material Properties and Initial Conditions -->
<!-- _____ -->
<MaterialProperties>
  <ICE>
    <material name="gas">
      <EOS type="ideal_gas"> </EOS>
      <dynamic_viscosity> 0.0
</dynamic_viscosity>
      <thermal_conductivity> 0.0
</thermal_conductivity>
      <specific_heat> 717.5 </specific_heat>
      <gamma> 1.4 </gamma>
      <geom_object>
        <difference>
          <box label="wholegrid">
            <min> [0.0, 0.0, 0.0 ] </min>
            <max> [5, 1.5, 1.5 ] </max>
          </box>
          <box label="rightpartition">
            <min> [0.05, 0, 0] </min>
            <max> [5, 1.0, 1.0 ] </max>
          </box>
        </difference>
      </geom_object>
      <res> [2,2,2] </res>
      <velocity> [0.0,0.0,0.0] </velocity>
    </material>
  </ICE>

```

```

        <temperature>      300.0                </temperature>
        <density>          11.768292682926831000 </density>
        <pressure>        1013250.0             </pressure>
    </geom_object>
    <geom_object>
        <box label="rightpartition">           </box>
        <res>              [2,2,2]             </res>
        <velocity>         [0.0,0.0,0.0]       </velocity>
        <temperature>      300.0                </temperature>
        <density>          1.1768292682926831000 </density>
        <pressure>        101325.0             </pressure>
    </geom_object>
</material>
</ICE>
</MaterialProperties>
<!-- _____ -->
<DataAnalysis>
  <Module name="lineExtract">
    <material>gas</material>
    <samplingFrequency> 1e10 </samplingFrequency>
    <timeStart>         0   </timeStart>
    <timeStop>          100 </timeStop>
    <Variables>
      <analyze label="press_CC"/>
      <analyze label="rho_CC"/>
      <analyze label="temp_CC"/>
      <analyze label="vel_CC"/>
    </Variables>
    <lines>
      <line name="X_line">
        <startingPt> [0.05, 0.0, 0.0] </startingPt>
        <endingPt>   [5, 0.0, 0.0] </endingPt>
      </line>
    </lines>
  </Module>
</DataAnalysis>
</Uintah_specification>

```

### A.3.2 Input file – 2D shock tube problem

```

<?xml version='1.0' encoding='ISO-8859-1' ?>
<Uintah_specification>
<!--Please use a consistent set of units, (mks, cgs,...)-->

  <Meta>
    <title> 2D shockTube </title>
  </Meta>

  <SimulationComponent type="rmpmice" />
  <doAMR>true</doAMR>

  <!-- _____ -->
  <!--   T I M E       V A R I A B L E S   -->
  <!-- _____ -->
  <Time>
    <maxTime>          0.003          </maxTime>
    <initTime>         0.0            </initTime>
    <delt_min>         0.0            </delt_min>
    <delt_max>         1.0            </delt_max>
    <delt_init>        1.0e-8        </delt_init>
    <!-- <max_Timesteps> 12</max_Timesteps> -->
    <timestep_multiplier>0.8 </timestep_multiplier>
  </Time>

  <!-- _____ -->
  <!--   G R I D       V A R I A B L E S   -->
  <!-- _____ -->
  <Grid>
  <BoundaryConditions>

    <LODI>
      <press_infinity> 1.0132500000010138e+05 </press_infinity>
      <sigma>          0.27              </sigma>
      <ice_material_index> 1
    </ice_material_index>
    </LODI>

    <Face side = "x-">
      <BCType id = "0"   label = "Pressure"   var = "Neumann">
        <value> 0.0 </value>
      </BCType>
      <BCType id = "all" label = "Velocity"   var = "Dirichlet">
        <value> [0.0,0.,0.] </value>
      </BCType>
      <BCType id = "all" label = "Temperature" var = "Neumann">
        <value> 0.0 </value>
      </BCType>
      <BCType id = "all" label = "Density"    var = "Neumann">
        <value> 0.0 </value>
      </BCType>

```

```

    <BCType id = "all" label = "SpecificVol" var =
"computeFromDensity">
        <value> 0.0 </value>
    </BCType>
</Face>

<Face side = "x+">
    <BCType id = "0" label = "Pressure" var = "Neumann">
        <value> 0.0 </value>
    </BCType>
    <BCType id = "all" label = "Velocity" var = "Neumann">
        <value> [0.,0.,0.] </value>
    </BCType>
    <BCType id = "all" label = "Temperature" var = "Neumann">
        <value> 0.0 </value>
    </BCType>
    <BCType id = "all" label = "Density" var = "Neumann">
        <value> 0.0 </value>
    </BCType>
    <BCType id = "all" label = "SpecificVol" var =
"computeFromDensity">
        <value> 0.0 </value>
    </BCType>
</Face>

<Face side = "y-">
    <BCType id = "all" label = "Symmetric" var = "symmetry">
    </BCType>
</Face>
<Face side = "y+">
    <BCType id = "0" label = "Pressure" var = "Neumann">
        <value> 0.0 </value>
    </BCType>
    <BCType id = "all" label = "Velocity" var = "Neumann">
        <value> [0.,0.,0.] </value>
    </BCType>
    <BCType id = "all" label = "Temperature" var = "Neumann">
        <value> 0.0 </value>
    </BCType>
    <BCType id = "all" label = "Density" var = "Neumann">
        <value> 0.0 </value>
    </BCType>
    <BCType id = "all" label = "SpecificVol" var =
"computeFromDensity">
        <value> 0.0 </value>
    </BCType>
</Face>

<Face side = "z-">
    <BCType id = "all" label = "Symmetric" var = "symmetry">
    </BCType>
</Face>

<Face side = "z+">
    <BCType id = "all" label = "Symmetric" var = "symmetry">

```

```

    </BCTYPE>
  </Face>
</BoundaryConditions>
  <Level>
    <Box label = "1">
      <lower>          [-1.37445, 0.0, -0.005]    </lower>
      <upper>          [0.62555, 0.4, 0.005]    </upper>
      <extraCells>    [1,1,1]                </extraCells>
      <patches>       [10,1,1]               </patches>
    </Box>
    <spacing>         [0.02,0.02,0.01]        </spacing>
  </Level>
</Grid>

<!-- _____ -->
<!-- O U P U T       V A R I A B L E S      -->
<!-- _____ -->
<DataArchiver>
  <filebase>MouseBrains.uda</filebase>
  <outputInterval>2e-5</outputInterval>
  <outputInitTimestep/>
  <save label = "press_CC"/>
<!--   <save label = "vol_frac_CC"/>  -->
  <save label = "sp_vol_CC"/>
  <save label = "vel_CC"/>
  <save label = "rho_CC"/>
  <save label = "temp_CC"/>
  <save label = "mach"/>
  <save label = "mom_L_ME_CC"/>
  <save label = "KineticEnergy"/>
  <save label = "TotalIntEng"/>
  <save label = "mag_grad_press_CC"/>

  <save label = "p.x"      levels="-1"/>
  <save label = "p.volume" levels="-1"/>

  <checkpoint walltimeStart = "600" walltimeInterval = "1200" cycle
= "2"/>
</DataArchiver>

<!-- _____ -->
<!--   I C E       P A R A M E T E R S      -->
<!-- _____ -->
<CFD>
  <cfl>0.4</cfl>
  <ICE>
    <advection type = "SecondOrder"/>
  </ICE>
</CFD>
<MPM>
  <time_integrator>explicit</time_integrator>
</MPM>
<!-- _____ -->
<!--   A M R   G R I D      -->
<!-- _____ -->

```

```

<AMR>
  <ICE>
    <do_Refluxing>          false    </do_Refluxing>
    <orderOfInterpolation>1          </orderOfInterpolation>
    <ClampSpecificVolume> true      </ClampSpecificVolume>

    <Refinement_Criteria_Thresholds>
      <Variable name = "press_CC" value = "1e6" mat1 = "0" />
    </Refinement_Criteria_Thresholds>
    <orderOf_CFI_Interpolation>1</orderOf_CFI_Interpolation>
  </ICE>
  <MPM>
    <min_grid_level>-1</min_grid_level>
    <max_grid_level>-1</max_grid_level>
  </MPM>

  <Regridder type="Tiled">
    <adaptive>              true      </adaptive>
    <min_patch_size>        [[8,8,1]] </min_patch_size>
    <max_levels>            3          </max_levels>
    <cell_refinement_ratio> [[4,4,1]] </cell_refinement_ratio>
    <cell_stability_dilation> [2,2,0]
  </cell_stability_dilation>
    <cell_regrid_dilation> [1,1,0] </cell_regrid_dilation>
    <max_timestep_interval> 100      </max_timestep_interval>
    <min_boundary_cells>    [1,1,0] </min_boundary_cells>
  </Regridder>

  <useLockStep>          true    </useLockStep>
</AMR>

<LoadBalancer type="DLB">
  <dynamicAlgorithm> patchFactorParticles</dynamicAlgorithm>
  <doSpaceCurve>        true      </doSpaceCurve>
  <timestepInterval>    100        </timestepInterval>
</LoadBalancer>

<!-- _____ -->
<!-- P H Y S I C A L C O N S T A N T S -->
<!-- _____ -->
<PhysicalConstants>
  <gravity>              [0,0,0]    </gravity>
  <reference_pressure> 101325.0 </reference_pressure>
</PhysicalConstants>

<!-- _____ -->
<!-- MATERIAL PROPERTIES INITIAL CONDITIONS -->
<!-- _____ -->
<MaterialProperties>
  <MPM>
    <material>
      <density>            8900.0    </density>
      <constitutive_model type = "comp_neo_hook_plastic">
        <useModifiedEOS> true      </useModifiedEOS>

```

```

        <bulk_modulus>      117.0e7      </bulk_modulus>
        <shear_modulus>    43.8e7      </shear_modulus>
        <yield_stress>     70.0e6      </yield_stress>
        <hardening_modulus> 43.8e5      </hardening_modulus>
        <alpha>            0.0          </alpha>
        <strain_limit>     3.05        </strain_limit>
        <reduction_factor> 1.0          </reduction_factor>
    </constitutive_model>
    <thermal_conductivity> 400.0
</thermal_conductivity>
    <specific_heat>      386.0      </specific_heat>
    <geom_object>
        <box label = "shockTubeWall">
            <min>        [-1.37445, 0.0126, -0.1] </min>
            <max>        [0.0, 0.02, 0.1] </max>
        </box>
        <res>            [2,2,1]      </res>
        <velocity>      [0.,0.,0.]    </velocity>
        <temperature>  300.          </temperature>
    </geom_object>
</material>
<contact>
    <type>null</type>
    <materials>        [0]          </materials>
</contact>
</MPM>
<ICE>
    <material name = "Nitrogen">
        <EOS type = "ideal_gas">      </EOS>
    <dynamic_viscosity> 0.0          </dynamic_viscosity>
    <thermal_conductivity> 0.0        </thermal_conductivity>
    <specific_heat>     743.0        </specific_heat>
    <gamma>             1.4          </gamma>
    <geom_object>
        <box label = "HighPressureRegion">
            <min>        [-1.37445, 0.0, -0.1] </min>
            <max>        [-1.31445, 0.0126, 0.1] </max>
        </box>
        <res>            [2,2,1]      </res>
        <velocity>      [0.0,0.0,0.0]    </velocity>
        <temperature>  300.0          </temperature>
        <density>      54.13111378      </density>
        <pressure>    4826330.105217853
    </pressure>
    </geom_object>

    <geom_object>
        <difference>
            <box label = "ComputationalDomain">
                <min>        [-2,-1.0,-0.1] </min>
                <max>        [1.5, 1.0, 0.1] </max>
            </box>
            <union>
                <box label = "shockTubeWall"/>
                <box label = "HighPressureRegion"/>
            </union>
        </difference>
    </geom_object>

```

```

        </difference>
        <res> [2,2,1] </res>
        <velocity> [0.0,0.0,0.0] </velocity>
        <temperature> 300.0 </temperature>
        <density> 1.1792946927374306000e+00 </density>
        <pressure> 101325.0 </pressure>
    </geom_object>
</material>
</ICE>

    <exchange_properties>
        <exchange_coefficients>
            <momentum> [1e15] </momentum>
            <heat> [1e15] </heat>
        </exchange_coefficients>
    </exchange_properties>
</MaterialProperties>
<!-- _____ -->
<DataAnalysis>
    <Module name="lineExtract">

        <material>Nitrogen</material>
        <samplingFrequency> 1e8 </samplingFrequency>
        <timeStart> 1e-7 </timeStart>
        <timeStop> 100 </timeStop>

        <Variables>
            <analyze label="press_CC" matl="0"/>
            <analyze label="rho_CC" matl="1"/>
            <analyze label="temp_CC" matl="1"/>
            <analyze label="vel_CC" matl="1"/>
            <analyze label="mach" matl="1"/>
        </Variables>

        <lines>

        <!-- sensor locations -->

            <line name="S1">
                <startingPt> [-0.093335, 0.0, 0] </startingPt>
                <endingPt> [-0.092096, 0.0, 0] </endingPt>
            </line>

        <!-- sample point outside the tube at 4 cm 60 deg -->

            <line name="P602@r_4_the_60">
                <startingPt> [0.02, 0.03464, 0] </startingPt>
                <endingPt> [0.02127, 0.03464, 0] </endingPt>
            </line>

        </lines>
    </Module>
</DataAnalysis>

</Uintah_specification>

```

### A.3.3 Input file – 3D shock tube problem

```

<?xml version='1.0' encoding='ISO-8859-1' ?>
<Uintah_specification>
<!--Please use a consistent set of units, (mks, cgs,...)-->

  <Meta>
    <title> 2D shockTube </title>
  </Meta>

  <SimulationComponent type="rmpmice" />
  <doAMR>true</doAMR>

  <!-- _____ -->
  <!--           T I M E           V A R I A B L E S           -->
  <!-- _____ -->
  <Time>
    <maxTime>           0.003           </maxTime>
    <initTime>          0.0             </initTime>
    <delt_min>          0.0             </delt_min>
    <delt_max>          1.0             </delt_max>
    <delt_init>         1.0e-8         </delt_init>
    <timestep_multiplier>0.8 </timestep_multiplier>
  </Time>

  <!-- _____ -->
  <!--           G R I D           V A R I A B L E S           -->
  <!-- _____ -->
  <Grid>
  <BoundaryConditions>
    <LODI>
      <press_infinity> 1.013250000010138e+05 </press_infinity>
      <sigma>          0.27             </sigma>
      <ice_material_index> 1           </ice_material_index>
    </LODI>

    <Face side = "x-">
      <BCType id = "0" label = "Pressure" var = "Neumann">
        <value> 0.0 </value>
      </BCType>
      <BCType id = "all" label = "Velocity" var = "Dirichlet">
        <value> [0.0,0.,0.] </value>
      </BCType>
      <BCType id = "all" label = "Temperature" var = "Neumann">
        <value> 0.0 </value>
      </BCType>
      <BCType id = "all" label = "Density" var = "Neumann">
        <value> 0.0 </value>
      </BCType>
      <BCType id = "all" label = "SpecificVol" var =
"computeFromDensity">
        <value> 0.0 </value>
      </BCType>

```

```

</Face>

<Face side = "x+">
  <BCType id = "0" label = "Pressure" var = "Neumann">
    <value> 0.0 </value>
  </BCType>
  <BCType id = "all" label = "Velocity" var = "Neumann">
    <value> [0.,0.,0.] </value>
  </BCType>
  <BCType id = "all" label = "Temperature" var = "Neumann">
    <value> 0.0 </value>
  </BCType>
  <BCType id = "all" label = "Density" var = "Neumann">
    <value> 0.0 </value>
  </BCType>
  <BCType id = "all" label = "SpecificVol" var =
"computeFromDensity">
    <value> 0.0 </value>
  </BCType>
</Face>

<Face side = "y-">
  <BCType id = "all" label = "Symmetric" var = "symmetry">
  </BCType>
</Face>
<Face side = "y+">
  <BCType id = "0" label = "Pressure" var = "Neumann">
    <value> 0.0 </value>
  </BCType>
  <BCType id = "all" label = "Velocity" var = "Neumann">
    <value> [0.,0.,0.] </value>
  </BCType>
  <BCType id = "all" label = "Temperature" var = "Neumann">
    <value> 0.0 </value>
  </BCType>
  <BCType id = "all" label = "Density" var = "Neumann">
    <value> 0.0 </value>
  </BCType>
  <BCType id = "all" label = "SpecificVol" var =
"computeFromDensity">
    <value> 0.0 </value>
  </BCType>
</Face>

<Face side = "z-">
  <BCType id = "all" label = "Symmetric" var = "symmetry">
  </BCType>
</Face>

<Face side = "z+">
  <BCType id = "all" label = "Symmetric" var = "symmetry">
  </BCType>
</Face>
</BoundaryConditions>
<Level>

```

```

        <Box label = "1">
            <lower>          [-1.37445, 0.0, 0.0] </lower>
            <upper>          [0.62555, 0.4, 0.4] </upper>
            <extraCells>     [1,1,1]           </extraCells>
            <patches>        [10,1,1]          </patches>
        </Box>
        <spacing>           [0.02,0.02,0.02]   </spacing>
    </Level>
</Grid>

<!-- _____ -->
<!-- O U P U T       V A R I A B L E S           -->
<!-- _____ -->
<DataArchiver>
    <filebase>MouseBrains.uda</filebase>
    <outputInterval>2e-5</outputInterval>
    <outputInitTimestep/>
    <save label = "press_CC"/>
    <save label = "sp_vol_CC"/>
    <save label = "vel_CC"/>
    <save label = "rho_CC"/>
    <save label = "temp_CC"/>
    <save label = "mach"/>
    <save label = "mom_L_ME_CC"/>
    <save label = "KineticEnergy"/>
    <save label = "TotalIntEng"/>
    <save label = "mag_grad_press_CC"/>
    <save label = "p.x"      levels="-1"/>
    <save label = "p.volume" levels="-1"/>

    <checkpoint walltimeStart = "600" walltimeInterval = "1200" cycle
= "2"/>
</DataArchiver>

<!-- _____ -->
<!-- I C E       P A R A M E T E R S           -->
<!-- _____ -->
<CFD>
    <cfl>0.4</cfl>
    <ICE>
        <advection type = "SecondOrder"/>
    </ICE>
</CFD>
<MPM>
    <time_integrator>explicit</time_integrator>
</MPM>
<!-- _____ -->
<!-- A M R       G R I D                       -->
<!-- _____ -->
<AMR>
    <ICE>
        <do_Refluxing>          false      </do_Refluxing>
        <orderOfInterpolation>1          </orderOfInterpolation>
        <ClampSpecificVolume> true       </ClampSpecificVolume>
        <Refinement_Criteria_Thresholds>
            <Variable name="press_CC" value="1e6" matl="0"/>

```

```

    </Refinement_Criteria_Thresholds>
    <orderOf_CFI_Interpolation>1</orderOf_CFI_Interpolation>
</ICE>
<MPM>
  <min_grid_level>-1</min_grid_level>
  <max_grid_level>-1</max_grid_level>
</MPM>
<Regridder type="Tiled">
  <adaptive> true </adaptive>
  <min_patch_size> [[8,8,8]] </min_patch_size>
  <max_levels> 3 </max_levels>
  <cell_refinement_ratio> [[4,4,4]] </cell_refinement_ratio>
  <cell_stability_dilation> [2,2,2] </cell_stability_dilation>
  <cell_regrid_dilation> [1,1,2] </cell_regrid_dilation>
  <max_timestep_interval> 100 </max_timestep_interval>
  <min_boundary_cells> [1,1,1] </min_boundary_cells>
  <dynamic_size>true</dynamic_size>
</Regridder>
<useLockStep> true </useLockStep>
</AMR>
<LoadBalancer type="DLB">
  <dynamicAlgorithm> patchFactorParticles</dynamicAlgorithm>
  <doSpaceCurve> true </doSpaceCurve>
  <timestepInterval> 100 </timestepInterval>
  <outputNthProc>1</outputNthProc>
  <cellCost>1</cellCost>
  <particleCost>1.25</particleCost>
  <patchCost>16</patchCost>
  <gainThreshold>0.050000000000000003</gainThreshold>
  <profileTimestepWindow>10</profileTimestepWindow>
  <doCostProfiling>true</doCostProfiling>
  <levelIndependent>true</levelIndependent>
  <collectParticles>false</collectParticles>
</LoadBalancer>

<!-- _____ -->
<!-- P H Y S I C A L C O N S T A N T S -->
<!-- _____ -->
<PhysicalConstants>
  <gravity> [0,0,0] </gravity>
  <reference_pressure> 101325.0 </reference_pressure>
</PhysicalConstants>

<!-- _____ -->
<!-- MATERIAL PROPERTIES INITIAL CONDITIONS -->
<!-- _____ -->
<MaterialProperties>
<MPM>
  <material>
    <density> 8900.0 </density>
    <constitutive_model type="comp_neo_hook_plastic">
      <useModifiedEOS> true </useModifiedEOS>
      <bulk_modulus> 117.0e7 </bulk_modulus>
      <shear_modulus> 43.8e7 </shear_modulus>
      <yield_stress> 70.0e6 </yield_stress>
      <hardening_modulus> 43.8e5 </hardening_modulus>
    </constitutive_model>
  </material>
</MPM>

```

```

    <alpha>                0.0                </alpha>
    <strain_limit>         3.05                </strain_limit>
    <reduction_factor>    1.0                </reduction_factor>
  </constitutive_model>
  <thermal_conductivity> 400.0                </thermal_conductivity>
  <specific_heat>        386.0                </specific_heat>
  <geom_object>
    <difference>
      <cylinder label="outer cylinder">
        <bottom>          [-1.37445, 0.0, 0.0] </bottom>
        <top>             [0.0, 0.0, 0.0]  </top>
        <radius>          0.02             </radius>
      </cylinder>
      <cylinder label="inner cylinder">
        <bottom>          [-1.37445, 0.0, 0.0] </bottom>
        <top>             [0.0, 0.0, 0.0]  </top>
        <radius>          0.0126           </radius>
      </cylinder>
    </difference>
    <res>                 [2,2,1]           </res>
    <velocity>            [0.,0.,0.]        </velocity>
    <temperature>        300.              </temperature>
  </geom_object>
</material>
<contact>
  <type>null</type>
  <materials>            [0]              </materials>
</contact>
</MPM>
<ICE>
  <material name="Nitrogen">
    <EOS type="ideal_gas">                </EOS>
  <dynamic_viscosity>    0.0                </dynamic_viscosity>
  <thermal_conductivity> 0.0                </thermal_conductivity>
  <specific_heat>        743.0              </specific_heat>
  <gamma>                1.4                </gamma>
  <geom_object>
    <cylinder label="HighPressureRegion">
      <bottom>          [-1.37445,0.0,0.0] </bottom>
      <top>             [-1.31445, 0.0, 0.0] </top>
      <radius>          0.0126             </radius>
    </cylinder>
    <res>                 [2,2,1]           </res>
    <velocity>            [0.0,0.0,0.0]      </velocity>
    <temperature>        300.0              </temperature>
    <density>            54.13111378        </density>
    <pressure>           4826330.105217853   </pressure>
  </geom_object>
  <geom_object>
    <difference>
      <box label="Computationaldomain">
        <min>            [-2, -1.0, -1.0] </min>
        <max>            [1, 1.0, 1.0]    </max>
      </box>
    <union>
      <difference>

```

```

        <cylinder label="outer cylinder"/>
        <cylinder label="inner cylinder"/>
    </difference>
    <cylinder label="HighPressureRegion"/>
</union>
</difference>
<res>                [2,2,1]                </res>
<velocity>           [0.0,0.0,0.0]           </velocity>
<temperature>        300.0                    </temperature>
<density>            1.1792946927374306000e+00 </density>
<pressure>           101325.0                 </pressure>
</geom_object>
</material>
</ICE>
<exchange_properties>
  <exchange_coefficients>
    <momentum>         [1e15]                 </momentum>
    <heat>              [1e15]                 </heat>
  </exchange_coefficients>
</exchange_properties>
</MaterialProperties>
<!-- _____ -->
<DataAnalysis>
  <Module name="lineExtract">
    <material>Nitrogen</material>
    <samplingFrequency> 1e8 </samplingFrequency>
    <timeStart>         1e-7 </timeStart>
    <timeStop>          100 </timeStop>

    <Variables>
      <analyze label="press_CC" matl="0"/>
      <analyze label="rho_CC" matl="1"/>
      <analyze label="temp_CC" matl="1"/>
      <analyze label="vel_CC" matl="1"/>
      <analyze label="mach" matl="1"/>
    </Variables>

    <lines>
<!--      sensor locations          -->

      <line name="S1">
        <startingPt>   [-0.093335, 0.0, 0] </startingPt>
        <endingPt>     [-0.092096, 0.0, 0] </endingPt>
      </line>

<!--      sample point outside the tube at 4 cm 60 deg    -->

      <line name="P602@r_4_the_60">
        <startingPt>   [0.02, 0.03464, 0] </startingPt>
        <endingPt>     [0.02127, 0.03464, 0] </endingPt>
      </line>
    </lines>
  </Module>
</DataAnalysis>

</Uintah_specification>

```

### A.3.4 Data processing

Once the simulation is run, the data is saved in the form of matrix inside the text files. These text files are huge in numbers. Hence, the C-shell and Octave scripts were written to extract the useful data from large number of files. C-shell script loops over each and every directory and selects the required file specified by different conditions in the script, while Octave script performs operation on the selected file to calculate peak pressure, positive phase duration, and negative phase duration.

#### A.3.4.1 C-shell script

```
#!/bin/csh

# find all files named "*_k0 in L-2 directory"
set these = `find . -name "*_FO"`

#echo $these

/bin/rm -f mf1.dat

echo "  x(m)          Pmax (KPa)          tpmx(sec)    tpos(sec)    tneg(sec)
Ldr" > mf1.dat

#(deg)          (cm)          (KPa)          (KPa)          (Sec)
(Sec)          (Sec)          (Sec)

foreach X ( $these[*]:q )

  # echo "now post processing $X "
  # remove the first line in the file and save it as a tmp
  sed /"press_CC"/d <$X >tmp

  # octave script
  /home/mukul/Octave_codes/tpos_1d tmp >> mf1.dat

  # remove the temporary file tmp
  /bin/rm tmp

end

sort -n mf1.dat > mf.dat
rm -rf mf1.dat
exit
```

## A.3.4.2 Octave script

```

#!/usr/bin/octave -qf

clear all;
close all;
file = argv ();
file_1=sprintf('%s',file);
f=load(file_1);

for i=1:length(f)
    if (f(i,5)>1.01325E+05)
        break
    end
end
R1 = i;
t1 = f(i,4);

for i=R1:length(f)
    if (f(i,5)<1.013250E+05)
        break
    end
end
R2 = i;
t2 = f(i,4);

for i=R2:length(f)
    if (f(i,5)>1.01325E+05)
        break
    end
end

R3 = i;
t3 = f(i,4);
tpos = (t2-t1);
tneg = (t3-t2);
Pmax = max(f(:,5));
Pmin = min(f(:,5));

k1=find(f(:,5)=Pmax);
k2=find(f(:,5)=Pmin);
h1=f(k1,1:5);
h2=f(k2,1:5);
x=h1(:,1);
y=h1(:,2);
tPmax=h1(:,4);
%r=100*sqrt(x^2+y^2);
%theta=atan(y/x)*180/pi;
%Pr=Pmax*0.000145038/14.75

ar=[x Pmax/1000 tPmax tpos tneg];
printf ("%02f      ",ar);
printf ("\n");

```

## REFERENCES

- [1] H. Mao, "Application of a Finite Element Model of the Brain to Study Traumatic Brain Injury Mechanisms in the Rat," *Stapp Car Crash Journal*, vol. 50, pp. 583-600, 2006.
- [2] N. M. Elsayed, "Toxicology of Blast Overpressure," *Toxicology*, vol. 121, pp. 1-15, 1997.
- [3] M. A. Saad, *Compressible Fluid Flow*, 2nd ed. Upper Saddle River, NJ: Prentice-Hall, Inc., 1993.
- [4] D. R. Richmond, J. T. Yelverton, E. R. Fletcher, and Y. Y. Phillips, "Biologic Response to Complex Blast Waves," Los Alamos National Laboratory, Los Alamos, New Mexico, Tech. Rep. A275383, 1985.
- [5] S. I. Svetlov, V. Prima, D. R. Kirk, H. Gutierrez, K. C. Curley, R. L. Hayes, and K. K. W. Wang, "Morphologic and Biochemical Characterization of Brain Injury in a Model of Controlled Blast Overpressure Exposure," *The Journal of Trauma*, vol. Publish Ahead of Print, p. 10.1097/TA.0b013e3181bbd885, 2009.
- [6] M. Griebel, T. Dornseifer, and T. Neunhoeffler, *Numerical Simulation in Fluid Dynamics: A Practical Introduction*. Philadelphia: Society for Industrial and Applied Mathematics, 1998.
- [7] J. E. Guilkey, T. B. Harman, and B. Banerjee, "An Eulerian-Lagrangian Approach for Simulating Explosions of Energetic Devices," *Computers and Structures*, vol. 85, pp. 660-674, 2007.
- [8] S. G. Parker, J. Guilkey, and T. Harman, "A Component-Based Parallel Infrastructure for the Simulation of Fluid-Structure Interaction," *Engineering with Computers*, vol. 22, pp. 277-92, 2006.
- [9] F. H. Harlow and A. A. Amsden, "Numerical Calculation of Almost Incompressible Flow," *Journal of Computational Physics*, vol. 3, pp. 80-93, 1968.
- [10] D. Sulsky, Z. Chen, and H. L. Schreyer, "A Particle Method for History-Dependent Materials," *Computer Methods in Applied Mechanics and Engineering*, vol. 118, pp. 179-96, 1994.

- [11] D. Sulsky, Z. Shi-Jian, and H. L. Schreyer, "Application of a Particle-In-Cell Method to Solid Mechanics," *Computer Physics Communications*, vol. 87, pp. 236-52, 1995.
- [12] B. A. Kashiwa, N. T. Padial, R. M. Rauenzahn, and W. B. VanderHeyden, "A Cell-Centered Ice Method for Multiphase Flow Simulations," Los Alamos National Laboratory, Los Alamos, New Mexico, Tech. Rep. LA-UR-93-3922, 1994.
- [13] B. A. Kashiwa, "A Multifield Model and Method for Fluid–Structure Interaction Dynamics," Los Alamos National Laboratory, Los Alamos, New Mexico, Tech. Rep. LA-UR-01-1136, 2001.
- [14] J. D. Anderson, "The Governing Equations of Fluid Dynamics," in *Computational Fluid Dynamics*. New York: McGraw-Hill, Inc., 1995, pp. 37-94.
- [15] J. D. Anderson, "Basic Aspects of Discretization," in *Computational Fluid Dynamics*. New York: McGraw-Hill, Inc., 1995, pp. 125-167.
- [16] E. F. Toro, "The Riemann Problem for the Euler's Equations," in *Riemann Solvers and Numerical Methods for Fluid Dynamics*. Heidelberg: Springer, 1997, pp. 115-158.
- [17] J. D. Anderson, "Some Simple CFD Techniques: A Beginning," in *Computational Fluid Dynamics*. New York: McGraw-Hill, Inc., 1995, pp. 216-281.
- [18] E. F. Toro, "Multidimensional Test Problems," in *Riemann Solvers and Numerical Methods for Fluid Dynamics*. Heidelberg: Springer, 1997, pp. 551-562.
- [19] E. F. Toro, "The HLL and HLLC Riemann Solvers," in *Riemann Solvers and Numerical Methods for Fluid Dynamics*. Heidelberg: Springer, 1997, pp. 293-312.
- [20] T. Poinsot, *Theoretical and Numerical Combustion*. Philadelphia: R. T. Edwards, Inc., 2001.